

Analysis of a PTEN-associated protein scaffold containing the transmembrane protein PRG2

Inaugural-Dissertation

to obtain the academic degree

Doctor rerum naturalium (Dr. rer. nat.)

submitted to the Department of Biology, Chemistry and Pharmacy

of the Freie Universität Berlin

by

Annika Brosig

from

Gardelegen, Germany

April, 2018

Die vorliegende Arbeit wurde in der Zeit von Juli 2013 bis April 2018 unter Anleitung von Prof. Dr. Britta Eickholt am Institut für Biochemie der Charité, Universitätsmedizin, Berlin durchgeführt.

1. Gutachter: Prof. Dr Britta Eickholt

2. Gutachter: Prof. Dr. Stephan Sigrist

Disputation am: 31.08.2018

Acknowledgements

I would like to express my gratitude to all the people, who have supported me during my PhD studies and contributed to this work.

First and foremost, I would like to thank my supervisor Prof. Britta Eickholt, who gave me the opportunity to work in her lab and to be part of this exiting project. I gratefully thank her for the excellent supervision and highly appreciate her constant support, enthusiasm and motivation that guided me through my PhD.

I want to thank Prof. Stephan Sigrist for accepting to be the second reviewer of this thesis.

My sincere thanks goes to Dr. George Leondaritis, who is an outstanding researcher and who highly contributed to my scientific education. Thanks for all the extensive discussions, your permanent support and patience during my PhD. It was great and inspiring to work with you.

For extensive help during the acquisition of the SIM data, I would like to thank our collaborators Dr. Jan Schmoranzer and Dr. Niclas Gimber. I also want to thank Dr. Thorsten Trimbuch for his help in generating the shRNA constructs.

Thanks to all the members of the Eickholt lab for creating a great working atmosphere including many chats and discussions in the lab as well as down by the fountain. I very much enjoyed working with you. Special thanks goes to Sandra, who I can always count on and who helped me through many, not only work-related, challenging phases during the time of my PhD. Thanks for being such a marvellous friend. Also, I greatly want to thank Patricia. She always found time to help me. Especially during hard phases, she was there to get me back on track. Also, special thanks to all the Kreis-Bintig family members for your support, in particular during the final days of thesis writing. Furthermore, thanks to Mayur for all the fruitful discussions and for inspiring thoughts about future career options. I would like to thank Kai for his insightful help, instructive suggestions and many chats about good old Bristol and Braunschweig. Thanks to all my office fellows former and current ones (Juliane, Joachim, Julia, Mayur, Sandra and Eugenia) for all the discussions and laughs we had. Also, I want to thank our technicians Beate, Kristin und Kerstin, who spend hours in the tissue culture preparing countless neuronal and cell line cultures.

Finally, I deeply want to thank my family and friends, who always stand by my side and support me in everything I do. Also, thanks for listening to all my PRG2 stories and the difficulties that came along with it. Special thanks to Nico. I am deeply grateful for his constant motivation, support and patience. Thanks for being at my side.

Contents

List of figures	V
List of tables	VI
Abbreviations	VII
Abstract	IX
Zusammenfassung	XI
1. Introduction	1
1.1 Establishment of neuronal architecture	1
1.2 The PI3K signalling pathway	2
1.3 The phosphatase and tensin homologue deleted on chromosome 10 (PTEN)	4
1.3.1 Specific function of PTEN in the central nervous system	4
1.3.2 PTEN structure	5
1.3.3 PTEN regulation	6
1.4 PI3K/PTEN pathway regulates the actin cytoskeleton	7
1.5 The role of the cytoskeleton in neuronal morphology and development	8
1.5.1 Microtubules	8
1.5.2 Actin	9
1.5.3 Actin cytoskeleton in the formation of axons	9
1.6 Impact of PI3K in the initial steps of neuronal development	11
1.6.1 Impact of PI(3,4,5)P ₃ in neuronal polarity	11
1.6.2 Impact of PI3K activity on axonal branching	12
1.7 The protein family of Plasticity Related Genes (PRGs)	13
1.7.1 PRGs are involved in filopodia formation	13
1.7.2 PRG function in the central nervous system	14
1.7.3 The role of the intracellular C-terminus on PRG function	15
1.8 Aim of study	17

2. Materials and Methods	18
2.1 Materials	18
2.1.1 Chemicals.....	18
2.1.2 Buffers and solutions	20
2.1.3 Cells and animals	22
2.1.4 Antibodies.....	22
2.1.5 Kits	23
2.1.6 Software	23
2.1.7 Plasmids.....	24
2.1.8 SiRNA	24
2.1.9 ShRNA	25
2.2 Methods.....	25
2.2.1 Cell culture	25
2.2.1.1 Cultivation and transfection of cell lines (HEK293T, N1E-115, COS-7).....	25
2.2.1.2 Cultivation of mouse primary neurons.....	25
2.2.1.3 Transfection of primary hippocampal neurons	25
2.2.1.3.1 Transfection using CaCl ₂	25
2.2.1.3.2 Transfection of hippocampal neurons using Lipofectamine 2000.....	26
2.2.1.4 Viral infection.....	26
2.2.1.5 Immunocytochemistry.....	26
2.2.2 Image acquisition and analysis	27
2.2.3 Biochemistry.....	27
2.2.3.1 Preparation of cell lysate for western blotting.....	27
2.2.3.2 SDS-polyacrylamide gel electrophoresis (SDS-PAGE).....	28
2.2.3.3 Western blotting.....	28
2.2.3.4 Immunoprecipitation (IP).....	28
2.2.3.4.1 Immunoprecipitation of exogenous/overexpressed proteins.....	28
2.2.3.4.2 Immunoprecipitation of PTEN and PRG2 from rat brain homogenate	29
2.2.3.4.3 Native PTEN-IP from cortical lysate.....	29
2.2.3.5 Affinity purification of the PRG2 antibody.....	30

2.2.3.6 PTEN phosphatase assay	30
3. Results	31
3.1 Generation and validation of PRG2 antibodies to study PRG2 function in neurons	31
3.1.1 Characterisation of commercially available PRG2 antibodies	31
3.1.2 Generation of PRG2 antibodies	33
3.1.3 Validation of the custom-made PRG2 antibody	35
3.2 PRG2 exists in a higher order complex	37
3.2.1 PRG2 forms homodimers in primary cortical neurons	37
3.2.2 The interaction of PRG2 monomers is independent of the intracellular C-terminus of PRG2	38
3.2.3 PRG2 interaction with other PRG family members	39
3.3 Temporal and spatial expression of PRG2	40
3.3.1 PRG2 is a developmentally regulated protein	40
3.3.2 PRG2 distribution in cell lines and in primary hippocampal neurons	42
3.3.2.1 Expression of PRG2 in N1E-115 cells	42
3.3.2.2 Subcellular localisation of PRG2 in primary hippocampal neurons	42
3.3.2.3 Super resolution microscopy unravels periodic distribution of PRG2 at the axonal plasma membrane	43
3.3.3 PRG2 localisation is maintained by the actin cytoskeleton	44
3.4 PRG2 binds to the lipid phosphatase PTEN	49
3.4.1 PRG2 interacts with PTEN	49
3.4.2 The PRG2 multimer binds PTEN	50
3.5 Analysis of the PRG2-PTEN complex	51
3.5.1 PRG2 modulates PI(3,4,5)P ₃ abundance through the inhibition of the PTEN phosphatase	51
3.5.2 PRG2 localisation is independent of PI3K induced PI(3,4,5)P ₃ generation	53
3.5.3 Functional characterisation of PRGs during neuronal development	54
3.5.4 BDNF facilitates PRG2-PTEN interaction	63
4. Discussion	65
4.1 PRG2 forms higher order complexes	65

4.2 Spatiotemporal organisation of PRG2.....	67
4.3 Regulation of the PRG2/PTEN complex.....	68
4.4 Regulation of axonal filopodia and branches by PRG2.....	69
4.5 Conclusion.....	70
4.6 Outlook.....	71
5. References.....	73
6. Supplementary information.....	85
6.1 Curriculum vitae.....	85
6.2 Poster and talks.....	86
7. Statement of authorship.....	87

List of figures

Figure 1: Development of primary neurons <i>in vitro</i>	2
Figure 2: PI3K/PTEN signalling pathway.	3
Figure 3: PTEN is present in the axonal shaft of developing neurons.	5
Figure 4: The domain structure of PTEN.	6
Figure 5: Model axonal filopodia formation.	10
Figure 6: The actin-spectrin scaffold provides axonal integrity and flexibility.	11
Figure 7: Schematic of the protein family of PRGs.	16
Figure 8: Examination of anti-PRG2 antibody (Abgent) specificity.	32
Figure 9: Mouse PRG2 amino acid sequence.	33
Figure 10: Generation of a custom-made PRG2 antibody.	34
Figure 11: SAB 70 after antibody purification.	35
Figure 12: Characterization of the custom-made PRG2 antibody.	36
Figure 13: Specificity of custom-made PRG2-antibody.	37
Figure 14: Complex formation of PRG2 <i>in vitro</i>	38
Figure 15: PRG2 dimerizes independent of its poly-E-box.	39
Figure 16: PRG2 binds to other members of the PRG family.	40
Figure 17: Developmental expression profile of PRG2 in brain and cortical neuronal lysate.	41
Figure 18: Exogenous PRG2 localises to filopodia in N1E-115 cells.	42
Figure 19: Subcellular distribution of PRG2 in primary hippocampal neurons.	43
Figure 20: Super resolution microscopy (SIM) of PRG2.	44
Figure 21: PRG2 partially localises to axonal actin rings.	46
Figure 22: Normal morphology of hippocampal neurons following Latrunculin B treatment.	47
Figure 23: PRG2 periodic pattern is defined by the actin cytoskeleton.	48
Figure 24: Verification of PRG2-PTEN interaction by immunoprecipitation.	50
Figure 25: PRG2 binds as a multimer to PTEN.	51
Figure 26: The PTEN-PRG2 interaction inhibits PTEN phosphatase activity.	53
Figure 27: PRG2 localization is not impaired by PI3K inhibition.	54
Figure 28: Loss of PRG2 during neuronal development reduces axonal branching.	56
Figure 29: Loss of PRG1 during neuronal development has a minor effect on arborization.	58
Figure 30: Synchronised loss of PRG1 and PRG2 reveals a more severe decrease in axonal arborization compared to single depletion of both PRGs.	60
Figure 31: Simultaneous loss of PRGs and PTEN does not restore axonal complexity.	61
Figure 32: PI3K signalling strength is altered by loss of PRG1/2 and PTEN.	63
Figure 33: BDNF promotes binding of PRG2 and PTEN.	64
Figure 34: Schematic of interacting PRG family members unravelled in the present thesis.	66
Figure 35: Model of axonal filopodia formation by the PRG2/PTEN protein complex.	71

List of tables

Table 1: List of chemicals	18
Table 2: List of buffers and solutions	20
Table 3: Cells and animals	22
Table 4: Primary antibodies	22
Table 5: Secondary antibodies	23
Table 6: Kits	23
Table 7: Software	23
Table 8: Plasmids	24
Table 9: Sequences coding for shRNAs	25
Table 10:Peptides injected in rabbits to raise the PRG2 antibodies	33

Abbreviations

ABP	Actin binding protein
AIS	Axon initial segment
Akt	Proteinkinase B
APS	Ammonium persulfate
ASD	Autism spectrum disorder
BCA	Bicinchoninic acid
BDNF	Brain-derived neurotrophic factor
BSA	Bovine serum albumin
CK2	Casein kinase 2
CNS	Central nervous system
Co-IP	Co-Immunoprecipitation
CO ₂	Carbon dioxide
CREB	Cyclic AMP response element-binding protein
dH ₂ O	Distilled water
DIV	Days <i>in vitro</i>
DMEM	Dulbecco's modified eagles medium
DNA	Deoxyribonucleic acid
DUSP	Dual specificity phosphatase
E	Embryonic day
FCS	Fetal calf serum
GAKIN	Guanylate kinase-associated kinesin
GAP	GTPase-activating protein
GEF	Guanine nucleotide exchange factor
GPCR	G-protein coupled receptor
GSK3β	Glycogen synthase kinase-3 beta
H	Hours
HEK	Human embryonic kidney cells
HRP	Horseradish peroxidase
IB	Immunoblot
IC	Immunocytochemistry
KD	Knock-down
kDa	Kilodalton
KO	Knock-out
LPA	Lysophosphatidic acid
LPP	Lipid phosphate phosphatase
LPT	Lipid phosphatase/phosphotransferase
LTP	Long term potentiation
mA	Milliampere
MAP2	Microtubule-associated protein 2
min	Minutes
mL	Milliliter
mM	Millimolar
NEP	Neutral endopeptidase
ng	Nanogram
NHERF	Na ⁺ /H ⁺ exchanger regulatory factor
nm	Nanometer

nM	Nanomolar
P	Postnatal day
PBS	Phosphate buffered saline
PFA	Paraformaldehyde
PH	Pleckstrin-homology
PI3K	Phosphoinositide-3-kinase
PI(4,5)P ₂	Phosphatidylinositol-4,5-bisphosphate
PI(3,4,5)P ₃	Phosphatidylinositol-3,4,5-trisphosphate
PPI	Pre-immun serum
PRG	Plasticity Related Gene
PREM	Platinum replica electron microscopy
PTEN	Phosphatase and tensin homologue deleted on chromosome ten
PTHS	PTEN hamartoma tumour syndrome
ROCK	Rho-associated containing protein kinase
rpm	Rounds per minute
RT	Room temperature
SDS	Sodium dodecyl sulfate
SDS-PAGE	SDS-polyacrylamide gel electrophoresis
sec	Seconds
S1P	Sphingosine 1-phosphate
SIM	Structured Illumination Microscopy
STORM	Stochastic optical reconstruction microscopy
Tab.	Table
TBS-T	Tris buffered saline with Tween20
TM	Transmembrane domain
V	Volt
WB	Western blot
WT	Wild type
μL	Microliter

Abstract

In the course of neuronal development, neurons undergo a well-defined maturation programme in order to establish their highly elaborate and characteristic morphology. Determined by extracellular cues and intracellular signalling pathways, an intrinsic sequence of developmental stages generates the formation of neuronal architecture. The PI3K signalling pathway is a key regulator of the neuronal growth program. Through phosphorylation of PI(4,5)P₂ to PI(3,4,5)P₃, PI3K activates downstream signalling processes mediating cytoskeletal reorganization and resulting in morphological changes. The phosphatase PTEN acts as the major suppressor of PI3K. PTEN predominantly functions at the membrane by dephosphorylating PI(3,4,5)P₃ to PI(4,5)P₂, thereby directly antagonises PI3K activity. PTEN is highly enriched in developing neurons and is known to dynamically localise to specific sub-domains of a cellular compartment. For example, PTEN is transiently recruited to the membrane of axonal growth cones mediating chemorepulsion induced morphological changes. However the function of PTEN within the axonal shaft has not been investigated yet.

The present thesis characterised the transmembrane protein PRG2 as a novel interaction partner of PTEN. PRG2 is one out of five members of the PRG protein family, which all constitute of a core structure encompassing six transmembrane spanning domains connected by intra- and extracellular loops. Unique within this protein family is the accumulation of 20 glutamic acid residues in the long intracellular C-terminal domain of PRG2. In the course of this project, we were able to show that PRG2 is highly developmentally regulated, with highest protein expression coinciding with the phase of neuronal branching and outgrowth. Interestingly, depletion of PRG2 by shRNA mediated knock down in early stages of neuronal development, severely impaired the emergence of axonal branches. Immunocytochemical approaches demonstrated a striking periodic appearance of PRG2 puncta along the axonal plasma membrane, which was dependent on actin cytoskeletal dynamics. This combined results identify the transmembrane protein PRG2 as a novel mediator of axon branch formation in developing neurons. Further, biochemical data revealed self-association ability of PRG2 as well as the possibility to interact with other PRG family members. We also provided evidence that PRG2 multimers interact with PTEN in primary neurons and that in association with PRG2, PTEN lipid phosphatase activity is inhibited.

We hypothesise that through its interaction with the lipid phosphatase PTEN, PRG2 spatiotemporally inhibits PTEN activity leading to local nanodomains of PI(3,4,5)P₃ accumulations along the axonal plasma membrane and to the formation of axonal branches. PI(3,4,5)P₃ domains are described to precede F-actin patch formation, which in turn drive the emergence of axonal filopodia. Through invading microtubules, filopodia eventually mature into collateral branches. In summary, this study presents a model, which describes PRG2 as

novel regulator of PTEN activity and thereby expands the understanding of the signalling mechanisms of how neurons adopt their characteristic morphology.

Zusammenfassung

Die Entwicklung neuronaler Zellen ist durch eine spezifische Sequenz innerhalb eines Wachstumsprogramm definiert. Das Durchlaufen der verschiedenen Wachstumsphasen wird durch extrazelluläre Reize sowie durch intrazelluläre Signaltransduktionskaskaden bestimmt. Diese sind, zum Beispiel, essenziell für die Ausbildung der charakteristisch stark verzweigten Morphologie neuronaler Zellen. Einer der wichtigsten Modulatoren während des neuronalen Reifungsprozesses ist der PI3-Kinase (PI3K) Signalweg. Infolge der Phosphorylierung des Phosphoinositides $PI(4,5)P_2$ zu $PI(3,4,5)P_3$ durch PI3K an der Zellmembran, werden nachgelagerte Proteine, wie beispielsweise Akt aktiviert, sowie Regulatoren des Zytoskelett angeschaltet. Diese Prozesse bewirken Veränderungen der zellulären Morphologie. Die Phosphatase PTEN wirkt dieser Reaktion entgegen indem sie $PI(3,4,5)P_3$ dephosphoryliert und $PI(4,5)_2$ bildet. Neben einer Anreicherung von PTEN in Axonen und Dendriten sich entwickelnder Neuronen erfolgt eine dynamische Lokalisation von PTEN in bestimmte neuronale Kompartimente. Ein prominentes Beispiel ist die vorübergehende Rekrutierung von PTEN an die Membran des axonalen Wachstumskegels, wo PTEN das Zurückziehen des Wachstumskegels mit Hilfe des Aktin Zytoskelett steuert. Trotz des substantiellen Wissens bezüglich der Rolle von PTEN im Wachstumskegel ist bisher noch nicht geklärt, welche Rolle PTEN im Axonschaft spielt. Diese Frage ist besonders interessant, da PI3K Aktivität wesentlich zum Auswachsen von axonalen Verzweigungen beiträgt.

Die vorliegende Arbeit charakterisiert das Transmembranprotein PRG2 als neuen PTEN Interaktionspartner. PRG2 gehört zur Proteinfamilie der Plasticity-Related Genes (PRGs), welche durch sechs Transmembrandomänen gekennzeichnet ist. Im Zuge dieser Arbeit konnten wir zeigen, dass PRG2 ein spezielles Expressionsmuster während der neuronalen Entwicklung aufweist, wobei die stärkste PRG2 Expression mit der Phase der neuronalen Verzweigung von Axonen und Dendriten zusammenfiel. Der Verlust von PRG2 während der frühen Phase der neuronalen Entwicklung in primären Neuronen des Hippocampus führt zu einer starken Verminderung des Auswachsens von axonalen Verzweigungen. Immunfärbungen in primären Neuronen zeigten eine periodische Anordnung von PRG2 in der Plasmamembran des Axonschafts. Weiterführende Experimente wiesen darauf hin, dass das Aktin Zytoskelett diese Anordnung reguliert. Die zusammengetragenen Resultate identifizieren das Transmembranprotein PRG2 als neuen Modulator in sich entwickelnden Neuronen während der Entstehung von axonalen Prozessen. Biochemische Analysen zeigten weiterhin, dass PRG2 in der Lage ist sowohl mit sich selbst als auch mit anderen PRGs zu interagieren. Wir können belegen, dass die PRG2-Multimere mit PTEN interagieren und dessen Phosphataseaktivität inhibieren.

Wir vermuten, dass die Interaktion von PRG2 und PTEN, sowohl eine räumliche als auch zeitliche Inhibition der PTEN Enzymaktivität hervorruft. Dieser Mechanismus unterstützt möglicherweise die Bildung von PI(3,4,5)P₃ Nanodomänen entlang der Axonmembran. Die lokale Ansammlung von PI(3,4,5)P₃ ist maßgebend für die Bildung von F-Aktin patches, welche die Vorstufe für axonale Filopodien bilden. Durch die Invasion von Mikrotubuli reifen kurze Filopodien zu einem vollentwickelten axonalen Prozess.

Zusammenfassend beschreibt diese Arbeit PRG2 als neuartigen Regulator der Phosphatase PTEN und erweitert damit das Verständnis, wie lokale PI(3,4,5)P₃ Domänen in Gegenwart von hohen PTEN Leveln gebildet werden können.

1. Introduction

The brain is a highly complex organ formed of neurons specialised for electrical signalling and the supportive nonneuronal cells. The nervous system gathers an enormous amount of information from the outside as well as from the inside of the body. Information is transmitted to the processing area within the brain or the spinal cord and further processed in order to ascertain the best response. Ultimately, information is sent to the effector tissue -for example muscles and organs- to implement an appropriate response.

The brain constitutes of around 100 billion neurons that form roughly 60 trillion connections with each other (Stiles and Jernigan, 2010). Neurons are highly polarized cells, which redirect information via two distinct compartments, the axon and the dendrites. An action potential is relayed throughout the neuronal soma towards the axon. Ultimately, axonal endings serve as presynaptic sites, which convert incoming electrical signals into chemical messengers thereby transmitting information to dendrites of adjacent cells. Dendrites receive synaptic inputs via their postsynaptic endings, which are small protrusions emerging from the dendritic shaft, termed dendritic spines.

During brain development, neurons migrate to their distinct target area within the brain and establish their polarized shape formed of a “leading” and a “trailing” process. The trailing process rapidly elongates and becomes the future axon, while the leading process forms the dendritic tree. Axons grow over considerable distances where they find their target with great accuracy. The distal tip of the growing axon contains a structure termed the growth cone, which enables the axon’s growth in response to chemotropic molecules. After the neuron reaches its final destination, the axon undergoes extensive branching and builds synaptic contacts with postsynaptic compartments of its target cells (Lewis, Courchet, and Polleux, 2013; Polleux and Snider, 2010).

Molecular signalling mechanism spatially and temporally control the establishment of neuronal maturation. Extracellular cues, such as growth factors, mediate the activation of intracellular signalling pathways and provide the dynamic reorganization of the neuronal cytoskeleton.

1.1 Establishment of neuronal architecture

In order to fulfil their complex functions, neurons need to mature through a temporally controlled sequence of events. The formation of the remarkable neuronal shape with highly arborized axonal and dendritic processes has been studied intensively in dissociated cultures of primary hippocampal neurons and can be investigated in vitro. The growth and maturation program is determined by five distinct stages establishing neuronal polarity and morphology (Dotti et al., 1988). In stage 1, plated neurons, derived from the embryonic hippocampus,

display a round shape with a unipolar distribution of lamellipodia and filopodial protrusions. 24 to 48 h later, around day in vitro (DIV) 1-2, various immature neurites extend from the cell body, still lacking the molecular and structural characteristics of axonal or dendritic processes (stage 2). Stage 3 is defined by the selection and rapid elongation of one neurite to form an axon with a pronounced developed growth cone. This phase is described as axon specification. From DIV5 onwards the axon extends and by ramification creates the axonal arbor. Meanwhile, the remaining neurites mature into dendrites and further generate an elaborated dendritic tree (stage 4), termed as phase of axonal and dendrite branching. Ultimately at stage 5, neurons acquire synaptic contacts and create neuronal connectivity (Dotti et al., 1988). A schematic of the neuronal maturation series is displayed in Figure 1.

The process of elaborating neuronal architecture includes highly dynamic morphological changes and requires a tight regulation of the actin and microtubule cytoskeleton. Activation of PI3-kinase (PI3K) and the generation of its phospholipid product implement a critical role in regulating neuronal architecture (Cosker and Eickholt, 2007; Kreis et al., 2014)

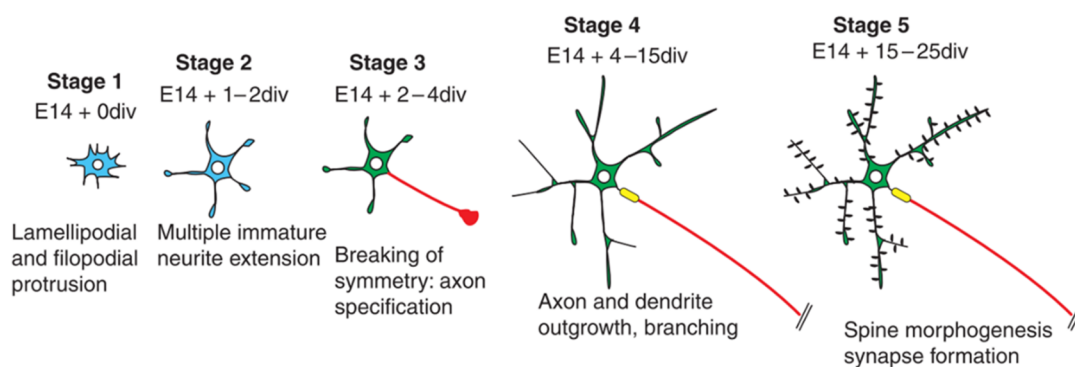


Figure 1: Development of primary neurons *in vitro*.

Stage 1 post-mitotic neurons display a circular formation with high lamellipodial and filopodial protrusive activity. These processes elongate in stage 2 and form immature neurites. Next, the selection and rapid elongation of one neurite creates the formation of the axon (red) whereas the remaining neurites acquire dendritic identity (stage 3). In stage 4 the maturation proceeds, neuronal outgrowth and branching processes shape the elaborated axonal and dendritic arbor. Finally, the formation of dendritic spines along the dendrites and the generation of synaptic contacts accomplishes neuronal maturation (stage 5) (Polleux and Snider, 2010).

1.2 The PI3K signalling pathway

One of the key regulators of neuronal morphology is the PI3-kinase (PI3K) signalling pathway (Cosker and Eickholt, 2007). PI3-kinases are divided into three classes according to their substrate preference and protein structure (Vanhaesebroeck, Guillermet-Guibert, Graupera, and Bilanges, 2010). The present study focuses on the class Ia PI3-kinase, which preferentially phosphorylates phosphatidylinositol 4,5-bisphosphate [PI(4,5)P₂] to phosphatidylinositol 3,4,5,-trisphosphate [PI(3,4,5)P₃] (Cantley et al., 2002). PI3K activation is accomplished by the activation of a number of different upstream receptors. Besides components of the extracellular

matrix and G-protein coupled receptor (GPCR) agonists, PI3K is activated upon growth factor binding to growth factor receptors, which can typically be classified as receptor tyrosine kinases. Following ligand binding, receptor tyrosine kinases dimerize, which leads to subsequent phosphorylation at specific tyrosine residues. This leads, in turn, to the activation of PI3K that then synthesizes PI(3,4,5)P₃ at the plasma membrane. Through phosphoinositide binding domains, such as PH (pleckstrin homology) domains, effector proteins are then recruited to the membrane and mediate the PI3K downstream signalling cascade. One of the most prominent effectors of PI(3,4,5)P₃ is Akt. This Serine/Threonine kinase, also known as Protein kinase B (PKB), binds PI(3,4,5)P₃ via its PH domain and subsequently is phosphorylated at Serine 473 and Threonine 308 by the kinases mTORC2 and PDK1, respectively. Phosphorylated Akt regulates the activity of several other proteins, such as mTORC1, BAD and Glycogen synthase kinase-3 beta (GSK3β). Thereby, PI3K regulates a number of fundamental cellular processes, such as cellular growth and survival, protein synthesis, as well as microtubule dynamics (Manning and Cantley, 2007). In parallel, guanine nucleotide exchange factors (GEFs) and GTPase-activating proteins (GAPs) of the Rho family of GTPases can localise to the membrane via PI(3,4,5)P₃ interactions, mediating actin based changes of the cytoskeleton (Cantrell, 2001) (Figure 2).

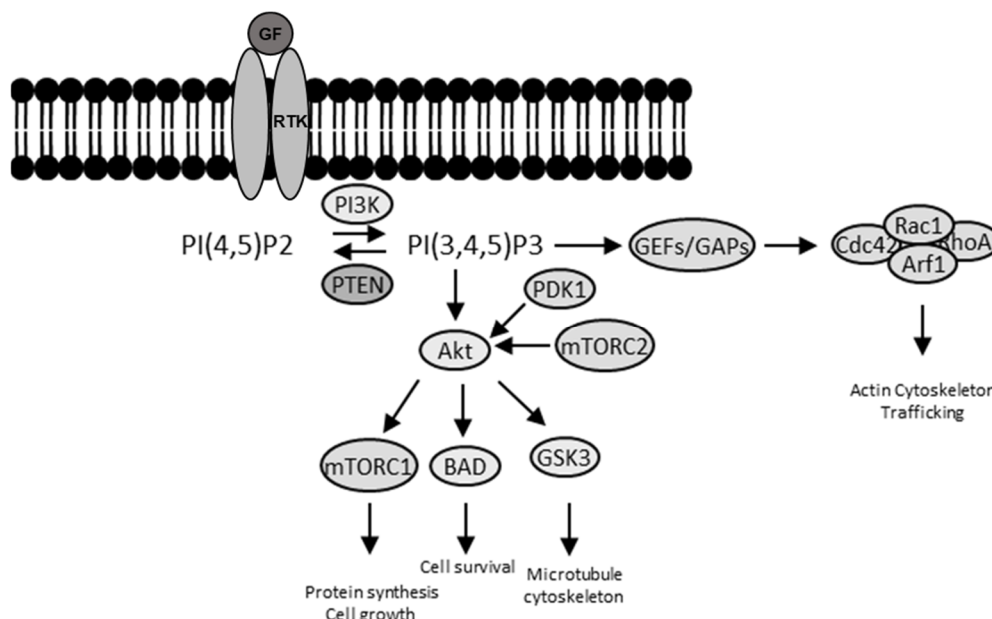


Figure 2: PI3K/PTEN signalling pathway.

PI3K is activated upon growth factor (GF) binding to the receptor tyrosine kinase (RTK). Active PI3K synthesizes PI(3,4,5)P₃ from PI(4,5)P₂. In turn PI(3,4,5)P₃ mediates the activation of Akt by PDK1 and mTORC2 and additionally recruits GEFs and GAPs to the membrane. Subsequently, processes, such as protein synthesis, cell survival as well as cytoskeletal dynamics are regulated by downstream signalling of phosphorylated Akt and GTPases. PI3K is directly antagonized by PTEN, which functions by dephosphorylating PI(3,4,5)P₃ to PI(4,5)P₂. (Kreis et al., 2014)

1.3 The phosphatase and tensin homologue deleted on chromosome 10 (PTEN)

PTEN is a lipid and protein phosphatase, which is mainly present in the cytosol. Predominantly PTEN functions, through its transient localisation to the plasma membrane, by dephosphorylating PI(3,4,5)P₃ to PI(4,5)P₂. Thereby negatively regulates the PI3K pathway and controls downstream signalling cascades involved in cytoskeletal dynamics (Figure 2). PTEN has also been described to be present in the nucleus, contributing to genomic stability and regulating cellular survival (Gil et al., 2006; Shen et al., 2007). Here, PTEN functions seem to be independent of its lipid phosphatase activity.

1.3.1 Specific function of PTEN in the central nervous system

Originally identified as a tumours suppressor, PTEN is highly mutated or deleted in various human cancers (Bigner et al., 1984; J. Li et al., 1997; Steck et al., 1997) and has evolved as key regulator in neuronal development. Humans carrying PTEN germline mutations present diverse pathologies ranging from the predisposition to the development of tumours to neurological abnormalities including macrocephaly, seizures, ataxia and autism spectrum disorders (ASD) (Zhou et al., 2003, Butler et al., 2005; Endersby and Baker, 2008; Zhou and Parada, 2012). PTHS (PTEN hamartoma tumour syndrome) including Cowden syndrome and Proteus syndrome are some of the well-known disorders (Hollander et al., 2011).

The importance of PI3K signalling regulation by PTEN in the central nervous system is revealed by data obtained in several PTEN conditional knock out mouse models. Kwon et al. showed that depletion of PTEN in subsets of differentiated neurons in the cortex and hippocampus of adult mice results in an impaired social behaviour reminiscent of ASD, accompanied by progressive macrocephaly (Kwon et al., 2006). In the same approach, PTEN mutant mice revealed a general neuronal hypertrophy phenotype, displaying increased soma size, axonal growth, dendritic arborization and spine density correlated with enhanced phospho-Akt levels. Loss of PTEN in postnatal stem cells of the hippocampus led to an impaired social interaction and appearance of seizures in PTEN mutant mice, as well as to hypertrophic PTEN deficient neurons (Amiri et al., 2012). In line with this, additional publications demonstrated high levels of phosphorylated Akt and a progressive growth phenotype in PTEN depleted neurons (Backman et al., 2001; Kwon et al., 2001 Fraser et al., 2004; Gallent and Steward, 2018). Interestingly, inhibition of PTEN has been shown to increase the regenerative potential of neurons by promoting growth of axonal processes after injury (Liu et al., 2010; Park et al., 2008). Altogether, downregulation of PTEN in the central nervous system, aberrantly modulates downstream effectors of PI3K leading to increased growth phenotypes.

At the cellular level, PTEN is located in the axon and dendrites of neurons, including dendritic spines. Following synaptic stimulation, PTEN is recruited to the post-synaptic membrane and appears to be involved in the modulation of synaptic plasticity (Jurado et al., 2010). In earlier stages of neuronal development, PTEN has been shown to localise to the axonal growth cone during neuronal outgrowth. PTEN is concentrated in the central region of the growth cone, and is transiently recruited to the membrane of the actin-rich periphery upon chemorepulsion or growth cone collapse to regulate PI(3,4,5)P₃ (Chadborn et al., 2006). PTEN is also highly abundant in the axon shaft of developing neurons (see Figure 3). However, the function of this axonal enrichment is poorly understood.

In summary, a large amount of work focusing on the analyses of PTEN function in the neuronal cell highlighted the importance of PTEN to dynamically localise to specific sub-domains of a cellular compartment, suggesting that PTENs distribution is highly regulated in a temporal and spatial manner.

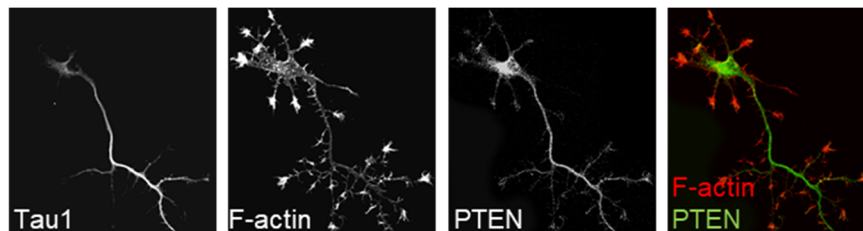


Figure 3: PTEN is present in the axonal shaft of developing neurons.

Primary hippocampal neuron: fixed at DIV5 and immunostained with anti-Tau1, anti-PTEN antibody and Phalloidin. Immunolabeling reveals a prominent enrichment of PTEN in the Tau1-positive axon.

1.3.2 PTEN structure

PTEN consists of 403 amino acids and shows a distinct domain structure (Figure 4). The first 15 amino acids of the N-terminus form the PI(3,4)P₂ binding domain (PBD), which determines PTENs association to the plasma membrane (Vazquez et al., 2006). PTEN further contains two core regions, namely the phosphatase (15-185) and the C2 (186-351) domain. The phosphatase domain possesses a catalytic signature motif (¹²³HCKAGKGR¹³⁰) that forms a phosphate binding loop (P loop), characteristic for dual specificity phosphatases (DUSPs). In addition to the classical protein phosphatase activity of dephosphorylating tyrosine residues, DUSPs can also dephosphorylate serine and threonine residues. In contrast to other DUSPs, a four residue insertion in the PTEN active site leads to an enlarged binding pocket determining phosphoinositide substrate specificity and providing PTENs catalytic ability on proteins and lipids (Lee et al., 1999). In addition to the PBD, the C2 domain appears to support PTEN membrane targeting (Lumb and Sansom, 2013; Shenoy et al., 2012). The C-terminus consists of a flexible C-tail (352-401) followed by a PDZ binding domain (401-403).

Interestingly, published data reveal the occurrence of a dimeric PTEN complex, which is catalytically active and displays an enhanced lipid phosphatase function compared to the PTEN monomer (Papa et al., 2014). Following phosphorylation of the C-tail domain, PTEN is described to induce a “closed” conformation status, which results in an intramolecular association of the C-tail and part of the C2 domain, leading to reduced membrane binding and phosphatase activity. In contrast, de-phosphorylation provokes an “open” conformation and increases membrane accessibility (Rahdar et al., 2009). In fact, post-translational modifications, such as phosphorylation, represent a key factor within the spectrum of PTEN regulatory mechanisms.



Figure 4: The domain structure of PTEN.

PTEN consists of 403 amino acids, compartmentalized into five domains: a PI(4,5)P₂-binding domain (PBD), a phosphatase domain, a C2 domain, a carboxy-terminal tail and a PDZ-binding domain. (Song, Salmena, and Pandolfi, 2012)

1.3.3 PTEN regulation

PTEN is regulated through various molecular mechanisms that specifically function to modulate expression, activity and localisation of the phosphatase. For example, transcriptional deregulation of PTEN by epigenetic silencing, is often associated with multiple tumour types (Ho et al., 2009; García et al., 2004; Salvesen et al., 2001). PTEN expression is further modulated by transcription factors. For example, EGR1 activates PTEN expression (Virolle et al., 2001). Whereas Snail1 and SALL4 have been described to inhibit PTEN expression (Escriva et al., 2008; Lu et al., 2009;). Post-transcriptional manipulation of PTEN levels, particularly by microRNAs such as miR-19 and miR-21, has been described to promote malignancies by downregulating PTEN (Meng et al., 2015; Olive et al., 2009; Zhang et al., 2010).

In a direct and acute fashion, post-translational modifications and the interaction with other proteins fundamentally drive cellular PTEN function further, for example, by localisation of the phosphatase to a cellular compartment and by altering protein stability. As briefly described previously, phosphorylation of PTEN’s C-tail induces specific conformational changes. In detail, phosphorylation of an amino acid cluster (Serine/Threonine 380, 382, 383, 385) by casein kinase 2 (CK2) provokes the alteration into a “closed” conformation that is more stable, which, however, exhibits reduced enzymatic activity through the loss of PTEN membrane attachment (Rahdar et al., 2009; Torres and Pulido, 2001). PTEN is also a substrate of Rho-associated containing protein kinase (ROCK). Phosphorylation in the C2 domain of PTEN by

ROCK, stimulates PTEN phosphatase activity (Z. Li et al., 2005). Ubiquitylation at Lysine 13 and Lysine 289 leads to nuclear localisation and degradation of PTEN. In turn, deubiquitylation by HAUSP causes an accumulation of PTEN in the cytosol (Song, Salmena, Carracedo, et al., 2012). Likewise PTEN is also target of acetylation and oxidation, regulating its subcellular distribution and enzymatic activity (Chae and Broxmeyer, 2011; Lee et al., 2002; Okumura et al., 2006).

PTEN protein-protein interactions mediate the regulation of the PTEN binding partner via PTENs protein phosphatase activity. For example, PTEN binds and dephosphorylates the actin binding protein Drebrin (Kreis et al., 2013). And interaction of PTEN with the transcription factor cyclic AMP response element-binding protein (CREB) leads to dephosphorylation of CREB (Gu et al., 2011).

Vice versa, PTEN itself is also regulated by protein-protein interaction. For example neutral endopeptidase (NEP) interacts with the phosphorylated C-tail of PTEN and facilitates its plasma membrane localisation as well as increases PTEN stability and activity (Sumitomo et al., 2004). The Na⁺/H⁺ exchanger regulatory factor (NHERF) binds and recruits PTEN to growth factors to restrict PI3K signalling (Takahashi et al., 2006). Additionally, the interaction of PTEN to MyosinV determines PTEN membrane transport and regulates PTEN phosphatase function in neurons (van Diepen et al., 2009).

Thus, through association with different proteins, PTEN localisation, activity and stability is highly regulated, thereby PTEN contributes to a plethora of cellular responses.

1.4 PI3K/PTEN pathway regulates the actin cytoskeleton

The PI3K/PTEN signalling pathway is highly involved in controlling the phosphoinositide composition along the plasma membrane of cells. The lipid composition at the membrane, in particular phosphoinositides, has been shown to influence the mobility and directionality of migrating cells by creating distinct membrane domains and recruit distinct effectors. Early evidence for the role of phospholipids and PI3K localisation on the regulation of cell motility and cytoskeletal changes are based on chemotactic experiments in fibroblasts, neutrophils and *Dictyostelium* (Iijima et al., 2002, Funamoto et al., 2002; Haugh et al., 2000; Servant et al., 2000). Upon exposure of cells to chemoattractants, polarisation required PI3K and PI(3,4,5)P₃ distribution towards the leading edge, whereas PTEN delocalised from the front of the cell. PI(3,4,5)P₃ contributes to actin dynamics mainly by regulating Rho family GTPases, whereas PI(4,5)P₂ controls cytoskeletal dynamics more directly by regulating actin binding proteins (ABPs) (Saarikangas, Zhao, and Lappalainen, 2010). Evidence shows that ABPs can bind to phosphoinositide-rich membranes through electrostatic interactions and laterally diffuse along the membrane (Senju et al., 2017).

The protein family of Rho GTPases connects the reorganization of the actin cytoskeleton with PI3K activation. GTPases alternate between an active GTP-bound and an inactive GDP-bound state. Guanine nucleotide exchange factors (GEFs) catalyse the conversion of GDP to GTP and thereby enhance GTPase activation. In contrast, GTPase activating proteins (GAPs) facilitate the hydrolysis of GTP to GDP, maintaining the inactivation of GTPases (Stankiewicz and Linseman, 2014). GEFs and GAPs are localised to the membrane and are activated upon binding with their respective PH-domains to phosphoinositides. Accordingly, changes in phosphoinositide levels lead to the tight regulation of GTPases. Members of the protein family of RhoGTPases, such as Rho, Rac and Cdc42, interact with their respective effector proteins in a GTP-bound constitution. Downstream targets of Rho include the LIM-kinase, which functions in inhibiting actin severing by the inhibition of Cofilin; as well as the actin polymerisation factor mDia2. Rac and Cdc42 interact with scaffold proteins belonging to the WASP/SCAR/WAVE complex, which activate key regulators of actin nucleation and polymerisation, such as Arp2/3 (Hanna and El-Sibai, 2013). Interestingly, WASP and WAVE can also directly bind to phosphoinositides contributing to their localisation and the activation of the ARP2/3 complex at the membrane (Senju et al., 2017).

1.5 The role of the cytoskeleton in neuronal morphology and development

The neuronal cytoskeleton encompasses three major components: neurofilaments, microtubules and actin. By providing structural support, cytoskeletal structures are essential during the formation of neuronal shape as well as in the maturation process of dendrites and axons during neuronal development.

1.5.1 Microtubules

Microtubules are composed of core structures termed protofilaments. These filaments are built by heterodimers of α - and β -tubulin. Through lateral interaction, protofilaments form the characteristic hollow cylindrical microtubule structure (Conde and Cáceres, 2009). Microtubules are polar structures containing a fast-growing “plus” and a slow-growing “minus” end (Letierrier, Dubey, and Roy, 2017). In neurons, microtubules-structures are modified by post-translational modifications as well as through regulatory factors. For example, spastin and katanin promote microtubules severing. Also, microtubule-associated protein (MAPs), such as Tau and MAP2, form crosslinked dense microtubule bundles in axons and dendrites, respectively (Hoogenraad and Bradke, 2009; Kapitein and Hoogenraad, 2015).

The establishment of neuronal architecture highly depends on the morphological changes induced by microtubule dynamics. In particular, by acting as mechanical force, microtubules

are involved in neurite outgrowth, axon elongation and neuronal branching (Hoogenraad and Bradke, 2009)

1.5.2 Actin

Actin is present in two principle forms, one being the monomeric globular G-actin and the other being the polymeric filamentous F-actin. Actin filaments are generated by polymerization of G-actin in an ATP dependent process. Under steady-state conditions, actin filaments undergo continuous “treadmilling” by constant polymerisation at the “barbed end” and depolymerisation at the “pointed end” of the filament, resulting in a highly dynamic structure with no net change in the length of the actin filament (Pollard, 2009). F-actin turnover is highly regulated by various actin binding proteins, such as Arp2/3 and Cofilin, promoting actin nucleation and elongation as well as filament severing and depolymerisation. This process of actin reorganization provides the basis for dynamic morphological changes of the cell. In neurons specific compartments such as the tip of the growing axon, the axonal growth cone and dendritic spines require high amounts of dynamic actin.

1.5.3 Actin cytoskeleton in the formation of axons

During axon specification, when the neuron starts to polarise, actin dynamics and instability is required in the growth cone of the neurite destined to become an axon (Bradke and Dotti, 1999). The enrichment of F-actin in growth cones allows the neuron to sense the environment, and constantly extend and retract membrane protrusions to direct its motility.

During branching, the emergence of filopodia from the axon shaft is the first step in the development of a collateral branch. This process requires dynamic cytoskeletal rearrangement. Here, local accumulation of F-actin underneath the plasma membrane, termed actin patches (Loudon, Silver, Yee, and Gallo, 2006), precede the growth of a filopodium (Spillane et al., 2011). PREM (platinum replica electron microscopy) images of the axonal cytoskeleton resemble the actin patches as a meshwork of branched filamentous actin (Spillane et al., 2011). Patches form spontaneously, grow in size and eventually dissipate. Interestingly, only a subset of patches gives rise to filopodia. Spillane et al. could show that axonal actin patches form at sites of high PI3K activity and that the actin nucleator Arp2/3 contributes to the emergence of F-actin patches. Following patch formation, filaments elongate and extend towards the membrane, and by polymerisation evoke a pushing force leading to the curvature of the plasma membrane. Further extension of the filopodium leads to a pronounced protrusion from the axon shaft. Subsequent maturation and stabilisation into a branch is accomplished by invading microtubules. Within the axon shaft, microtubules are arranged in a parallel fashion. At sites of branching, microtubules undergo localised fragmentation. Severing is mediated by proteins, such as spastin and katanin (Yu et al., 2008),

and may provide a facilitated entry of microtubules into filopodia, a process that requires Septin7 (Hu et al., 2012). A schematic model of axonal filopodia formation is shown in Figure 5.

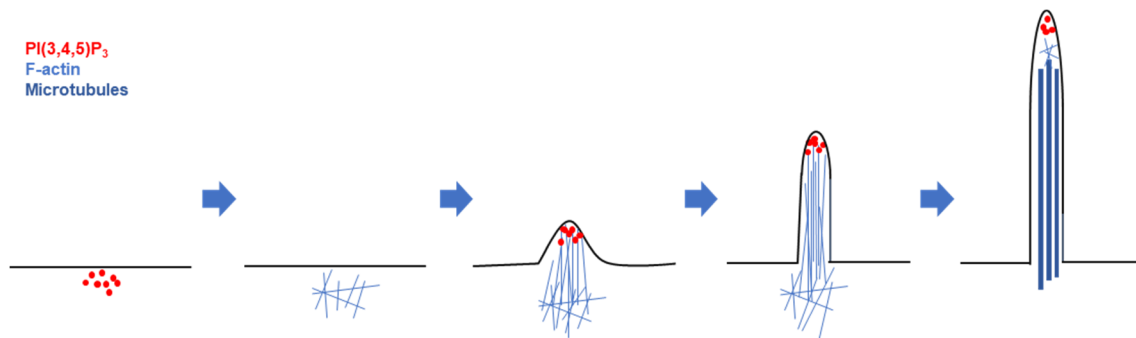


Figure 5: Model axonal filopodia formation.

Local PI3K activity depicted by the accumulation its lipid product PI(3,4,5)P₃ (red) leads to the formation of a meshwork of actin filaments (dark blue) underneath the plasma membrane, termed F-actin patches. Actin patches are precursors for filopodia formation. Elongation of actin filaments towards the plasma membrane leads to membrane curvature and the outgrowth of a protrusion from the axon shaft. Axonal filopodia mature into a branch by the invasion of microtubules (light blue).

The development of super-resolution microscopy techniques, such as structured illumination microscopy (SIM) and stochastic optical reconstruction microscopy (STORM), enabled a gain in resolution when compared to conventional light microscopy and allowed insights into the interaction, distribution and dynamics of proteins down to nanometer scale. Data based on these techniques revealed novel axonal actin structures, which will be described in the following.

In 2013, Xu et al. detected a remarkable periodic actin organisation within the axon shaft of fixed cultured hippocampal neurons. They found actin filaments arranged into isolated rings wrapped around the circumference of axons. These actin ring structures display a spatial sequential distribution of ~190nm. Likewise, immunolabeling with anti-spectrin antibody revealed a similar periodic pattern and showed that actin ring distribution is regulated by spectrin tetramers. Additional data, combining live cell imaging and novel F-actin fluorogenic probes (for example SiR-Actin) demonstrate the formation of actin rings in living neurons (D'Este et al., 2015; Lukinavičius et al., 2014). In stage 3, neurons (DIV2) that had just polarised (see Figure 1), neurons already display spectrin structures, which are built gradually from proximal to distal parts in the axon shaft upon development. In its mature state, the actin-spectrin scaffold seem to be highly stable and immobile (Zhong et al., 2014), and is believed to function as mechanical support for the axonal membrane. Earlier studies in the nematode *Caenorhabditis elegans* prove that assumption. Here, mature axons that lack β -spectrin break under acute movement of the animal due to acute strain (Hammarlund, Jorgensen, and Bastiani, 2007). This demonstrates that the formation of an actin-spectrin structure underneath the plasma membrane highly contributes to the integrity and flexibility of the axon (Figure 6).

Further the structure may serve as a regulator for the distribution of proteins, such as sodium channels along the plasma membrane, (Xu et al., 2013).

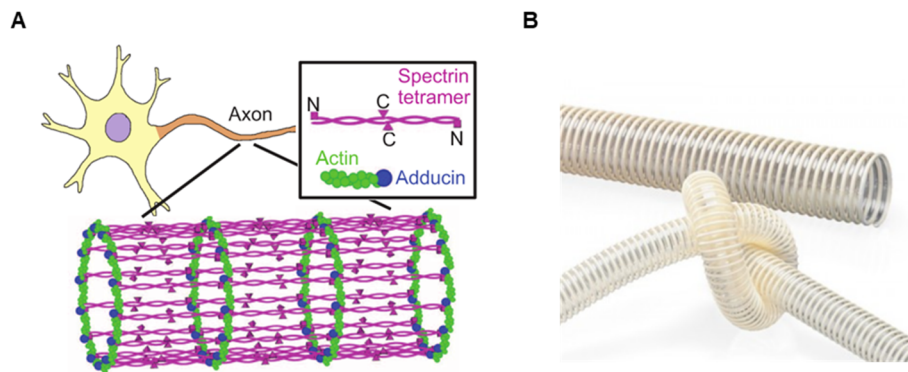


Figure 6: The actin-spectrin scaffold provides axonal integrity and flexibility.

A) Schematic representation of the actin spectrin structure in axons. Actin filaments (green) capped by adducin (blue) form ringlike structures wrapping around the circumference of the axon. Spectrin tetramers (magenta) connect the adjacent actin rings along the axon and generate a lattice structure with a periodicity of ~180-190 nm. C: C-terminus, N: N-terminus. B) Image of a flexible tube. The actin-spectrin lattice formation in neurons highly promotes the integrity and flexibility in the axon, similar to the helix in a conventional tube. (Xu et al., 2013 and <https://www.kf-betriebstechnik.de/>)

Besides the sub-plasmalemmal actin rings, recent studies examined structures of the deep actin network in axons. Dynamic actin hotspots, with a duration time of ~30, are distributed along the axon and undergo continuous polymerisation and depolymerisation (Ganguly et al., 2015). Additionally, dynamic bidirectional actin polymers, with an average length of approximately 9 μm , are present within the axonal shaft. These structures are termed actin trails and often seem to originate from actin hotspots, suggesting that the spots serve as a domain for actin elongation (Ganguly et al., 2015). The function of these deep actin network structures is still not clear. It is hypothesised that the actin hot spots operate as storage zones, providing actin supply once it is needed, for example during actin ring formation (Roy, 2016). Further, actin spots and trails are supposed to have a role in axonal transport.

1.6 Impact of PI3K in the initial steps of neuronal development

1.6.1 Impact of PI(3,4,5)P₃ in neuronal polarity

The establishment of neuronal architecture by the well-defined maturation programme (see Figure 1) is highly dependent on PI3K signalling. Published data shows a relevance of local PI(3,4,5)P₃ distribution and the PI3K signalling cascade especially during the phase of neuronal polarisation. This stage is described as point of `breaking the morphological symmetry` where rapid elongation of one neurite determines polarity through the formation of an axon (Dotti, Sullivan, and Banker, 1988). Inhibition of PI3K activity by LY-294002 in primary hippocampal neurons leads to the prevention of axon specification (Shi, Jan, and Jan, 2003). In the same approach, the main effector of PI3K signalling, phosphorylated Akt localises to the

tip of the growing axon, but not to other processes. Further, Akt phosphorylation mediates the inhibition of GSK3 β , which is critical for microtubule formation via collapsin response mediator protein 2 (CRMP2). CRMP2 promotes the assembly of microtubule subunits at ends of existing microtubules (Conde and Cáceres, 2009) Overexpression of wild type or a constitutive active form of GSK3 β prevents axon specification in hippocampal neurons (Yoshimura et al., 2005). Whereas shRNA-mediated knock down or pharmacological and peptide inhibition of GSK3 β leads to the formation of multiple axons (Jiang, Guo, Liang, and Rao, 2005). Also, visualisation of PI(3,4,5)P $_3$ by PH domain containing proteins, such as Akt, fused to GFP, proposed PI(3,4,5)P $_3$ accumulation at the distal end of the longest neurite (Ménager et al., 2004). Additionally, Horiguchi et al. published that the guanylate kinase-associated kinesin (GAKIN) transports PI(3,4,5)P $_3$ itself or may transports factors that stimulate the production of PI(3,4,5)P $_3$ to the prospective axon. In summary, published data propose that the PI3K signalling pathway substantially contributes to the establishment of neuronal polarity. In addition, PI(3,4,5)P $_3$ and local PI3K activity have been described to be implicated in the process of axonal branching by affiliation to the process of filopodia formation (Ketschek and Gallo, 2010).

1.6.2 Impact of PI3K activity on axonal branching

The outgrowth of filopodia from the axon is the initial step for the development of an elaborated collateral branch. Axonal filopodia are finger-like protrusions emerging from the axonal shaft. They arise from precursor F-actin patches. Published data demonstrate the PI3K dependent emergence of actin patches along the axon shaft of embryonic sensory axons (Ketschek and Gallo, 2010). Accordingly, NGF dependent activation of the PI3K signalling pathway results in an increase in F-actin patch formation. Usage of a GFP-Akt-PH construct monitored PI(3,4,5)P $_3$ microdomains at sites that subsequently gave rise to filopodia. Further, simultaneous visualisation of F-actin patches via mCherry-Actin and PI(3,4,5)P $_3$ revealed a synchronised formation of actin patches and PI(3,4,5)P $_3$ accumulations. Interestingly, although actin patch number was increased, the percentage of patches transitioning into filopodia did not change, suggesting that PI3K affects the frequency of patch formation rather than changing the possibility to build a filopodium from a patch. Also, experiments without NGF treatment and usage of the PI3K inhibitor LY-294002, as well as direct activation of PI3K by a cell permeable peptide, suggested a requirement of localised PI3K activity for F-actin patch initiation. Besides the enhanced number of filopodia, direct activation of PI3K also promoted the formation of mature axon branches (Ketschek and Gallo, 2010), indicating a clear link between PI3K activity and axonal arborization. However, the mechanism how local accumulation of PI3K activity is achieved remains elusive. In particular, with regard to the high concentrations of the lipid phosphatase PTEN in the axon shaft.

1.7 The protein family of Plasticity Related Genes (PRGs)

A mass spectrometry approach, performed by a former member of the Eickholt laboratory, Michiel van Diepen, that was aimed at isolating neuron specific PTEN interaction partners, identified Plasticity Related Gene 2 (PRG2) as an interaction partner of PTEN in mouse brain. The interaction was initially verified by co-immunoprecipitation experiments by Michiel van Diepen. In my PhD work, I set out testing the significance of the PTEN-PRG2 protein-protein interaction in neurons.

PRG2 is one out of five members of the protein family of Plasticity Related Genes. The first member within the protein family of PRGs, PRG1, has been identified by Bräuer et al. (2003) in a cDNA screen to discover mRNAs specifically upregulated during neuronal development and in lesioned hippocampus. PRGs are brain enriched proteins (Bräuer and Nitsch, 2008). Due to the pre-existing abbreviation “PRG” for an unrelated protein family of proteoglycans and the relation of Plasticity Related Genes to lipid phosphate phosphatases (LPPs), the alternative acronym LPPR (LPP related proteins) has been established. Similar to LPPs, PRGs are subclassified into the superfamily of lipid phosphatases/phosphotransferases (LPTs). LPT family members are characterised by a core region consisting of six transmembrane spanning domains connected by intra- and extracellular loops. Within their extracellular loops, LPPs possess three catalytic domain sequences, which are essential in maintaining the phosphatase activity that targets hydrolysis of bioactive lipid substrates, such as lysophosphatidic acid (LPA) and sphingosine 1-phosphate (S1P) (Sigal, McDermott, and Morris, 2005). Alignment studies of PRGs and LPPs revealed non-conservative substitutions within the proposed catalytic motif of PRGs (Sigal, Quintero, Cheney, and Morris, 2007), suggesting that PRGs are catalytically inactive. However, early studies investigating PRG1 function described a role for PRG1 in LPA dependent processes. The current consensus appears to be that PRG1 may control or sense LPA levels rather than effectively dephosphorylating them (Bräuer et al., 2003; McDermott, Sigal, Sciorra, and Morris, 2004; Trimbuch et al., 2009).

To date, five PRG family members have been discovered, named PRG1-PRG5. Intriguingly, PRG members are able to form higher order complexes by interaction with their family members. In 2015 Yu et al. showed the interaction of PRG3 with PRG1 as well as with PRG2 and PRG5 in overexpression experiments of tagged PRG variants in Neuro2A cells. However, the formation of PRG higher order complexes on endogenous protein level is not yet determined.

1.7.1 PRGs are involved in filopodia formation

Initial studies investigating PRG function demonstrate a profound induction of filopodia formation upon PRG overexpression. In that effect, Sigal et al. showed that PRG3-GFP

localises to the actin-rich membrane protrusions and significantly increased the number of filopodia in PRG3-GFP expressing HeLa and Cos7 cells (Sigal et al., 2007). Interestingly, in the same approach data support the idea, that the formation of filopodia by PRG3 is not dependent on the well characterised actin promoting factor Cdc42 (Sigal et al., 2007), suggesting that PRG induced filopodia may generated through the activation of other RhoGTPases.

In line with the PRG3 induced phenotype, expression of the lately identified PRG family member, PRG5, in P19 embryonic carcinoma cells revealed drastic morphological changes through emergence of spiky-like membrane extensions (Broggini et al., 2010). When PRG5 was expressed together with PRG3 the effect on filopodia formation was enhanced compared to single expression of both family members (Yu et al., 2015). Altogether, these data demonstrate that members of the PRG family induce filopodia formation. However the underlying mechanism by which PRGs direct the induction of filopodia is not fully understood.

1.7.2 PRG function in the central nervous system

Examination of the neurodevelopmental expression pattern of PRGs displayed a differential abundance of PRGs during development. Whereas PRG3 and PRG5 are present from early embryonic stages onwards (E15), PRG1 expression is restricted to the postnatal phase (Bräuer et al., 2003; Coiro et al., 2014; Velmans et al., 2013).

Localisation studies during early stages of development show PRG3 distribution in neurites and the axonal growth cone, whereas in later stages (after DIV14) PRG3 is mainly located in the axon (Velmans et al., 2013). In line with the data obtained in nonneuronal cells, PRG5 expression induced filopodia-like protrusion at neurites and located to the tips of filopodia and neurites (Broggini et al., 2010; Coiro et al., 2014). Recently, Strittmatter and Cafferty (2017) showed accumulation of PRG3 in actin-rich protrusion along the neurite shaft as well as in the growth cone. Additionally, they demonstrate enhanced neurite outgrowth following PRG3 expression in cortical neurons and analysed the role of PRG3 in neurite sprouting. Indeed, *in vivo* overexpression of PRG3 in corticospinal motor neurons enhanced the sprouting of axonal tracts after unilateral brainstem lesion in wild type mice and identified PRG3 as a new axon-growth modulator that drives axonal sprouting (Strittmatter and Cafferty, 2017).

Data focusing on the closely related PRG2, revealed the importance of PRG2 in thalamocortical axon guidance (Cheng et al., 2016). Radixin is a crosslinker of the cortical actin cytoskeleton and the plasma membrane, and has been shown to bind PRG2 (Cheng et al., 2016). This protein complex is essential in the LPA dependent repulsion of thalamocortical axons, restricting them in the intermediate zone of the cortex. *In vivo* loss of PRG2 leads to a misrouting and protruding of thalamocortical fibers into the cortical plate due to the lack of

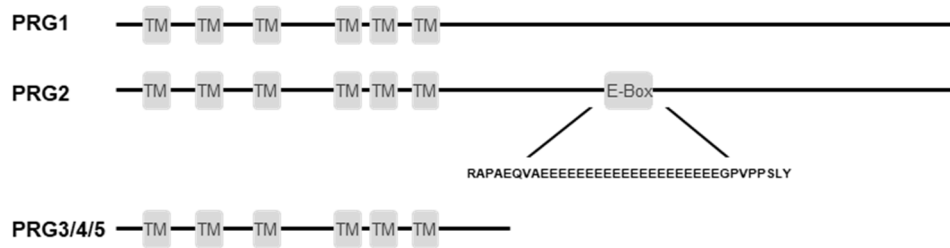
sensitivity for LPA as a chemorepellent for axonal growth cones. *In vivo* recordings and whisker-specific behavioural test exhibited altered processing of cortical information and sensory discrimination deficits of adult PRG2 deficient mice, revealing an essential role of PRG2 in axon guidance (Cheng et al., 2016).

The highly related family member PRG1 has been shown to be implicated in synaptic plasticity. PRG1 deficiency in hippocampal neurons resulted in a reduced number of dendritic spines accompanied by an impaired long term potentiation (LTP) ability of excitatory synapses compared to control (Liu et al., 2016). Further, depletion of PRG1 leads to severe hippocampal overexcitability and epileptic seizures in juvenile PRG1 mutant mice (Trimbuch et al., 2009).

Taken together, PRGs are involved in diverse functions during neuronal development ranging from early events, such as neurite outgrowth processes and axon guidance to the modulation of synaptic plasticity in mature neurons. This is presumably attributed to the diverse neurodevelopmental expression of the PRG family members.

1.7.3 The role of the intracellular C-terminus on PRG function

Although all PRGs display the core domain structure of LPTs, encompassing six transmembrane domains connected by intra - and extracellular loops, they are distinct in the length of the intracellular C-terminal tail. Whereas PRG3 and PRG5 harbour rather short C-termini, corresponding to 43 and 50 amino acids, respectively; PRG1 and PRG2 bear a 400 amino acid C-terminus each (Figure 7). These intracellular C-terminal extensions are suspected to represent a regulatory or signal transduction domain. Indeed, the C-terminal domain of PRG1 serves as a putative binding region for interaction partners mediating intracellular signalling. In this respect, PRG1 has been shown to localise to the postsynaptic density of hippocampal neurons (Trimbuch et al., 2009), where it binds the Ca^{2+} signal transducer protein Calmodulin. This interaction is accomplished in between the residues Ser⁵⁵⁴ and Gln⁵⁸⁸ within the PRG1 C-terminus and maintains postsynaptic function via intracellular Ca^{2+} signalling (Tokumitsu et al., 2010). Further the PRG1 C-terminal region associates with the protein phosphatase 2A (PP2A) via the Calmodulin binding motif and modifies its enzymatic activity at the postsynaptic density (X. Liu et al., 2016). Likewise, the interaction of the PRG family member, PRG2 with Radixin during thalamocortical axon guidance is dependent on the PRG2 C-terminus (Cheng et al., 2016). Notably, unique upon PRGs is a 20 glutamic acid residue stretch (poly-E-box) within the C-terminus of PRG2. This unusual acidic region may provide an additional level in regulating PRG2 function. However, data demonstrating a fundamental role of the PRG2 poly-E-box is missing.



TM: Transmembrane domain
 E-box: PRG2 specific Poly-E-box

Figure 7: Schematic of the protein family of PRGs.

The protein family of PRGs includes 5 members (PRG1-5). These integral membrane proteins share a common domain structure consisting of six transmembrane domains connected by intra- and extracellular loops. The length of the intracellular C-terminus varies. The highly homologous PRG1 and PRG2 possess a long C-terminal tail of 400 amino acids. Whereas PRG3-5 display a rather short C- tail of 40-50 residues. Unique upon PRGs is an highly acidic stretch within the intracellular C-tail of PRG2, displayed by a sequence of 20 glutamic acid residues.

1.8 Aim of study

This study was motivated by an initial mass spectrometry approach, conducted by Michiel van Diepen, identifying the interaction of the lipid and protein phosphatase PTEN with the transmembrane protein PRG2. The protein family of PRGs is described to be mainly enriched in brain tissue. Throughout neuronal development, PRG members display a differential expression pattern and mediate neuronal outgrowth processes as well as synaptic transmission. PRG2 was shown to function in association with the actin binding adaptor Radixin in axon guidance (Cheng et al., 2016), suggesting a role for PRG2 in actin dynamics in early events of neuronal maturation. PRGs are involved various steps during neuronal maturation, however signalling events mediating PRG function are less clear.

PTEN, which is abundantly expressed in dendrites and axons, directly antagonises the PI3K pathway, which links growth cues from the membrane to the cytoskeleton, regulating neuronal growth and architecture. The present study is aimed at investigating, if and how the association of PRG2 and PTEN influences neuronal PTEN functions in developing neurons. PTEN has been demonstrated to be highly regulated by its interaction partners. However, less is currently known regarding the regulation of PTEN based scaffolds during the course of neuronal development. This thesis focuses on the examination of the spatiotemporal dynamics of the PRG2-PTEN complex during neuronal development and will extend the understanding of PTENs impact on neuronal function.

The present study shows a highly developmentally regulated expression profile of PRG2 during neuronal development, with a striking appearance of PRG2 during the phase of neuronal outgrowth and branching. Subcellular distribution analysis in primary neurons demonstrate a highly periodic organisation of PRG2 along the axonal plasma membrane. ShRNA mediated depletion of PRG2 in hippocampal neurons during early stages of neuronal development significantly decreased axonal branching. Examination of PTEN phosphatase activity in association with PRG2 revealed a PRG2-dependent inhibition of PTEN enzymatic activity. Taken together, this study proposes a novel protein complex containing PTEN and PRG2, acting at the axonal plasma membrane to create domains of high PI3K activity. We hypothesise that through inhibition of PTEN activity by PRG2, local PI3K/PI(3,4,5)P3 accumulations lead to the formation of axonal filopodia, which serve as precursors for collateral branches

2. Materials and Methods

2.1 Materials

2.1.1 Chemicals

Table 1: List of chemicals

<u>Name</u>	<u>Company</u>	<u>Catalog number</u>
Ammonium persulfate (APS)	Roth	No. 9592.2
Acrylamide	National Diagnostics	No. EC-890
B27	Life Technologies	No. 17504044
β -Mercaptoethanol	Sigma	No. M7522
BDNF	R&D Systems	No. 248-BD-005
Bovine Serum Albumin (BSA)	Roth	No. 8076.4
DABCO	Roth	No. 0718.1
Di-C8-PI(3,4,5)P ₃	Echelon	No. P-3908
Dulbecco's Modified Eagle Medium (DMEM)	Invitrogen	No. 31331028
ECL Western Blotting Substrate	Promega	No. W1001
Ethanol	Roth	No. P075.5
Fetal calf serum (FCS)	Biochrom	No. S0115
Flag M2 Affinity Gel	Sigma	No. A2220
GDC-0941	Selleckchem	No. S1065
GlutaMax	Invitrogen	No. 25030-024
Goat Serum	Gibco	No. 16210-072
Laminin	Corning	No. 354232
Latrunculin B	Calbiochem	No. 428020
Lipofectamine 2000	Invitrogen	No. 11668019
Milk powder	Roth	No. T145.3
Mowiol	Sigma	No. 81381
Neurobasal-A	Invitrogen	No. 21103-049
NP-40	US Biological	No. 3500
Optimem	ThermoFisher	No. 31985062
PageRuler Protein ladder	ThermoFisher	No. 112289
Paraformaldehyde (PFA)	Merck	No. 1040051000
Penicillin/Streptomycin	Invitrogen	No. 15070-063

Phalloidin	ThermoFisher	No. A12379 No. A12380
Phosphate Buffered Saline (PBS)	Applichem	No. A9191,0012
Ponceau Red	Sigma	No. 09189
Poly-L-Ornithine	Sigma	No. P8638
Protease Inhibitor Cocktail 3	Calbiochem	No. 539134
Protein G Agarose (Hi-Bind)	BioVision	No. 6513
Resolving Buffer	National Diagnostics	No. EC-892
Roti [®] -Load	Roth	No. K929.1
Roti [®] -Load 3 (LDS)	Roth	No. 3359.1
Sodium Chloride (NaCl)	Roth	No. 9265.1
Sodium Dodecyl Sulfate (SDS)	Calbiochem	No. 428029
Temed	Merck	No. 1107320100
Tris-Hydrochloride (Tris-HCl)	Roth	No. 9090.3
Triton-X-100	US Biological	No. T8655
Tween-20	Calbiochem	No. 655205
Vectashield	Vector Laboratories	No. H-1000

2.1.2 Buffers and solutions

Table 2: List of buffers and solutions

<u>Solution</u>	<u>Ingredients</u>
Blocking solution	1% Goat serum 2% BSA 0,2 % Triton PBS
2x BBS buff	50mM BES 280 mM NaCl 1,5 mM Na ₂ HPO ₄ dH ₂ O pH 7,3
HBSS buffer	135mM NaCl 4mM KCl 1mM Na ₂ HPO ₄ 2mM CaCl ₂ x2H ₂ O 1mM MgCl ₂ x6H ₂ O 20mM HEPES 20mM d-Glucose dH ₂ O pH7,3
PTEN lysis buffer	50 mM Tris 150 mM NaCl 1 mM EDTA 1 mM EGTA 1 % NP-40 0,1 % β-Mercaptoethanol Protease inhibitors dH ₂ O
RIPA buffer	150 mM NaCl 50 mM Tris 0,5% Sodium deoxycholate, 1% NP-40 0,1% SDS dH ₂ O

Running gel (8%)	4,8 ml dH ₂ O 2,5 ml Resolving Buffer 2,7 ml Acrylamide 100 µl APS (10%) 10 µl TEMED
Stacking buffer	0,5 M Tris-HCl 0,4% SDS dH ₂ O pH 6,8
Stacking gel (4%)	3,1 ml dH ₂ O 1,25 ml Stacking Buffer 0,65 ml Acrylamide 25 µl APS (10%) 5 µl TEMED
TBS-T (10x)	50mM Tris-HCl 150 mM NaCl 0,05% Tween-20 dH ₂ O pH 7,4
Transfer buffer (1x)	20 mM Tris-HCl 190 mM Glycine 20% Methanol dH ₂ O
Mowiol	10g Mowiol 4-88 40 ml PBS 20 ml Glycerol 2 g DAPCO

2.1.3 Cells and animals

Table 3: Cells and animals

<u>Name</u>	<u>Company</u>
HEK293T cells	stock in the lab
N1E-115 cells	stock in the lab
COS-7 cells	stock in the lab
C57/bl6 mice	FEM, Charité Berlin
PTEN ^{floxed/floxed} C57/bl6 mice	FEM, Charité Berlin
PRG2 KO C57/bl6 mice	FEM, Charité Berlin
Wistar rats	FEM, Charité Berlin

2.1.4 Antibodies

Table 4: Primary antibodies

(IB: Immunoblot, IC: Immunocytochemistry, IP: Immunoprecipitation)

<u>Name</u>	<u>Company</u>	<u>Source</u>	<u>Dilution</u>
Akt-pan	Cell Signaling, #9272	rabbit	IB: 1:1000
p(Thr308)Akt	Cell Signaling, #2965	rabbit	IB: 1:1000
p(Ser473)Akt	Cell Signaling, #4060	rabbit	IB: 1:1000
Flag-M2	Sigma, #F3165	mouse	IB: 1:1000 IC: 1:1000
GAPDH	Calbiochem, #CB1001	mouse	IB: 1:2000
GFP	Abcam, #ab13970	chicken	IB: 1:1000 IC: 1:1000
Map2	Sigma, #M9942-200UL	mouse	IC: 1:1000
PRG1	R&D Systems, #MAB2874	mouse	IB: 1:500
PRG2	Abgent, #AP5732c	rabbit	IB: 1:500
PRG2	Chemicon International, #AB 15170	rabbit	IB: 1:500
PRG2 (SAB70)	Custom made, Peptides (Eurogentec)	rabbit	IB: 1:1000 IF: 1:100
PTEN	Cell Signaling, #9559	rabbit	IB: 1:1000
PTEN (N-19)	Santa Cruz, #sc-6818	goat	IP
Tau1	Millipore, #MAB3420	mouse	IC: 1:1000
α -Tubulin	Sigma, #T6199	mouse	IB: 1:2000 IC: 1:1000

Table 5: Secondary antibodies

<u>Name</u>	<u>Company</u>	<u>Dilution</u>
Alexa Fluor 488 donkey anti-chicken	Dianova, #703-545-155	IC: 1:500
Alexa Fluor 647 donkey anti-mouse	Dianova, # 715-605-150	IC: 1:500
Alexa Fluor 488 goat anti-mouse	ThermoFisher, #A-10680	IC: 1:500
Alexa Fluor 568 goat anti-mouse	ThermoFisher, #A-11031	IC: 1:500
Alexa Fluor 488 goat anti-rabbit	Dianova, #711-545-152	IC: 1:500
Alexa Fluor 568 goat anti-rabbit	ThermoFisher, #A-11011	IC: 1:500
Alexa Fluor 488 Phalloidin	ThermoFisher, #A-12379	IC: 1:100
Alexa Fluor 568 Phalloidin	ThermoFisher, #A-12380	IC: 1:100
Alexa Fluor 647 Phalloidin	ThermoFisher, #A-22287	IC: 1:100
HOECHST	Sigma, #14530	IC: 1:50.000
HRP-conjugated anti-chicken-IgG	Promega, #G135A	IB: 1:1000
HRP-conjugated anti-mouse-IgG	Vector Laboratories, #PI2000	IB: 1:3000
HRP-conjugated anti-rabbit-IgG	Vector Laboratories, #PI1000	IB: 1:3000

2.1.5 Kits

Table 6: Kits

<u>Name</u>	<u>Company</u>	<u>Catalog number</u>
Malachite Green Assay	Echelon	No. K-1500
Pierce® BCA Protein Assay Kit	ThermoFisher	No. 23225
SulfoLink® Immobilization Kit for Peptides	ThermoFisher	No. 44999

2.1.6 Software

Table 7: Software

<u>Name</u>	<u>Company</u>
ImageJ	National Institutes of Health, USA
Imaris	Bitplane AG, Switzerland
Prism 5	GraphPad Software, USA
R-studio	Boston, USA

2.1.7 Plasmids

Majority of plasmids used in this thesis, were generated in the Eickholt lab and validated by sequencing. Origin of other plasmids is stated in brackets.

Table 8: Plasmids

<u>Plasmid</u>	<u>Description</u>
pCAG-PRG1-Flag	PRG1 full length protein fused to Flag
pCAG-PRG2-Flag	PRG2 full length protein fused to Flag
pCAG-PRG2 Δ C-Flag	Truncated variant of PRG2 lacking the Poly-E-box fused to Flag
pCAG-PRG2-YFP	PRG2 full length protein fused to YFP
pCAG-PRG2DC _a -YFP	Truncated variant of PRG2 (amino acid 1-407)
pCAG-PRG2DC _b -YFP	Truncated variant of PRG2 (amino acid 1-305)
pCAG-GFP-PTEN	PTEN full length protein fused to GFP
U6-shPRG1-syn-GFP	shRNA mediated knockdown of PRG1 and expression of GFP
U6-shPRG2-syn-GFP	shRNA mediated knockdown of PRG2 and expression of GFP
U6-shPRG1/2-syn-GFP	shRNA mediated knockdown of PRG1 and PRG2 and expression of GFP
Syn-GFP (AG Rosenmund)	Expression of GFP
PRG3-GFP (AG Bräuer)	PRG3 full length fused to GFP
PRG4-GFP (AG Bräuer)	PRG4 full length fused to GFP
PRG5-Flag (AG Bräuer)	PRG5 full length fused to Flag
pcDNA3.1 (ThermoFisher)	Expression vector
pEGFP-N1 (Clontech)	Expression vector for fusion proteins with GFP
P3xFlag_CMV (Sigma)	Expression vector for fusion proteins with Flag

2.1.8 SiRNA

SiRNA was purchased from ThermoScientific.

siPRG2 (ON TARGET plus SMARTpool) is comprised of 4 individual siRNAs (GAAGCGAGCCAGCGUGGAU,CCAGGCAGCUUAUCGGUGA,CUGUCUACGUGUCGAUGUA, CCUCAAUCAUGGUCGGCGA). As control the ON-Target plus Non-Targeting pool (D-001810-10) has been used.

2.1.9 ShRNA

Table 9: Sequences coding for shRNAs

<u>Target mRNA</u>	<u>shRNA sequence 5'→3'</u>
PRG1	GAGTCTTAGCATGCCGTACAT
PRG2	GCTTCAGAAGCAGCTGTAAAC
PRG1/2	GCTGCAACTTCAACTCCTTC

2.2 Methods

2.2.1 Cell culture

2.2.1.1 Cultivation and transfection of cell lines (HEK293T, N1E-115, COS-7)

HEK293T, N1E-115 and COS-7 cells were cultured in DMEM containing 10% heat inactivated FCS, 200 mM Glutamax and 100 U/ml Penicillin/Streptomycin at 37°C and 5% CO₂. Per 6 well dish, 200.000 cells were seeded and transfected one day after plating using Lipofectamine 2000 according to manufacturer's instructions. 24 h after transfection cells were lysed in indicated buffers and prepared for Western Blot analysis.

2.2.1.2 Cultivation of mouse primary neurons

Dissection of hippocampi and cortices and subsequent preparation of primary hippocampal and cortical neurons from E16.5 wild type, PTEN flox/flox and PRG2 KO C57/bl6 mice (see Tab. 3) was kindly done by Kerstin Schlawe and Kristin Lehmann. Primary neurons were routinely kept in Neurobasal-A medium supplemented with 200 mM Glutamax, 2% B27 and 100 U/ml Penicillin/Streptomycin at 37°C and 5% CO₂. Cortical neurons were seeded on 30 µg/µL Poly-L-Ornithine coated coverslips. Hippocampal neurons were plated on 30 µg/µL Poly-L-Ornithine and 20 µg/µL Laminin coated coverslips. For immunocytochemistry 110.000 primary hippocampal neurons/well of a 12 well plate and for biochemical approaches 200.000 cortical cells/well of a 6 well plate, were seeded.

2.2.1.3 Transfection of primary hippocampal neurons

2.2.1.3.1 Transfection using CaCl₂

Hippocampal neurons were plated in a 24 well dish at a density of 50.000 cells per well. One day after plating neurons were transfected using CaCl₂. The following protocol corresponds to four wells of a 24 well dish. Neurobasal medium supplemented with 200 mM Glutamax and 2% B27 was prewarmed in the incubator for 30 min. Subsequently, 37.5 µL dH₂O and 12.5 µL

1M CaCl₂ were gently mixed. By pipetting up and down, first 7-9 µg of DNA and second 50 µL of 2x BBS buffer was added to the transfection mix. Finally, 900 µL prewarmed Neurobasal-A medium was added to the transfection mix and incubated for 15 min at RT. Conditioned Neurobasal medium has been removed from the dish and was stored in a falcon tube at 37°C. 250 µL transfection mix was applied to each well and neurons were kept in the incubator for 45-60 min. Then, the transfection mix was washed off 8x with HBSS buffer and conditioned media was applied. Cells were kept until 7 DIV.

2.2.1.3.2 Transfection of hippocampal neurons using Lipofectamine 2000

Primary hippocampal neurons were seeded in a 12 well dish with a density of 110.000 neurons per well. Transfection was performed using Lipofectamine 2000 after two DIV. First, 2 µg of DNA were mixed with 100 µl Optimem. In parallel, 2 µL of Lipofectamine and 100 µL Optimem were combined in a separate tube. Both solutions were pooled and incubated for five minutes. Meanwhile, half of the conditioned medium was collected in a falcon tube and the same volume of fresh Neurobasal medium (with additives) was added. Medium was kept at 37°C. 200 µl of transfection mix was added dropwise to the cells, followed by 15-20 minutes incubation at 37°C and 5% CO₂. Medium was aspirated and mix of conditioned and fresh medium was added. Cells were kept until 7 DIV.

2.2.1.4 Viral infection

For *in vitro* experiments, PTEN flox/flox primary neurons were infected with lentiviruses purchased from the Viral Core Facility, Charité. Here, syn-Cre-RFP and syn-nls-RFP viruses were applied at DIV1 or DIV2. PTEN expression was assessed after different days in culture by western blotting and Immunocytochemistry.

2.2.1.5 Immunocytochemistry

Cells were fixed in 4% prewarmed PFA in PBS for 15-20 minutes and coverslips were rinsed three times with PBS. Permeabilization and blocking of unspecific binding sites was performed by application of blocking solution (Tab.2) for 1h. The primary antibody (Tab. 4) diluted in blocking solution was applied for either 2-3h at RT or overnight at 4°C in a wet chamber. Coverslips were washed three times with PBS and secondary antibody (Tab. 5) labelling was undertaken for 1-2 h at RT. Coverslips were mounted in Mowiol.

For SIM microscopy cells were seeded on square coverslips (Roth, #LH24.1). Antibody labelling was performed as described above. Coverslips were embedded in Vectashield mounting media for analysis.

2.2.2 Image acquisition and analysis

Confocal images of transfected N1E-115 cells and primary hippocampal neurons were acquired using the Leica TCS SP5 Laser Scanning Microscope. Images were analysed using ImageJ software.

For investigation of axonal arborization of primary hippocampal neurons, images were obtained with an inverted epifluorescence microscope (Nikon Eclipse Ti) using the 20x objective. Data analysis was undertaken using the NeuronJ plugin of ImageJ and R-Studio software.

Further, in order to resolve precise positioning of PRG2 nanodomains and specifically PRG2 periodicity at the axonal plasma membrane Structured Illumination Microscopy (SIM) was performed. SIM as a technique of super-resolution microscopy generates a 2-fold resolution gain compared to conventional microscopy methods. Here, SIM images were captured using the OMX V4 Blaze system (GE Healthcare) in collaboration with Dr. Jan Schmoranzner and Dr. Niclas Gimber (AMBIO Super-Resolution Microscopy Z02 SFB958, part of SFB958). Images were analysed using ImageJ software. The 'measurement points' tool of the Imaris software was used to generate PRG2 periodicity data by selection of central single sections of a stack and subsequent distance measurement between two consecutive PRG2 spots. In order to obtain membrane/cytosol abundance data, once more central sections were used and PRG2 puncta in both compartments were counted and analysed using GraphPad software.

2.2.3 Biochemistry

2.2.3.1 Preparation of cell lysate for western blotting

Lysates were generated from cell lines (HEK293T, N1E-115), cortical neurons and whole brains from either mouse or rat. Before lysis cells were washed once with ice cold PBS. Cell lines were lysed in RIPA buffer (including protease and phosphatase inhibitors). Cortical and brain lysates were homogenized in buffer containing 10 mM Tris pH 7.8, 140 mM NaCl, 5mM EDTA, 0.5% NP40, 0.1% β -Mercaptoethanol as well as protease and phosphatase inhibitors. All lysates were vortexed and incubated rotating at 4°C for 20 min. Subsequently, samples were centrifuged for 20 min, at 14.000 rpm at 4°C and the supernatant was transferred in a new Eppendorf tube. Protein concentration was measured using the Pierce®BCA Protein Assay kit. To denature the samples 4x Roti load buffer was applied to the lysates and they were heated at 95°C for 3 min. Samples were kept at -20°C until analysis by SDS-polyacrylamide gel electrophoresis (SDS-PAGE).

For experiments under semi-native conditions, homogenates were generated under non-reducing conditions. Lysis buffer did not contain β -Mercaptoethanol and lysate was

supplemented with non-reducing 4x Roti load 3(LDS) buffer. Samples were not boiled but kept at RT and immediately run for SDS-polyacrylamide gel electrophoresis.

2.2.3.2 SDS-polyacrylamide gel electrophoresis (SDS-PAGE)

Sodium dodecyl sulfate-polyacrylamide gel electrophoresis is an analytical method to separate proteins in a gel matrix according to their molecular weight. SDS-PAGE consisted of a stacking gel (Tab.2) with 3,75% acrylamide and a running gel (Tab.2) with either 8% or 10% acrylamide, depending on the molecular weight of the protein of interest. Lysates were loaded on SDS-PAGE and an electric field was applied, first 80 V for 30 min followed by 140 V until the dye front of the Roti load buffer reaches the bottom of the running gel.

2.2.3.3 Western blotting

After gel electrophoresis, proteins were immobilized on a membrane and detected by specific antibodies. Here, proteins were transferred from the polyacrylamide matrix to a nitrocellulose membrane using the WET/Tank Blotting System from Bio-Rad. The blotting process was performed in transfer buffer for 2.5 h at 400 mA. Post-transfer, membrane was incubated in 5 milk diluted in TBS-T for 1 h to block unspecific binding sites. Then, the primary antibody (Tab.4) diluted in blocking solution was applied for 2 h at RT or overnight at 4°C. Membranes were washed 3x with TBS-T and incubated with the respective horseradish peroxidase (HRP)-coupled secondary antibody (Tab.5) for 1 h at RT. After a final washing step (3x 15 min in TBS-T), proteins were detected using 'Enhanced Chemiluminescence (ECL)' reagents (Promega, #0000280623). Visualization was carried out by using the Vilber Lourmat System®.

2.2.3.4 Immunoprecipitation (IP)

Immunoprecipitation is a powerful technique to identify protein-protein interactions. The protein of interest is being isolated out of the cell lysate by affinity to its specific antibody. Subsequently, interaction partners can be identified by probing the IP samples with potential antibodies in Western Blot experiments.

2.2.3.4.1 Immunoprecipitation of exogenous/overexpressed proteins

For IP of exogenous protein, cell lines were plated in 6 well dishes and transfected with Flag and GFP-tagged plasmids. 24 h post-transfection cells were lysed in 300 µL RIPA buffer containing protease and phosphatase inhibitors per well. Cell lysate was generated as described in section 2.2.3.1. 10% of total protein lysate was mixed with 4x Roti load buffer and were probed as input control. 20 µL Anti-Flag Affinity Gel was used per condition. Prior to the IP, Flag beads were washed twice with lysis buffer by centrifugation for 3 min at 5000 rpm. All centrifugation steps were conducted at 4°C. Beads were resuspended in lysis buffer in same volume, respectively. IP was undertaken rotating and overnight at 4°C. Mixture of beads and

lysate were spun down and supernatant was transferred to a fresh tube and probed later for IP efficiency. Beads were washed 3x with lysis buffer, followed by resuspension in 25 μ L 2x Roti load buffer and boiling at 95°C for 3 min. Once beads settled to the bottom of the tube, supernatant was transferred to a fresh tube. Remaining pellet was boiled in 25 μ L 1x Roti load buffer and supernatant was added to the previous supernatant. Immunoprecipitated samples and inputs were analysed by Western Blot using anti-Flag (Sigma) and anti- GFP (ThermoFisher) antibody.

2.2.3.4.2 Immunoprecipitation of PTEN and PRG2 from rat brain homogenate

Brains from P1 rat embryos were weighed and homogenized in 4x volume lysis buffer (10 mM Tris at pH 7.5; 140 mM NaCl; 5mM EDTA; 0,5% NP-40; 0,1% β -Mercaptoethanol) containing protease and phosphatase inhibitors. Here, 2 ml lysis buffer were used per brain. 10% of brain lysate has been used as input control. In order to preclear the lysate 20 μ L Protein G agarose beads per sample were washed twice with lysis buffer (3 min, 5000 rpm, 4°C) and resuspended in original volume lysis buffer. Beads were incubated with generated lysate for 1 h at 4°C. Next, bead-lysate mixture was spun down and the supernatant was transferred to a fresh tube. Cleared brain lysates were incubated overnight (rotating, 4°C) using anti-PTEN antibody (2 μ g, N-19, Santa Cruz), anti-PRG2-antbody (1,5 μ g, custom-made) and corresponding IgG controls. On the next day, 20 μ L Protein G agarose beads per sample were prepared as described above and were added to lysate-antibody mixture. Samples were incubated 2 h at 4°C on the roller. Following several washing steps, beads were boiled in 45 μ L 2x Roti load buffer for 3 min. The supernatant was transferred into a fresh Eppendorf tube, when beads sank down to the bottom of the tube. Again remaining beads were incubated with 1x Roti load at 95°C, for 3 min and supernatants were pooled in the previous tube. Subsequently, SDS-PAGE and Western Blot with indicated antibodies (anti-PTEN 138G6, Cell Signaling; anti-PRG2, custom-made) was performed.

2.2.3.4.3 Native PTEN-IP from cortical lysate

Cortical neurons were lysed at 9 DIV in buffer containing 10 mM Tris (pH 7.5); 140 mM NaCl; 5 mM EDTA; 0,5% NP-40; protease and phosphatase inhibitors. Per condition one 6 well plate was lysed in 700 μ L buffer. 20% of lysate was taken for input control. The input was divided and supplemented with either 4x Roti load (containing β -Mercaptoethanol) or 4x Roti load 3(LDS). Preclearing of lysate was performed as described before (2.2.3.4.2). Cleared lysates were incubated overnight with anti-PTEN antibody (3 μ g, N-19, Santa Cruz). The following day, incubation with Protein G agarose beads was performed as described above (2.2.3.4.2). Post-incubation, the lysate-bead mixture was spun down for 3 min, 5000 rpm. The supernatant was harvested and beads were washed four times with lysis buffer. To elute the IP sample, 50 μ L Glycine (0,1 M, pH 2.5) was applied. Elution was immediately neutralized by addition of 5 μ L

Tris-HCl (1M, pH 8.5) and pH was controlled by pH indicator stripes. Volume of IP samples was divided in half. One sample was supplemented with 4x Roti load (containing β -Mercaptoethanol), and the other was completed with 4x Roti load 3(LDS) to preserve non-reducing conditions. Native IP was performed as described in Papa et. al, 2014.

2.2.3.5 Affinity purification of the PRG2 antibody

In order to affinity purify the PRG2 antibody, the SulfoLink® Immobilization Kit for Peptides has been used. Prior to purification, 4 sera (two per epitope) have been tested for unspecific binding via Western Blotting. Based on these results, one serum was chosen for purification. According to manufactures protocol the affinity column was equilibrated for purification and coupled with the peptide. 2 ml of respective serum was incubated with the column for 1 h while rocking. Column was rinsed 6x with PBS and antibody was eluted by addition of 5 mL Glycine (0,2 M, pH 2.5). Eluate was collected in 1 ml aliquots and the pH was monitored. Immediately after the pH switch to 2.5, the elutions were neutralized with Tris-HCl (1 M, pH 8.5). Then the antibody concentration of the different elutions was estimated by using the plate reader to measure absorbance at 280nm. Elutions with the highest protein concentration were pooled, aliquoted and stored at -20°C. The antibody was tested for biochemistry and immunocytochemistry.

2.2.3.6 PTEN phosphatase assay

GFP-PTEN immunoprecipitants from transfected COS-7 cells were washed four times with PTEN lysis buffer and three times with PTEN assay buffer (100 mM Tris pH 8.0, 2 mM DTT). After the final wash, beads were resuspended in assay buffer and distributed in 25 μ l aliquots and placed on ice. One-tenth of IP reactions was kept for analysis of PTEN levels by western blotting. Reactions were started by the addition of 3 μ L of 1 mM di-C8-PIP₃ to a 25 μ L-aliquot of immunoprecipitated PTEN. Samples were incubated at 37°C under constant rotation for up to 60 min. Reactions were terminated by addition of 100 μ l malachite green reagent and, after a further incubation for 15 min at room temperature, the absorbance at 620 nm was measured.

3. Results

The phosphoinositide 3-kinase (PI3K) signalling pathway is one of the major regulators of neuronal development including the establishment of neuronal morphology (Rodgers and Theibert, 2002). During the course of neuronal development, PI3K signalling and the associated generation of increased levels of the second messenger PI(3,4,5)P₃ determines axon specification and elongation (Cosker and Eickholt, 2007). PI3K/PI(3,4,5)P₃ also mediates neuronal outgrowth and branching, revealing a fundamental role of PI3K for intrinsic neuronal maturation processes (Jaworski et al., 2005; Ketschek and Gallo, 2010). PTEN, originally identified as tumour suppressor, directly antagonises PI3K activity by dephosphorylating PI(3,4,5)P₃ to PI(4,5)P₂. Thereby PTEN prevents elevated levels of PI3K signalling strength and functions as a key regulator of neuronal growth. Intriguingly, PTEN is highly abundant in dendrites and axons throughout neuronal development (Kreis et al., 2014). To date, the emergence of neuronal protrusions from neurites to form the elaborate neuronal architecture in a PTEN rich environment is poorly understood.

A mass spectrometry approach, identifying PTEN interaction partners (Diepen et al., 2009), defined Plasticity Related Gene 2 (PRG2) as a novel target of PTEN in rat brain. The protein family of PRGs was first identified in a cDNA screen to find mRNAs specifically upregulated during neuronal development and in the lesioned hippocampus (Bräuer et al., 2003). Members of PRGs have been shown to be dynamically regulated during neuronal development and appear to induce neurite outgrowth (Broggini et al., 2010; Strittmatter and Cafferty, 2017). Recent data on the function of PRG2 demonstrate a role in axon guidance (Cheng et al., 2016).

The present thesis aimed on investigating the functional relevance of the formation of a PRG2/PTEN complex during neuronal development.

3.1 Generation and validation of PRG2 antibodies to study PRG2 function in neurons

3.1.1 Characterisation of commercially available PRG2 antibodies

In order to analyse the localisation and function of the PRG2 protein, we tested the specificity of commercially available antibodies. A search for PRG2 antibodies identified two antibodies from different companies. The first antibody was a polyclonal antibody generated in rabbit and raised against an epitope in the intracellular C-terminal domain of PRG2 (amino acid residues 316-344) and was supplied by Abgent. The second commercially available PRG2 antibody was also a polyclonal rabbit antibody, which was offered by Chemicon. The epitope of this antibody was not indicated by the supplier. Western blot data, provided by the suppliers,

obtained from HEK293 and NCI-H292 cell lysates probed with both antibodies, showed the recognition of a single band at the molecular size of 77 kDa. This corresponds to the calculated molecular size of PRG2 based on its amino acid sequence. Both antibodies had not been cited before in publications. In the present study both commercial antibodies were used for initial experiments. E17.5 mouse brain lysate, P1 rat brain lysate, untransfected and PRG2-Flag transfected HEK293T cell lysates were probed with the anti-PRG2 antibody from Abgent in western blotting. Figure 8 shows the recognition of a signal at ~62 kDa (arrow) in all samples tested, resembling a much lower molecular size than the predicted one of 77 kDa, suggesting that this band is unspecific. P1 rat brain lysate showed a strong signal at ~90 kDa, which differs from the amino acid based predicted molecular size of PRG2 being 76 kDa. It is possible that this shift in molecular weight may be caused by post-translational modifications of the PRG2 protein. Untransfected and PRG2-Flag transfected HEK293T cell lysate as well as E17.5 mouse brain lysate, displayed a slightly lower faint signal at ~90 kDa (arrowhead). In fact, the anti-PRG2 antibody revealed a double band in PRG2-Flag HEK293T cell lysate. We presume that the upper band corresponds to PRG2-Flag. However, the lower band is likely to reflect unspecific binding, as the size difference between the two bands is too large for the lower one to be endogenous PRG2. An additional unspecific signal was detected at 120 kDa in E17.5 mouse brain lysate. Taken together, the clear identification of PRG2 by this commercially available antibody in western blot analysis was impeded by the recognition of various unspecific bands. Similar experiments, performed with the PRG2 antibody from Chemicon, also revealed unspecific western blot bands in all samples tested (data not shown).

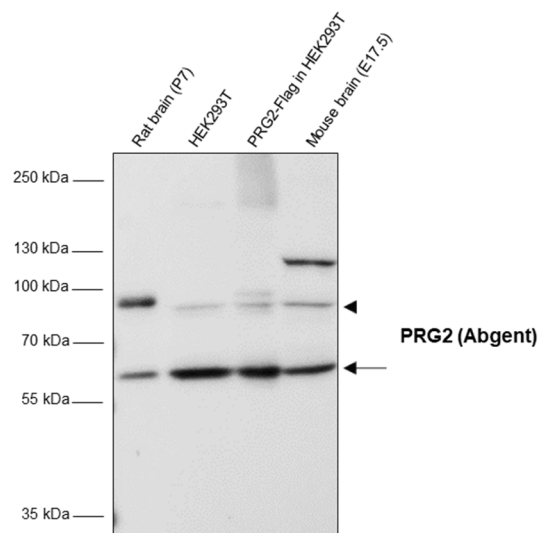


Figure 8: Examination of anti-PRG2 antibody (Abgent) specificity.

Brain lysate from different developmental stages of rat (P1) and mouse (E17.5), non-transfected HEK 293T cells and PRG2-Flag transfected HEK293T cells, were probed with anti-PRG2 antibody (Abgent) in western blotting for antibody specificity. Detection of PRG2 expression reveals multiple bands in all samples tested (arrows).

3.1.2 Generation of PRG2 antibodies

Based on the data obtained in 3.1.1, we decided to generate a custom-made PRG2 antibody. In general, before raising an antibody, decisions have to be made about whether to generate a polyclonal or a monoclonal antibody. Polyclonal antibodies are produced by the injection of a peptide antigen into an animal, such as rabbit, mouse or goat. Following immune response, B-cells become activated and produce a heterogeneous collection of antibodies specific to multiple epitops on an antigen. Each antibody recognises a unique epitope located on the same antigen. After immunization, the serum therefore contains a large number of antibodies with different specificities and affinities to the antigen. The production of monoclonal antibodies also requires the injection of an antigen. After immunization, B-lymphocytes are harvested from the animal's spleen and are fused to a myeloma cell line. This creates immortalized B cell-myeloma hybridomas, that are able to grow in culture while producing antibodies. In contrast to polyclonal antibodies, monoclonal antibodies are specific to only one epitope on the antigen, because they derived from a single B-cell. The production of monoclonal antibodies is more time-consuming and much more expensive than the procedure of polyclonal antibody generation. For these reasons, we decided to raise a polyclonal PRG2 antibody.

Two polyclonal anti-sera were generated. Whereas one serum was raised against an epitope in the extracellular domain (between transmembrane domain (TM) 3 and TM 4) of PRG2, the other serum was raised against the most distal part of the PRG2 intracellular C-terminal tail (as depicted in light green and dark green in Figure 9 and listed in Table10). A schematic presentation of the PRG2 amino acid sequence is shown in Figure 9. For each epitope two animals were injected. In total, four samples of the pre-immune serum (PPI, before injection) and the final bleed (SAB) were obtained.

```
MLAMKEKNKTPKDSMTLLPCFYFVELPIVASSIVSLYFLELTDLFKPAKVGFQCYDRALSMPYVETNEELIPLLMLLSLAFAAPA
ASIMVGEQMVYCLQSRLWGRGPGGVEGSINAGGCNFSNLRRTVRFVGVHVFGLCATALVTDVIQLATGYHTPFLLTVCKPN
YTLTGTSCEENPYITDICSGHDTAILSARKTFPSQHATLSAFAAVYVSMYFNAVISDTTKLLKPILVFAFAIAAGVCGLTQITQY
RSHVPDYYAGFLIGAGIAAYLACHAVGNFQAPPAEKVPTPAPAKDALRALTRQGHESMYQQNKSVSTDELGPPGRLEGVPRP
VAREKTSLGSLKRASVDVLLAPRSPMGKEGMVTFSENTLPRVSTPSLDDPARRHMTIHVPLDASRSRQLIGEWKQKSLEGRG
LGLPDEASPVHLRAPAEQVAEEEEEEEEEEEEEEEEEEEEGPVPPSLYPTVQARPLGPRVILPPRPGPQLVHIPEEGVQA
GAGLSPKSSSSSVRAKWLSMAEKGPPVAVAPSQPRVANPPRLQVIAMSKAAGGPKAETASSSSASSDSSQYRSPSDRD
SASIVTIDAHAPHPVHLSAGSTPWEWKAKVVEGEGSYELGDLARGFRSSCKQPGMGPGSPVSDVDQEEPRFGAVATVNL
ATGEGLPVPPGASEGALGAGSRESTRLRQVGGLAEREVEAAESYRRMQARRYQD
```

Figure 9: Mouse PRG2 amino acid sequence.

Blue: Transmembrane domains, Red: Poly-E-box, Light Gray: Cytosolic C-terminal tail, Light Green: Extracellular epitope B (SAB71/72), Dark Green: Intracellular epitope A(SAB69/70)

Table 10:Peptides injected in rabbits to raise the PRG2 antibodies

Peptide	Peptide sequence	Epitope	Serum (SAB)
A	H-CAE SYY RRM QAR RYQ D-NH2	Intracellular, end of C-terminus	SAB 69, SAB 70
B	H-CTL LGT SCE SNP YIT Q-NH2	Extracellular, between TM3 and TM4	SAB 71, SAB 72

Prior to antibody purification, the final bleed was examined by western blot analysis in order to identify the serum with the strongest affinity to PRG2 (Figure 10). Lysates previously used in Figure 8, were run on SDS-PAGE and membranes were probed with all four sera (SAB 69, 70, 71, 72) and PPI of two animals. The PPI membrane shows the background detection profile of serum. By comparing blots probed with SAB 69 (Figure 10I) and SAB 70 (Figure 10I') with the membrane of PPI 1 (Figure 10I''), samples of P1 rat brain lysate and HEK293T cells overexpressing PRG2-Flag exhibit a strong western blot signal at the molecular size of 90 kDa, suggesting that this band resembles PRG2 expression. In contrast, the comparison of SAB 71 (Figure 10II) and SAB 72 (Figure 10II') with PPI 2 (Figure 10II'') did not display an additional western blot band in the rat brain and the PRG2-Flag transfected HEK293T cell lysate.

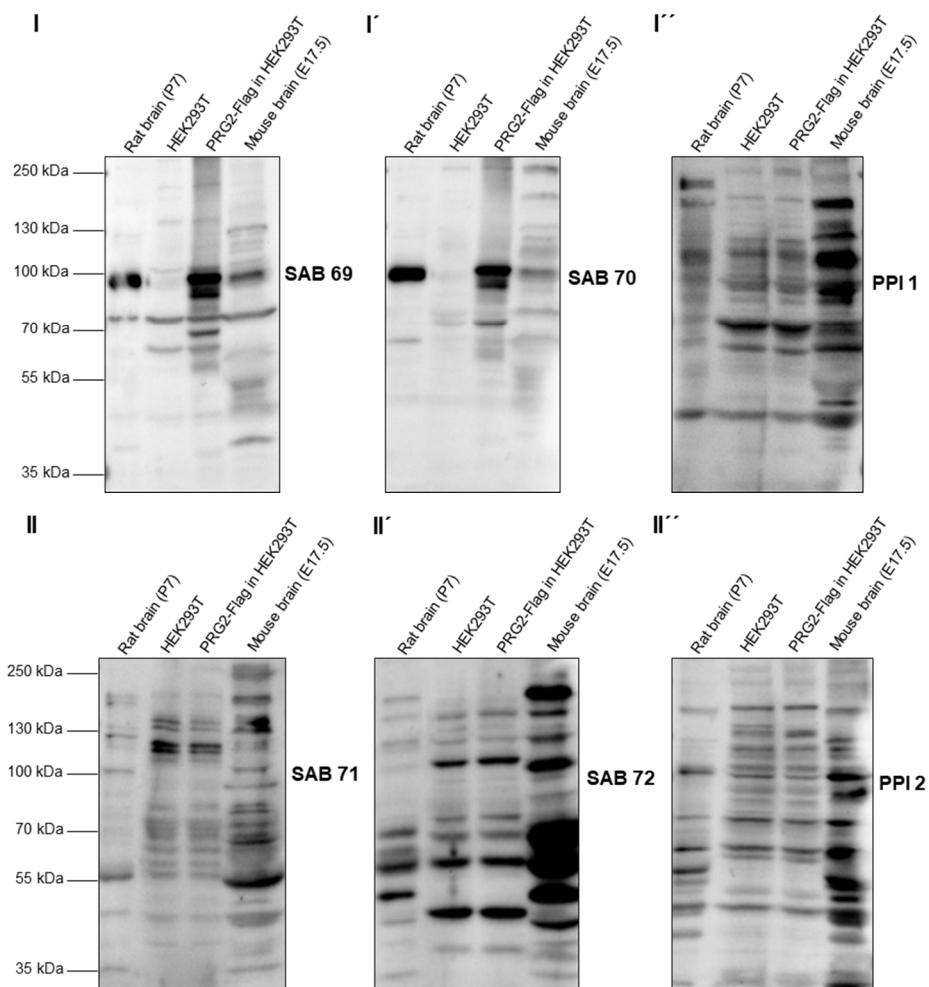


Figure 10: Generation of a custom-made PRG2 antibody.

Examination of anti-sera and pre-immune serum to identify serum with highest PRG2 affinity. Western blot analysis was performed with lysates described earlier (see Figure 8). I: Serum 69, I': Serum 70 (intracellular epitope), I'': Pre-immune serum 1, II: Serum 71, II': Serum 72 (extracellular epitope), II'': Pre-immune serum 2. Sera and PPIs were diluted 1:1000 in blocking solution. SAB 69 and SAB 70 sera detect a protein with the correct molecular size of PRG2.

In summary, results reveal strong detection of a band with a molecular weight resembling the weight of PRG2 using serum 69 and 70. When compared to serum 69, serum 70 displayed less background labelling and was therefore chosen for further antibody purification using the SulfoLink® Immobilization Kit for Peptides. Affinity purification was undertaken as described in Material and Methods (2.2.3.5). The antibody elution fractions with highest protein concentrations were tested by western blot analysis using the previously described lysates (see Figure 8 and Figure 10). Membranes probed with Elution 1 and Elution 2 show less background signal when compared to blots with non-purified serum and detect a prominent single band in the P1 rat brain lysate sample (Figure 11). Elutions tested in Figure 11 were pooled and stored at -20°C until further use and the specificity of the antibody was investigated by biochemical and immunocytochemical approaches.

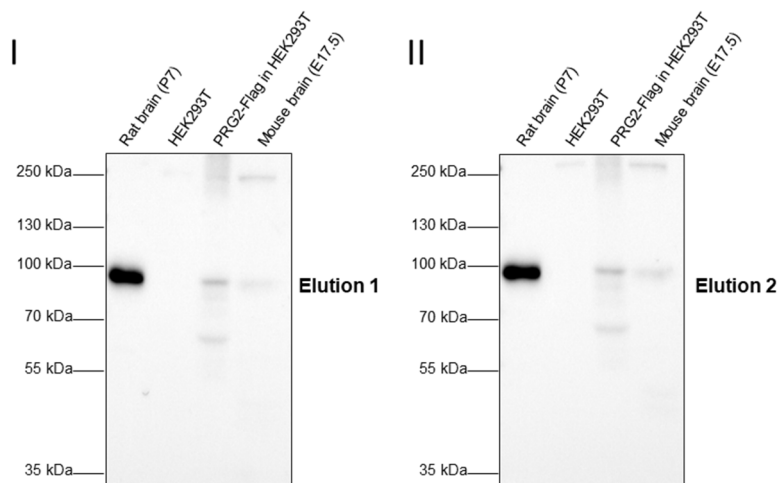


Figure 11: SAB 70 after antibody purification.

Testing two elutions after antibody purification by Western Blot. I: Elution 1, II: Elution 2. Both elutions tested display a high affinity to PRG2.

3.1.3 Validation of the custom-made PRG2 antibody

In order to test if the newly generated PRG2 antibody is specific, a siRNA targeting PRG2 was purchased from Thermo Scientific. The siRNA consists of a pool of four individual siRNA sequences targeting PRG2. Sequences are indicated in Material and Methods (2.1.8). For control conditions, the non-targeting siRNA pool from Thermo Fisher was used. HEK293T cells were triple-transfected with GFP, PRG2-Flag and increasing amounts of siPRG2 or non-targeting siRNA. After two days of incubation, cell lysates were analysed by western blotting. Membranes probed with anti-Flag and anti-PRG2 antibody demonstrated a dose-dependent reduction in PRG2 abundance in siRNA-mediated knock down conditions. In addition, endogenous PRG2 was not detected with the PRG2 antibody (Figure 12).

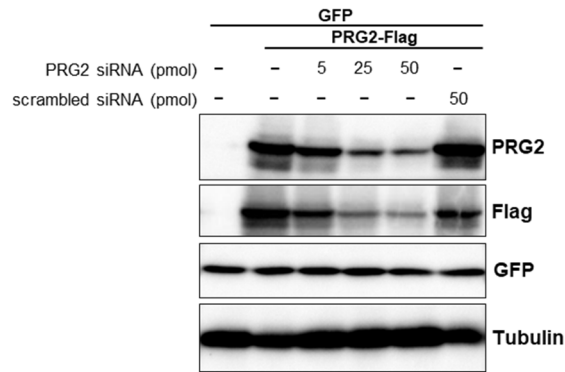


Figure 12: Characterization of the custom-made PRG2 antibody

PRG2-Flag (and control GFP) was expressed in HEK293T cells in the presence of PRG2 siRNA or non-targeting siRNA, as indicated. Cells were lysed two days after transfection and lysates were probed in western blotting with indicated antibodies. Custom-made anti-PRG2 antibody shows reduction of PRG2 in siPRG2 treated samples.

The specificity of the antibody was additionally assessed by immunocytochemistry. In these experiments, we used N1E-115 cells, an adrenergic cell line derived from mouse neuroblastoma tissue. N1E-115 cells express general neuronal markers, such as the neuronal tubulin antigen recognised by the Tuj-1 antibody, but do not express members of the PRG family (data not shown). Here, PRG1-Flag and PRG2-Flag plasmids were expressed in N1E-115 neuroblastoma cells. 24 h post-transfection cells were fixed and stained with anti-Flag and anti-PRG2 antibody. Counter-staining of the nucleus and F-actin was achieved through the application of Hoechst and Phalloidin, respectively (Figure 13). Cells expressing PRG2-Flag displayed a co-labelling of Flag and PRG2. In contrast, non-transfected cells observed in the same confocal image, did not reveal PRG2 antibody staining (Figure 13A). This indicates that the newly generated antibody specifically detects PRG2 in PRG2-expressing cells. To further confirm specificity of the obtained PRG2 signal, we tested the antibody in cells expressing the closely related family member PRG1. The results demonstrate that the anti-PRG2-antibody failed to detect in PRG1-Flag expressing cells (Figure 13B). Taken together, the biochemical data generated from siRNA-mediated PRG2 knockdown cell lysate and overexpression experiments of PRG2 in N1E-115 cells validate the custom-made anti-PRG2 antibody in detecting PRG2 and establishes the antibody as a novel tool to further investigate PRG2 localisation and function.

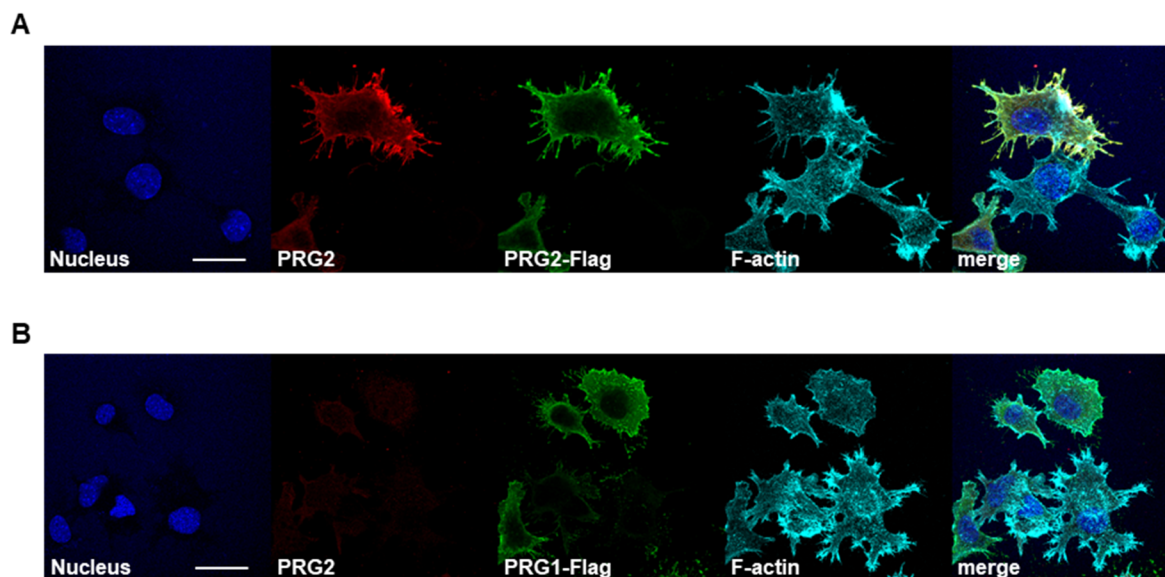


Figure 13: Specificity of custom-made PRG2-antibody

PRG2-Flag (A) and PRG1-Flag (B) were expressed in N1E-115 cells. 24 h after transfection cells were fixed and stained with purified anti-PRG2 and anti-Flag antibody. Additionally, Hoechst and Phalloidin were used for counterstaining. A: Anti-PRG2 and anti-Flag show same staining pattern. B: Purified PRG2 antibody does not detect PRG1-Flag. Scale bar: 20 μ m

3.2 PRG2 exists in a higher order complex

A common feature associated with transmembrane proteins, possessing multiple membrane domains, is the possible role of aggregation and oligomerisation in the cell membrane, providing functional implications in the transduction of signalling events and resulting cellular responses. For example, dimerization or oligomerization between 7-transmembrane GPCRs is recognised to modulate pharmacological characteristics of the receptors and influence their coupling to G proteins (Rivero-Müller et al., 2013; Gahbauer and Böckmann, 2016). Similarly, transient receptor potential (TRP) proteins, which are 6-transmembrane ion channels assemble in homo- and heterotetrameric complexes to enhance ion permeation property (Hellwig, 2005; Schindl and Romanin, 2007). Considering its overall domain organisation into 6 transmembrane domains, we examined whether PRG2 could form higher order complexes.

3.2.1 PRG2 forms homodimers in primary cortical neurons

In order to test PRG2 multimerization, we cultured wild type mouse primary cortical neurons for 9 days and lysed cells in non-reducing conditions. The total cell lysate was either mixed with loading buffer containing or lacking SDS. Samples without SDS were incubated at different temperatures ranging from 90 $^{\circ}$ C to 20 $^{\circ}$ C to preserve the native protein state in low temperature conditions. The SDS condition was boiled at 90 $^{\circ}$ C. All probes were loaded on a 8% SDS-PAGE and PRG2 expression was detected by western blotting using the custom-made anti-PRG2 antibody. Figure 14 shows the appearance of a second PRG2 band at a molecular weight of \sim 250 kDa in non-reducing, low temperature conditions. This clearly

suggests that in addition to its monomeric form, PRG2 exists also as a higher order protein complex in primary neurons. Considering the molecular weight of PRG2 being 90 kDa and the molecular weight of the second PRG2 form, we propose the complex detected in these experiments might be a PRG2 dimer or trimer.

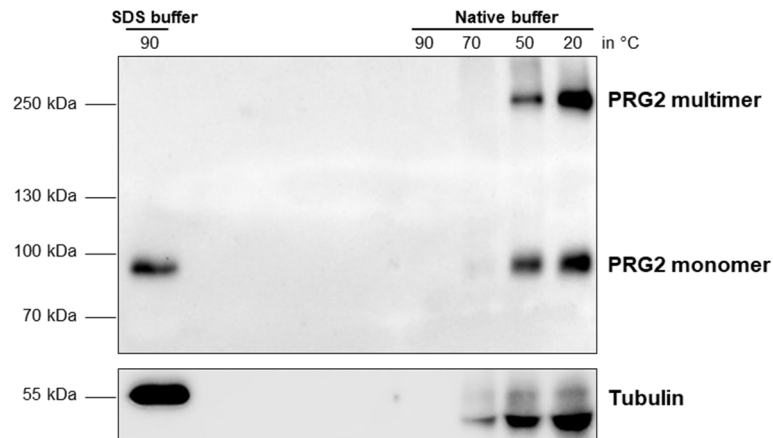


Figure 14: Complex formation of PRG2 *in vitro*.

Mouse primary cortical neurons were cultured for 9 days and lysed under non-reducing conditions. 1/5 of total lysate was incubated with loading buffer containing SDS (4x Roti load) and boiled for 3min at 95°C. Rest of lysate was mixed with loading buffer lacking SDS (4x Roti load 3(LDS)) and heated at indicated temperature for 3 min. Samples were loaded on 8% SDS-PAGE with subsequent Western Blotting using anti PRG2-antibody and Tubulin. Endogenous PRG2 exists in a higher order form.

3.2.2 The interaction of PRG2 monomers is independent of the intracellular C-terminus of PRG2

A different experimental paradigm to analyse multimerization was used to confirm interaction. Here, we expressed differentially tagged PRG2 proteins (PRG2-Flag and PRG2-YFP) and carried out co-immunoprecipitation experiments in cell lines deficient in PRG2 expression. We generated C-terminal deletion mutants of PRG2, whereas PRG2DC_a lacks the C-terminus from the poly-E-box onwards, and the entire C-terminus was depleted in PRG2DC_b. A schematic of full-length PRG2 and the deletion mutants is shown in Figure 15A. N1E-115 cells were transiently transfected with indicated constructs. Following co-transfection of differentially tagged PRG2 variants, we performed immunoprecipitation of PRG2-Flag from cell lysate (Figure 15B+C). Subsequently, western blot analysis of total cell lysate and immunoprecipitated samples, probed with anti-Flag and anti-GFP antibodies, was performed. Results demonstrate PRG2 interaction of full length PRG2-Flag and full length PRG2-YFP. Similarly, PRG2DC_a-YFP and PRG2DC_b-YFP binds to immunoprecipitated full length PRG2-Flag (Figure 15B+C). In addition to this, PRG2DC_a-YFP also co-immunoprecipitated with PRG2DC_a- Flag (Figure 15C). This indicates that the interaction of PRG2 monomers is not dependent on the C-terminal and raises the exciting possibility that PRG2 dimerization/oligomerization can occur as a result of interactions between the transmembrane sections of the proteins.

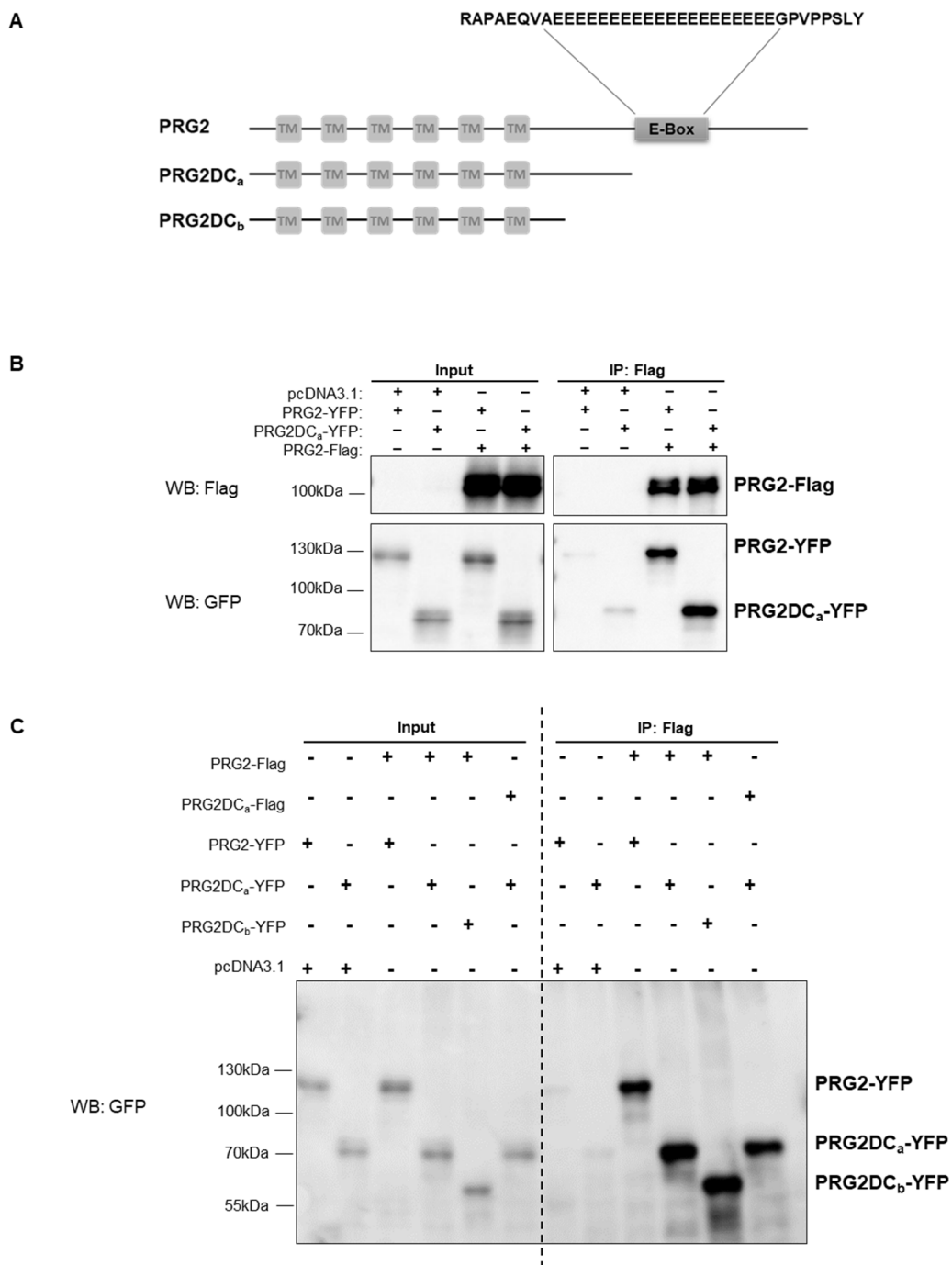


Figure 15: PRG2 dimerizes independent of its poly-E-box.

A) Schematic of PRG2 full length (top) and PRG2 Δ C mutant (bottom) lacking the poly-E-box. B+C) N1E-115 cells were co-transfected with PRG2-Flag (or control vector) and PRG2/PRG2DC_a/PRG2DC_b-YFP. Cells were lysed after 24 h. PRG2-Flag was immunoprecipitated using Flag M2 affinity gel. Subsequently, Western Blot was performed and membranes were probed with anti-GFP and anti-Flag antibody. PRG2 homodimerization occurs independent of the intracellular C-terminal tail.

3.2.3 PRG2 interaction with other PRG family members

In the previous section we identified the formation of PRG2 homomeric complexes. We further were interested, if PRG2 forms heteromeric protein complexes with other PRG family members. Therefore, we co-expressed PRG3-GFP (or control) with PRG2-Flag (or control)

(Figure 16A) as well as PRG2-YFP (or control) with PRG5-Flag (or control) (Figure 16B) in N1E-115 cells for one day and immunoprecipitated PRG2-Flag and PRG5-Flag, respectively from the cell lysate with Flag M2 Affinity Gel. Western blot analysis of total cell lysate and immunoprecipitated samples using anti-Flag and anti-GFP antibodies identified protein complexes consisting of PRG2-Flag and PRG3-GFP as well as of PRG2-YFP and PRG5-Flag (Figure 16). Results show that PRG2 forms heterologous protein complex with its family members. However, the function of PRG complex formation remains elusive.

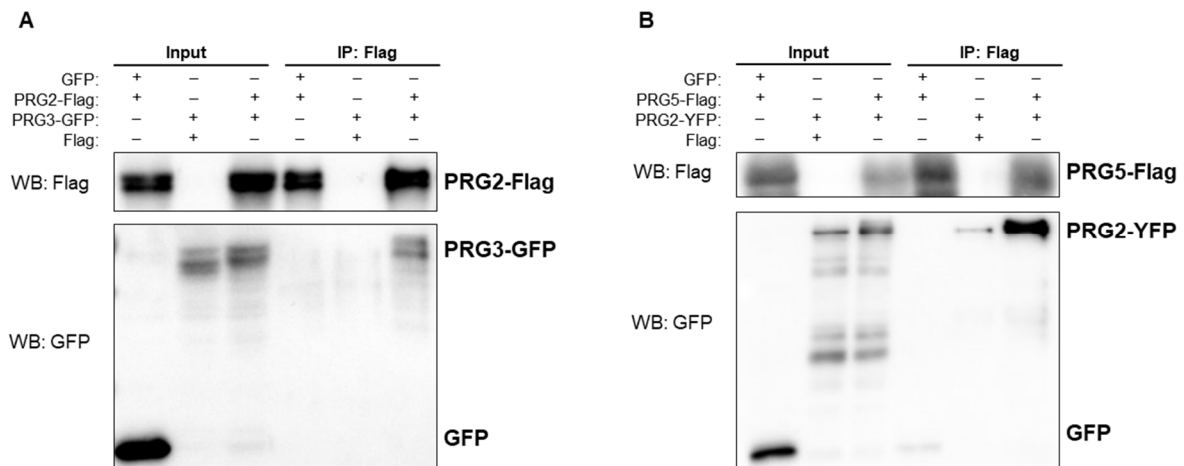


Figure 16: PRG2 binds to other members of the PRG family.

Transfection of YFP- and Flag-tagged plasmids was performed in N1E-115 cells. 1d after transfection cells were harvested and PRG2-Flag (A) and PRG5-Flag (B) were immunoprecipitated from protein lysate. Co-immunoprecipitation was detected in Western Blot using indicated antibodies. PRG2 interacts with PRG3 (A) and PRG5 (B).

Summarizing, PRG2 forms higher order complexes of PRG2 monomers independent of the intracellular poly-E-box of PRG2. PRG2 is further capable of generating heterologous PRG2 complexes with its family members PRG3 and PRG5. Based on this data, we started a collaboration with the AG Scheerer/Spahn (Charité, Berlin) to identify these complexes and to elucidate the crystal structure of PRG2. So far, data indicated the existence of a tetrameric and/or hexameric constitution of PRG2 homomers.

3.3 Temporal and spatial expression of PRG2

3.3.1 PRG2 is a developmentally regulated protein

PRGs are mainly expressed in brain tissue and have been described to undergo a differentially regulated expression pattern during neuronal development. Biochemical data demonstrate, that PRG3 expression starts during early embryonic development and declines postnatally. In contrast, PRG1 expression is restricted to postnatal stages (Velmans et al., 2013; Bräuer et al., 2003). In order to elucidate the developmental profile of PRG2 expression during brain development, we performed western blot analysis from rat brain lysate collected at different

time points during embryonic development (E13-E19) and at postnatal stages (P1-W40). The results demonstrate a highly dynamically regulated expression pattern of the PRG2 protein during neuronal development (Figure 17A). PRG2 levels were hardly detected at E13, but gradually increased until P1 and declined postnatally. In comparison, the expression of the family member PRG1 starts later in development when compared to PRG2, and peaks at postnatal stages. Therefore, PRG2 expression coincides with the early phases of brain development, which are characterised by neuronal migration and axon guidance, whilst expression of PRG1 overlaps with synaptogenesis.

In order to obtain further detailed information of PRG2 expression during neuronal development, and, more importantly, during the different stages of the neuronal maturation program, we generated protein lysates from primary cortical neuronal cultures that were cultured to different stages in neuronal development between DIV3 and DIV21. Figure 17B displays western blot analysis of neuronal lysates, which exhibits a gradual increase of PRG2 expression during early stages of neuronal development. We found that PRG2 expression peaks at around DIV7-DIV9, followed by attenuation of expression from DIV16 onwards. Neurons cultured *in vitro* go through a well defined maturation program (Dotti et al., 1988), in which immature neurons with less protrusive activity (DIV0) develop into highly arborized neurons harbouring dendritic spines (DIV20). Our expression analysis identifies that PRG2 expression correlates with the phase of neuronal outgrowth concomitant with the formation of axon and denritic branches (DIV7-DIV9). At the same time, the protein expression of PTEN, a major regulator of neuronal cell growth remains constant throughout neuronal maturation (see Figure 17A and B), indicating that PTEN expression is not developmentally regulated.

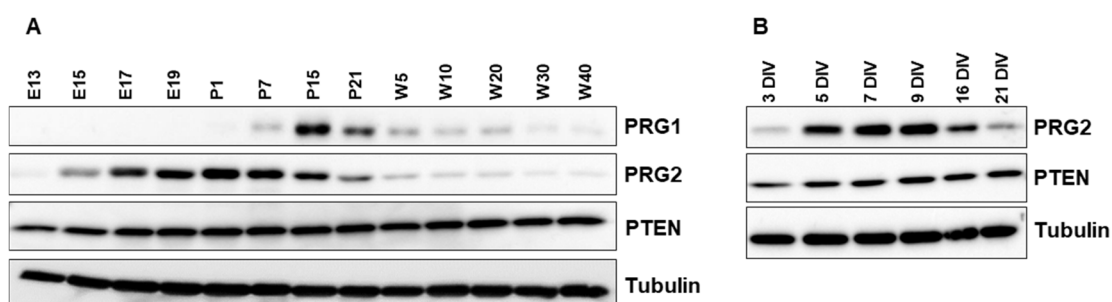


Figure 17: Developmental expression profile of PRG2 in brain and cortical neuronal lysate.

A) Rat brain homogenates from different developmental (E13-E19) and postnatal (P1-W40) stages were generated and analysed by western blotting. B) Cultured primary cortical neurons were harvested at specified time points (DIV3-DIV21) and lysates were probed with indicated antibodies by western blotting. PRG2 shows a well-defined expression pattern in particular phases of brain development and during the maturation primary cortical neurons.

3.3.2 PRG2 distribution in cell lines and in primary hippocampal neurons

3.3.2.1 Expression of PRG2 in N1E-115 cells

To date, data describing the subcellular distribution of PRG2 are missing. We started to address that question by a gain-of-function approach in N1E-115 cells. For that purpose, PRG2-Flag was transiently transfected for 48 h in the neuroblastoma cell line N1E-115. Following, fixation and staining with Hoechst, Phalloidin and anti-Flag antibody was performed. Transfected cells were identified by Flag-labelling. Counterstaining with the F-actin marker, Phalloidin, reveals localisation of PRG2 in the actin rich filopodia (arrows) of the cells. PRG2 was also occasionally enriched at the tip of the filopodium (arrowheads) (Figure 18). In line with this finding, previous studies overexpressing PRGs in different cell models demonstrate a localisation of the PRG family members, PRG3 and PRG5, in filopodial structures (Sigal et al., 2007; Brogini et al., 2010). Taken together, exogenous PRG2, similar to PRG3 and PRG5 locates to the F-actin rich filopodial protrusions of a cell.

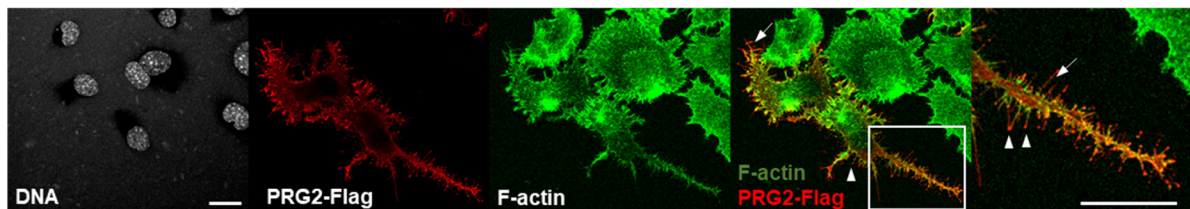


Figure 18: Exogenous PRG2 localises to filopodia in N1E-115 cells.

PRG2-Flag was transiently expressed in N1E-115 cells for 48 h, fixed and stained with anti-Flag antibody, Phalloidin and Hoechst. Overexpression of PRG2-Flag in N1E-115 cells leads to accumulation of PRG2 in filopodial processes (arrows) and to occasional enrichment of PRG2 at the tip of these filopodia (arrowheads). Scale bar: 20 μ m

3.3.2.2 Subcellular localisation of PRG2 in primary hippocampal neurons

Next, we set out to investigate the subcellular distribution of endogenous PRG2 in primary hippocampal neurons. Based on our data presented in 3.3.1 (Figure 17B), which identified highest PRG2 expression around DIV7 and DIV9 in primary neuronal cultures, we assessed PRG2 localisation during this period in neuronal development. Primary hippocampal neurons were immunolabeled with the custom-made anti-PRG2 antibody. Additionally, counterstaining with the axonal and dendritic markers, anti-Tau1 and anti-MAP2 antibody, was performed. Confocal images, displayed in Figure 19, revealed high anti-PRG2 signals at the plasma membrane of Tau positive axons (Figure 19A), but not at the membrane of MAP2-positive neurites. This finding is confirmed by the quantification of PRG2 plasma membrane enrichment in axons and dendrites. Figure 19C shows a significant discrepancy between both compartments, in which PRG2 is distributed along the membrane in 90% of axons, and is only enriched in the membrane in 20% of dendrites analysed. In addition to that, PRG2 localisation seemed to be a sequential organisation of PRG2 clusters with little spacings along the axonal

plasma membrane. This striking distribution of PRG2-dense puncta along the membrane encouraged us to examine PRG2 localisation exploiting super resolution microscopy.

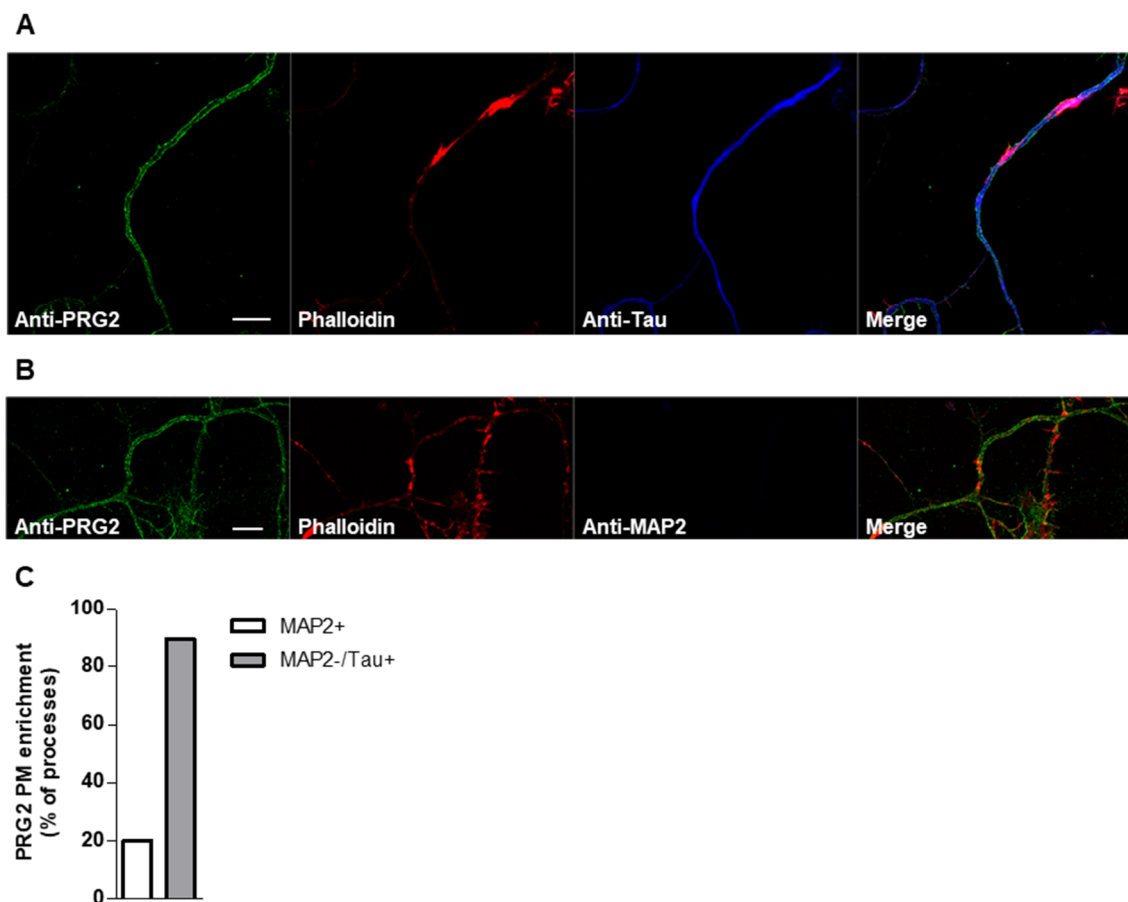


Figure 19: Subcellular distribution of PRG2 in primary hippocampal neurons.

Primary hippocampal neurons were cultured until DIV9 and subsequently fixed and stained with anti-PRG2 antibody, Phalloidin, Hoechst and either anti-Tau1 (Figure 19A) or anti-Map2 (Figure 19B) antibody. Counterstaining using axonal (Tau1) and dendritic (MAP2) markers reveals a strong plasma membrane enrichment of PRG2 in Tau1 positive processes. Scale bar: 10 μ m. Quantification of PRG2 plasma membrane (PM) enrichment of MAP2+ (dendritic) and MAP2-/Tau+ (axonal) processes.

3.3.2.3 Super resolution microscopy unravels periodic distribution of PRG2 at the axonal plasma membrane

In recent years, new technologies in microscopy have extended the optical resolution limit of standard confocal microscopy, allowing a detailed acquisition of, for example, the subcellular distribution, the interaction and the dynamic reorganization of proteins. Structured Illumination Microscopy, SIM, as a technique of high resolution microscopy, creates a 2-fold gain in resolution compared to conventional methods and thereby enables a x-y resolution of 100-130 nm (Schermele et al., 2010). SIM is based on the illumination of the sample with periodic light patterns leading to the Moiré effect. The effect is caused by the superposition of two patterns with distinct frequencies that creates a third pattern, the Moiré pattern. In SIM, the

mathematical reconstruction of up to 15 patterns of excitation per slice leads to the generation of a high-resolution image (Letierrier, Dubey, and Roy, 2017; Schermelleh et al., 2010).

To obtain a detailed insight into the subcellular distribution of PRG2 in primary neurons we collaborated with Dr. Jan Schmoranzler and Dr. Niclas Gimber (AMBIO, Charité; SFB958). We captured SIM images of hippocampal neurons that were cultured for 9DIV and labelled cells with anti-PRG2 and anti-Tau1 (axon marker) antibody. PRG2 appeared to localise in a periodic punctate pattern along the axonal plasma membrane (Figure 20A and B). The continuous arrangement of PRG2 dots was quantified using the measurement point tool of the Imaris software. A frequency analysis, plotting the occurrence of the measured distances between two consecutive PRG2 spots is depicted in Figure 20C. The diagram demonstrates the existence of different spacings between PRG2 molecules. However, the most frequent occurred spacing in between two PRG2 spots is 260 nm. Other highly abundant PRG2 distances are 220 nm, 240 nm and 300 nm. In combination with the 260 nm value, these distances display the majority of measured distances of consecutive PRG2 spots. This indicates that spacings from 220 to 280 nm between two PRG2 puncta are the most frequent one, whereas longer or shorter distances were less frequently observed. In summary, these findings show a periodically organised appearance of PRG2 along the axonal plasma membrane and raised the question of how this distribution is coordinated.

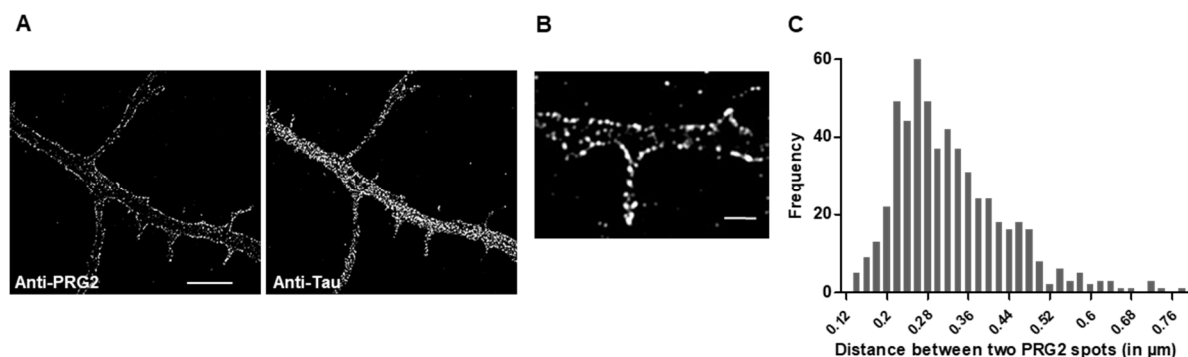


Figure 20: Super resolution microscopy (SIM) of PRG2.

Hippocampal neurons (DIV9) were fixed and stained with anti-Tau1 and anti-PRG2 antibody. Z-stacks were acquired using the SIM OMX V4 Blaze system. A) Representative central single section of a stack. Scale bar: 5µm. B) Specimen image of higher magnification reveals a highly periodic appearance of PRG2 at the axonal plasma membrane. Scale bar: 1µm. C) Analysis of PRG2 periodicity. Distance between PRG2 dots at the axonal plasma membrane were measured and quantified using Imaris/Fiji. Most abundant distance between two PRG2 spots is 0,26 µm.

3.3.3 PRG2 localisation is maintained by the actin cytoskeleton.

The actin cytoskeleton in the axon shaft of neurons has recently gained attention by the investigation of a periodic, circumferential and lattice-like F-actin structure underneath the plasma membrane (Roy, 2016). Uncovered by super resolution microscopy, the now called actin rings are cytoskeletal structures spaced by ~190 nm (Xu et al., 2013). Providing a

supporting architecture for the axon, the actin rings function as a mechanical scaffold, but can also assist in the periodic arrangement of membrane proteins. (Xu et al., 2013). Recent work supports this assumption. Data showed that membrane protein motility in the axon initial segment (AIS) is restricted to a repetitive pattern of ~190 nm spaced segments, which alternates with the periodic lattice of actin rings, indicating that the actin/spectrin structure functions as a mechanistic barrier modulating lateral diffusion along the axon (Albrecht et al., 2016).

Considering the periodic organisation of PRG2 along the axonal membrane, we first analysed the possibility that axonal PRG2 clusters follow the periodic arrangement of axonal F-actin rings. We performed SIM on cultured hippocampal neurons stained with Phalloidin, anti-PRG2 and anti-Tau1 (not shown) antibody. Sections of a z-stack are displayed in Figure 21. Images show the periodic appearance of actin rings (green) labelled through Phalloidin. Sequential PRG2 puncta, shown in red, localised along the plasma membrane. The merged image revealed that PRG2 partially localises at the exact position of an actin ring (arrow), suggesting that actin rings may mediate the localisation of PRG2 within the membrane by, for example tethering to actin structures. However, PRG2 was also present in between two consecutive actin rings (arrowhead), demonstrating that arrangement of PRG2 is not restricted to actin rings. In summary, the partial, but not exclusive co-localisation of PRG2 with the F-actin ring structures suggests that PRG2 distribution does not follow the periodic profile of actin rings, indicating that anchoring of PRG2 exclusively to actin rings is unlikely.

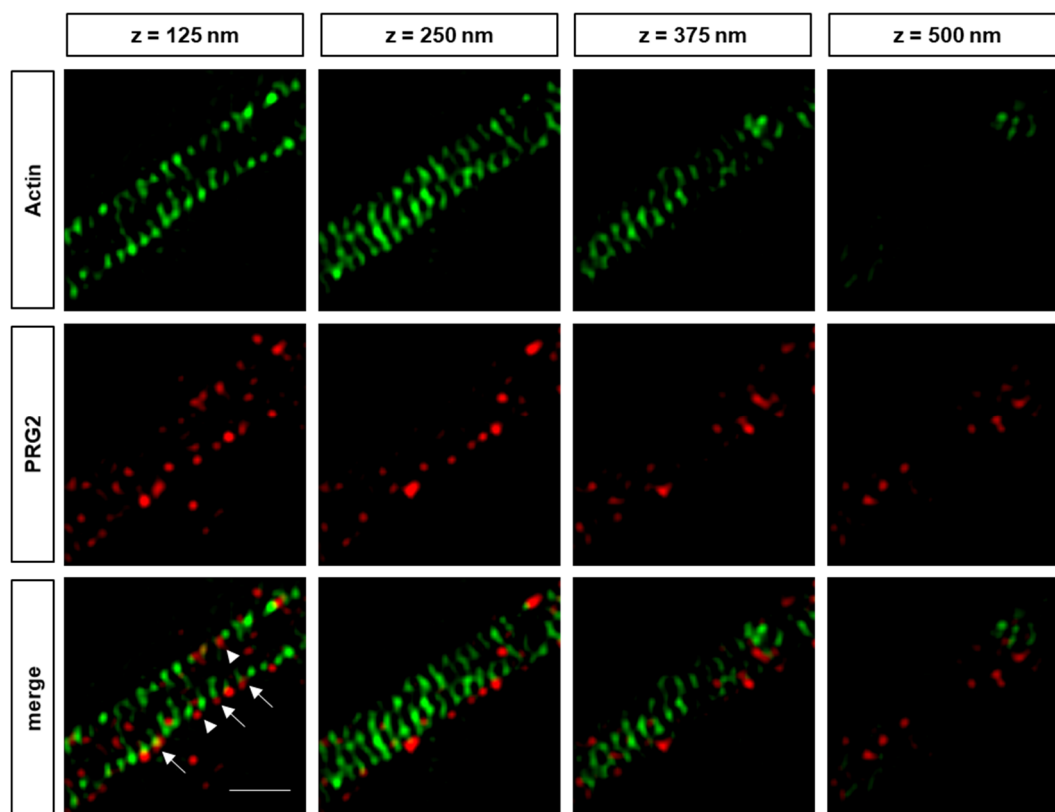


Figure 21: PRG2 partially localises to axonal actin rings.

DIV9 hippocampal neurons were stained with Phalloidin, anti-PRG2 and anti-Tau1 (not shown) antibody. Phalloidin staining allowed visualisation of actin rings in the neuronal axon. PRG2 occasionally localises with the axonal rings at the plasma membrane. Scale bar: 1 μ m.

In order to determine if the actin cytoskeleton actively instructs the localisation of PRG2, we treated primary hippocampal neurons with an F-actin destabilising drug (Latrunculin B) and assessed PRG2 distribution along the axonal plasma membrane. Figure 22 shows confocal images of neurons under control conditions as well as cells pre-treated with 5 μ M Latrunculin B for 1 h and 3 h. Both treatment conditions exhibited a decrease in F-actin structures compared to control but preserved normal morphology of the cells.

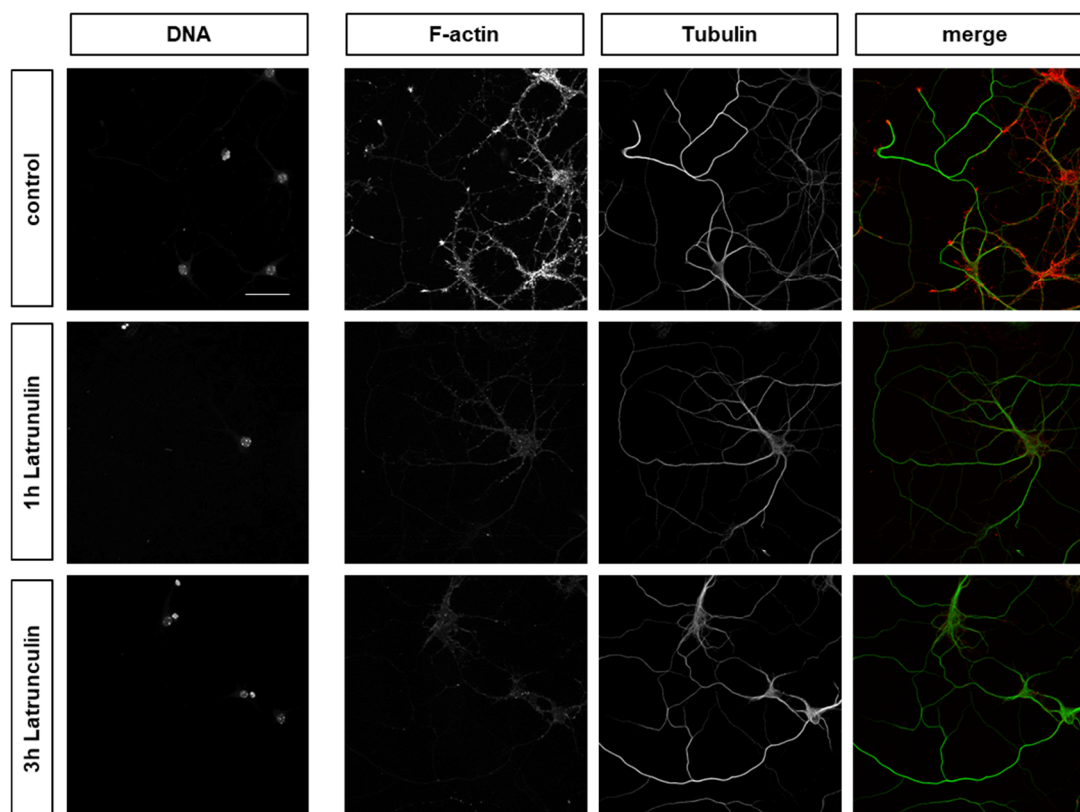


Figure 22: Normal morphology of hippocampal neurons following Latrunculin B treatment.

Confocal images of neurons treated with Latrunculin and stained with Hoechst, Phalloidin and anti- α -Tubulin antibody. Scale bar: 50 μ m. Latrunculin treatment does not alter normal neuronal morphology. Actin labelling is diminished in Latrunculin treated neurons.

SIM images of hippocampal neurons, pre-treated with 5 μ M Latrunculin for 1 h and for 3 h, were captured and analysed for PRG2 membrane enrichment and PRG2 periodicity (Figure 23). Representative images of all conditions are displayed in Figure 23A. Analysis of PRG2 membrane localisation shows that under control conditions ~70 % of analysed PRG2 puncta in the axon distributed in the plasma membrane (Figure 23B). This membrane enrichment was not affected after 1 h Latrunculin B treatment. After 3 h, Latrunculin B significantly reduced the PRG2 distribution at the axonal plasma membrane (Figure 23B).

A frequency plot of PRG2 spacings showed an aberrant spreading of frequencies in Latrunculin B treated neurons compared to control (Figure 23C). In control conditions, PRG2 distance measurements displayed a distinct appearance of most frequent spacings between two PRG2 puncta being 220 nm, 240 nm, 260 nm and 280 nm. The disruption of F-actin structures led to a decreased occurrence of these particular distances. Instead longer spacings, such as 440 nm and 560 nm as well as 700 nm, occurred more often compared to control.

Quantification of the mean distances in each treatment identified that actin disruption significantly increased the distance between two PRG2 puncta compared to control (Figure 23D). Taken together, the periodic distribution of PRG2 is vulnerable to F-actin disruption. PRG2 localisation along the membrane is preserved after 1 h treatment but collapses with 3 h

of actin inhibition. This indicates that the actin cytoskeleton is crucial for the periodic positioning of PRG2 and maintains its localisation at the axonal plasma membrane.

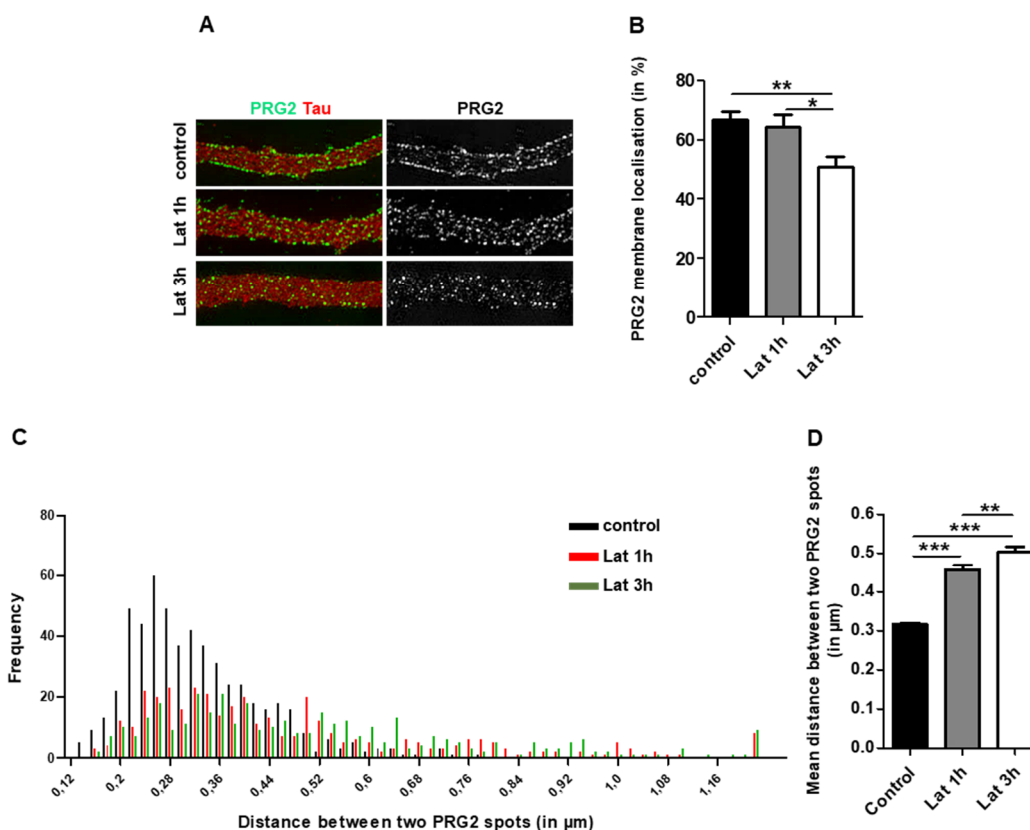


Figure 23: PRG2 periodic pattern is defined by the actin cytoskeleton.

Hippocampal neurons (DIV9) were treated with 5 μM Latrunculin for either 1h or 3h. After treatment cells were fixed and labelled with anti-PRG2 and anti-Tau1 antibody. SIM images were obtained as described previously. A) Exemplary images of indicated conditions. B) Data presents the ratio of PRG2 dots at the axonal plasma membrane to dots in the cytosol. Quantification shows a significant reduction of PRG2 membrane localization after treatment with Latrunculin for 3h. C) Frequency plot of PRG2 distances shows attenuation of the main PRG2 intervals after actin disruption by Latrunculin treatment. D) Mean distance between two PRG2 spots is significantly increased after treatment. B,C;D) n=9 axons per condition, at least 10 μm axon length per neuron were analysed. B,D) One way ANOVA with Bonferroni post hoc test was used to determine significance between various conditions. *p<0.05, **p<0.01, ***p<0.001. Data represent mean \pm SEM.

3.4 PRG2 binds to the lipid phosphatase PTEN

The lipid phosphatase PTEN directly antagonises the PI3K signalling pathway by dephosphorylating PI(3,4,5)P₃ to PI(4,5)P₂. As the major negative regulator of PI3K signalling, PTEN activity tightly controls PI3K/PI(3,4,5)P₃ dependent cellular responses (Kreis et al., 2014). Published data demonstrates that PTEN localisation, stability and enzymatic activity is highly controlled by its association to other proteins (Wu et al., 2000; Diepen et al., 2009; Song, Salmena, and Pandolfi, 2012). An unbiased mass spectrometry screen performed in the Eickholt laboratory identified PRG2 as a novel interaction partner of PTEN.

3.4.1 PRG2 interacts with PTEN

To verify the result of the mass spectrometry approach, the interaction of PRG2 and PTEN was examined using co-immunoprecipitation experiments. Therefore, HEK293T cells were co-transfected with GFP-PTEN (or control vector) and PRG2-Flag. Cell lysates were collected and PRG2-Flag was immunoprecipitated. Subsequent western blot analysis using anti-Flag and anti-GFP antibodies identified GFP-PTEN in complex with PRG2-Flag (Figure 24A).

The interaction was further confirmed at endogenous protein expression level in rat brain lysate (Figure 24B). For that purpose, both proteins, PTEN and PRG2, were immunoprecipitated individually from P1 rat brain lysate. In addition to a PRG2 immunoprecipitation with the custom-made anti-PRG2 antibody, a second PRG2 immunoprecipitation using the anti-PRG2 antibody from Chemicon (Chem) was conducted. Rat brain lysate (input) and immunoprecipitated samples were probed with the anti-PTEN and anti-PRG2 (custom-made) antibody by western blotting. Results showed a prominent interaction of the two proteins, when PTEN was immunoprecipitated from rat brain lysate. Although PRG2 was effectively pulled down from the lysate with both PRG2-antibodies, PRG2-PTEN interaction was not detected in these sample conditions. This might be due to sterical hinderance or masking of the interaction domain by the antibody prevented co-immunoprecipitation in this direction. Summarizing, the association of PRG2 and PTEN was validated by co-immunoprecipitation. Further experiments are required to specify structural requirements responsible for this interaction.

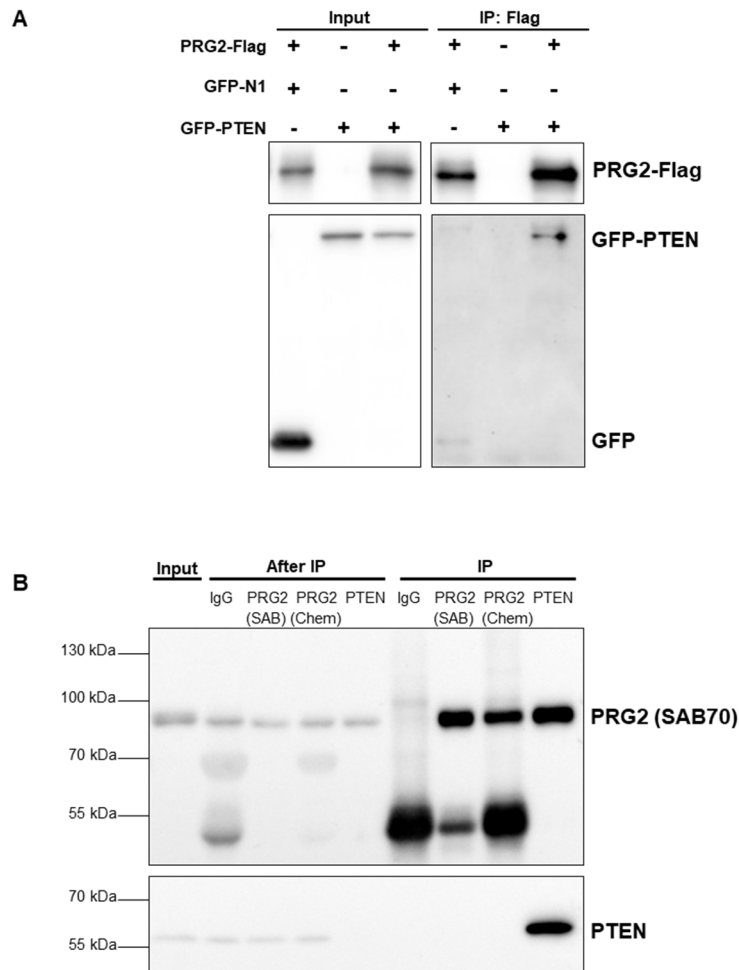


Figure 24: Verification of PRG2-PTEN interaction by immunoprecipitation.

A) Immunoprecipitation of exogenous protein. HEK293T cells were co-transfected with PRG2-Flag and GFP-PTEN (or control vector). 24 h post-transfection, cells were lysed in RIPA buffer and PRG2-Flag was immunoprecipitated from protein lysate. The lysate and immunoprecipitated samples were analysed by western blotting. PRG2-Flag was co-immunoprecipitated with GFP-PTEN. B) Endogenous immunoprecipitation of PRG2 and PTEN from rat brain lysate. Rat brain was homogenised in lysis buffer and immunoprecipitation was performed using anti-PRG2 (custom-made, SAB70), anti-PRG2 (Chemicon), anti-PTEN (SantaCruz) antibodies and rabbit IgG. Samples were analysed by western blotting using corresponding antibodies. Interaction was confirmed by PTEN immunoprecipitation and detection with anti-PRG2 antibody.

3.4.2 The PRG2 multimer binds PTEN

As described previously in chapter 3.2, PRG2 multimerizes in cortical neurons (see Figure 14). Therefore, we asked if the higher order form of PRG2 interacts with PTEN. To address this question, immunoprecipitation of PTEN from cortical lysate (DIV9) was combined with subsequent native elution. Elution was performed as published in Papa et al., 2014 and is described in material and methods (see 2.2.3.4.3). Each input and elution fraction of three replicates was split in half. One half was mixed with sample buffer containing SDS, the other one was incubated with sample buffer lacking the denaturing compound. Subsequently all samples were run on 8 % SDS-PAGE. Western blot analysis of non-native samples (Figure 25, bottom) revealed PTEN immunoprecipitation in three replicates tested. Non-native PTEN-

IP samples were probed with the anti-PRG2 antibody and showed a striking appearance of the PRG2 multimer at around 250 kDa (Figure 25, top). This finding suggests that PRG2 multimers are able to interact with PTEN and that this large protein complex may influence the formation of local phosphoinositide domains.

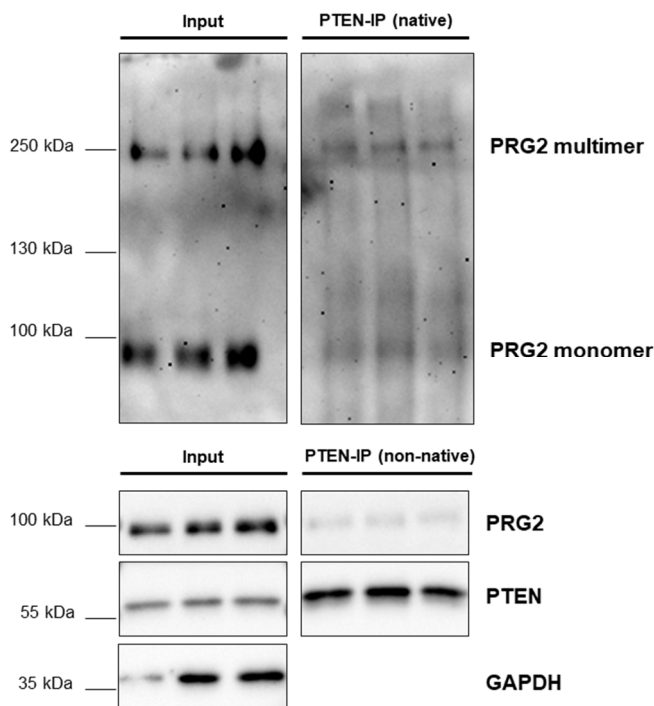


Figure 25: PRG2 binds as a multimer to PTEN.

DIV9 cortical neurons were lysed under non-reducing conditions. PTEN was immunoprecipitated from cortical lysates. Input and immunoprecipitated samples were split and were supplemented with loading buffer lacking SDS (top: PTEN-IP native) and buffer containing SDS (bottom: PTEN-IP non-native). Probes were investigated by SDS-PAGE (8%) and western blotting. The multimeric form of PRG2 interacts with PTEN.

3.5 Analysis of the PRG2-PTEN complex

3.5.1 PRG2 modulates PI(3,4,5)P₃ abundance through the inhibition of the PTEN phosphatase

Protein scaffolds spatially and temporally can regulate cellular signalling through confinement of signalling to specific compartments and/or by modulation of enzymatic activity (Chen et al., 2014). Kinases and phosphatases are highly regulated through association with other proteins thereby providing dynamic control of phosphorylation events and its associated downstream signalling targets (Antal and Newton, 2013). In order to test, if PTEN enzymatic activity is altered in association with PRG2, we, in collaboration with Dr. George Leondaritis, performed PTEN lipid phosphatase assays. Therefore, COS-7 cells were co-transfected with GFP-PTEN and control vector, or with GFP-PTEN and increasing concentrations of PRG2 (Figure 26A+B). PTEN was then immunoprecipitated from protein cell lysate and the release of phosphate product was measured in a standard Malachite Green based colorimetric assay (Maehama et

al., 2000) at indicated time points. The orthophosphate concentration was normalised to relative PTEN concentration immunoprecipitated.

Results, displayed in Figure 26A, showed that in contrast to control conditions (PTEN only), PRG2 co-expression decreased PTEN phosphatase activity in a dose dependent manner. Interestingly, experiments conducted with increasing concentrations of a truncated mutant of PRG2 (PRG2 Δ C_a, see Figure 15A), revealed that PTEN activity remains unaffected in the presence of this specific PRG2 variant lacking the PRG2 specific poly-E-box (Figure 26B). In order to directly compare PTEN activity in different treatments and to exclude the possibility of sample variation in PTEN abundance in different treatments, we normalised phosphate produced to the relative PTEN concentration immunoprecipitated. These results demonstrate that PRG2 can reduce PTEN activity to approximately 50% at the highest PRG2 concentration tested (Figure 26C). The specificity of this inhibition was further confirmed by assaying phosphatase release of the 5' phosphatase SHIP2 in the presence of PRG2. Here, PRG2 expression did not affect the amount of SHIP2 produced phosphate (Figure 26D).

Results demonstrated that the attenuation of PTEN enzymatic activity by PRG2 occurs in a dose dependent manner and potentially requires the poly-E-box containing C-terminus of PRG2. This suggests further that PRG2 is capable to manipulate the phosphoinositide composition at the axonal plasma membrane through its association with PTEN. In particular, the inhibitory role of PRG2 may lead to an enrichment of PI(3,4,5)P₃ at sites of PRG2-PTEN complex formation.

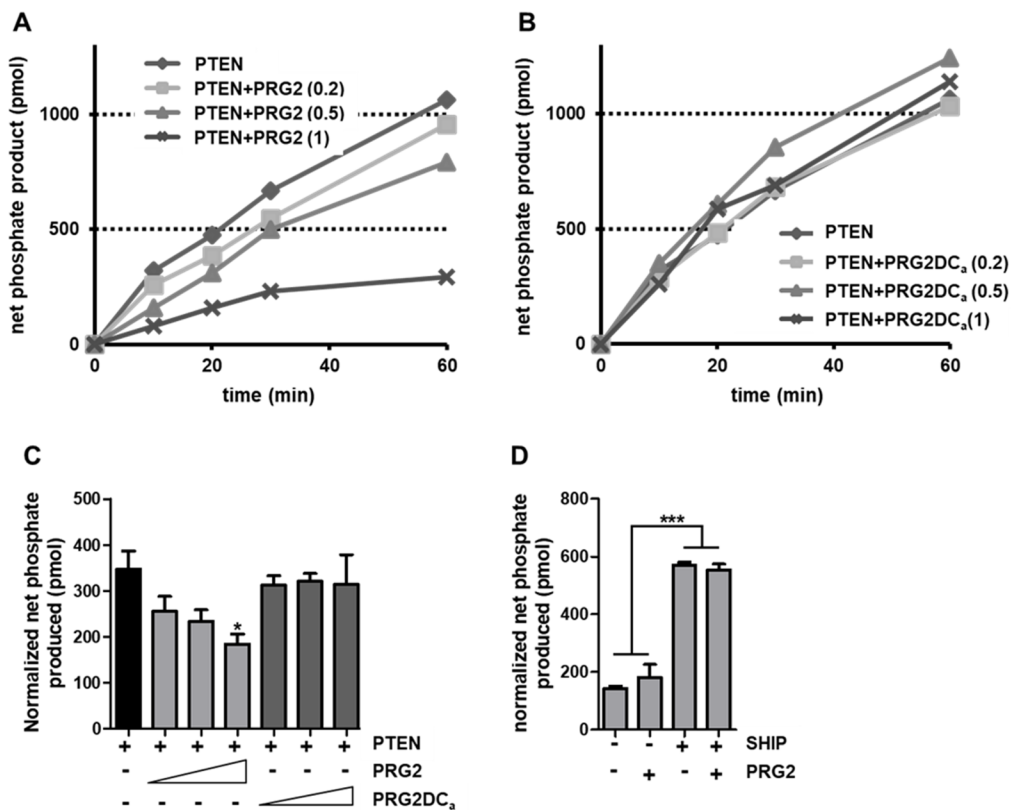


Figure 26: The PTEN-PRG2 interaction inhibits PTEN phosphatase activity.

COS-7 cells were co-transfected with GFP-PTEN and control vector, or with GFP-PTEN and increasing concentration of PRG2 or PRG2DC_a (A and B, respectively) Numbers indicated represent μg DNA transfected. Subsequently, PTEN was immunoprecipitated and enzymatic activity (phosphate product release) was measured in a standard colorimetric assay (Malachite Green Assay; Maehama et al., 2000). Phosphate release was normalized to PTEN concentration immunoprecipitated (C). Bar graphs represent 4 discrete measurements from two independent experiments. * $p < 0.05$, ** $p < 0.001$. Data represent mean \pm SEM. PRG2 expression did not change phosphate product release of the 5' phosphatase SHIP (D). Upon increasing concentrations of PRG2, PTEN phosphatase activity declines. In the presence of PRG2DC_a, PTEN activity is not affected.

3.5.2 PRG2 localisation is independent of PI3K induced PI(3,4,5)P₃ generation

The, previously described, inhibitory role of PRG2 on PTEN phosphatase activity may lead to a change of the balance between phosphoinositides, favouring generation of PI(3,4,5)P₃. In order to understand, if in turn the balance between PI(3,4,5)P₃ and PI(4,5,)P₂ influences PRG2 localisation, we inhibited PI3K to decrease the amount of PI(3,4,5)P₃ and performed SIM microscopy in primary neurons. Hippocampal neurons were pre-treated with GDC-0941 (PI3K inhibitor) and PRG2 periodicity and membrane enrichment was quantified. In parallel, cortical neurons treated with PI3K inhibitor were lysed at indicated time points and cell lysate was analysed by western blotting (Figure 27A). Akt is the most prominent effector of PI3K. Hence, phospho-S473-Akt levels were detected as readout for PI3K signalling strength. Figure 27A displays a significant reduction of phospho-Akt in GDC-0941 treated conditions, confirming effective inhibition of the kinase. Distance measurements of consecutive PRG2 spots at the

axonal plasma membrane reveal, compared to untreated samples, a modest but significant difference in the mean spacing between PRG2 puncta in GDC-0941 treated neurons (Figure 27C). However, representative images of all conditions (Figure 27B) showed that the general appearance of PRG2 puncta at the membrane does not change greatly after PI3K inhibition. Analysis of PRG2 membrane localisation of untreated and GDC-0941 treated neurons demonstrated that PRG2 enrichment at the axonal plasma membrane is unaffected by PI3K inhibition (Figure 27D). In summary, results show that $PI(3,4,5)P_3$ and $PI(4,5)P_2$ abundance at the plasma membrane have no impact on PRG2 membrane localisation.

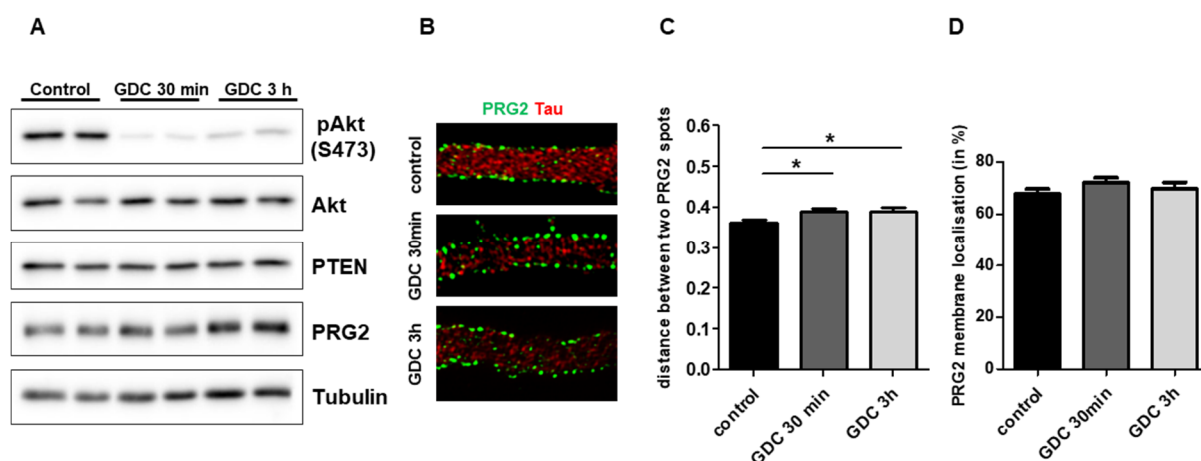


Figure 27: PRG2 localization is not impaired by PI3K inhibition.

A) Cortical neurons were treated with the PI3K inhibitor (GDC-0941, 500nM), cells were lysed in RIPA buffer and probed for western blot with indicated antibodies. Phospho Akt levels, as a read out for PI3K signaling strength, are decreased in GDC treated conditions. B+C+D) DIV9 hippocampal neurons were treated with PI3K inhibitor, fixed and stained with anti-PRG2 and anti-Tau1 antibody. SIM images were captured. B) Representative images of control and GDC treated samples. C) Distance measurement of consecutive PRG2 spots. D) Ratio of PRG2 puncta at the axonal plasma membrane to puncta in the cytosol. N= 6 axons per condition, One way ANOVA with Bonferroni post hoc, * $p < 0.05$.

3.5.3 Functional characterisation of PRGs during neuronal development

Previous studies, presented in this thesis, described PRG2 as a highly developmentally regulated protein, which interacts with the lipid phosphatase PTEN. In addition to this, the analyses of the developmental expression of PRG2 identified a well-defined timeframe in early neuronal development that correlates precisely with branching morphogenesis of both axonal and dendrite processes (see Figure 17). Therefore, we next asked if PRG2, which we found to be particularly enriched in axonal membranes, is required for axonal branching. To achieve this goal, we aimed to deplete PRG2 during this particular phase of the neuronal maturation program and generated a shRNA construct specifically silencing PRG2 expression whilst simultaneously expressing GFP (collaboration with Thorsten Trimbuch; Viral Core Facility, Charité). The shPRG2 sequence binds at the end of the intracellular C-terminus of PRG2. The newly generated plasmid was validated by expression in HEK293T cells with subsequent western blot analysis (Figure 28B). Results showed, in contrast to control conditions in which

PRG2-Flag was co-expressed with an empty vector construct, PRG2 level was highly decreased through co-expression of PRG2-Flag with the shPRG2 construct. Next, primary hippocampal neurons were transfected at DIV2 using either the shRNA construct or a control plasmid expressing GFP. Analysis of neurons was performed at DIV7, when neurons typically showed solid PRG2 expression. Following fixation, immunolabeling with anti-GFP and anti-Tau1 antibody allowed the detection of transfected neurons as well as the identification and tracing of all axonal processes of transfected cells. A schematic of the experimental time line is depicted in Figure 28A. Representative images of shPRG2 and control transfected neurons are shown in Figure 28C. Quantification of primary axon length in each treatment revealed a moderate, but significant decrease of the longest axonal process extending from the neuronal cell body in PRG2 depleted neurons, when compared to control transfected neurons (Figure 28D). However, when comparing the length of all axonal processes, including the axonal branches emerging from axonal projections, PRG2 silenced neurons exhibited a robust reduction in the total axon length in comparison to control neurons (Figure 28E). This effect was due to a severe reduction in the number of primary (Figure 28F) and total branches per axon in neurons transfected with the shRNA targeting PRG2 (Figure 28G). Taken together, loss of PRG2 during early neuronal development leads to a minor effect on primary axon length but drastically impairs axonal branching. The aberrant neuronal phenotype induced by PRG2 depletion suggests a fundamental role of the transmembrane protein PRG2 in neuronal maturation.

PRG1 loss may affect maturation of axonal architecture. Therefore, in collaboration with Thorsten Trimbuch (Viral Core Facility, Charité), we generated a shRNA construct silencing PRG1 expression. Sufficient knock-down of PRG1 expression was confirmed through western blot analysis of HEK293T cell lysate, previously transfected with PRG1-Flag and the shPRG1 (or control) plasmid (Figure 29B). Accordingly, shRNA mediated knock down of PRG1 in primary hippocampal neurons was performed. Neurons were transfected at DIV2 with control-GFP or shPRG1-GFP constructs. Fixation and staining was conducted at DIV7, similar to the previous experiments assessing PRG2 function. Figure 29C shows representative images of control and PRG1 deficient neurons. The analysis of primary axon length in control and PRG1 silenced neurons revealed that the outgrowth of the longest axonal process from the neuronal cell body is not affected by PRG1 loss (Figure 29D). However, quantification of the length of all axonal processes showed a modest but significant attenuation of the total axon length. This trend appeared to be based on the reduction of secondary and tertiary branches in PRG1 knock-down neurons compared to control (Figure 29G), whereas the number of primary axonal branches did not change in control and PRG1 depleted neurons (Figure 29F).

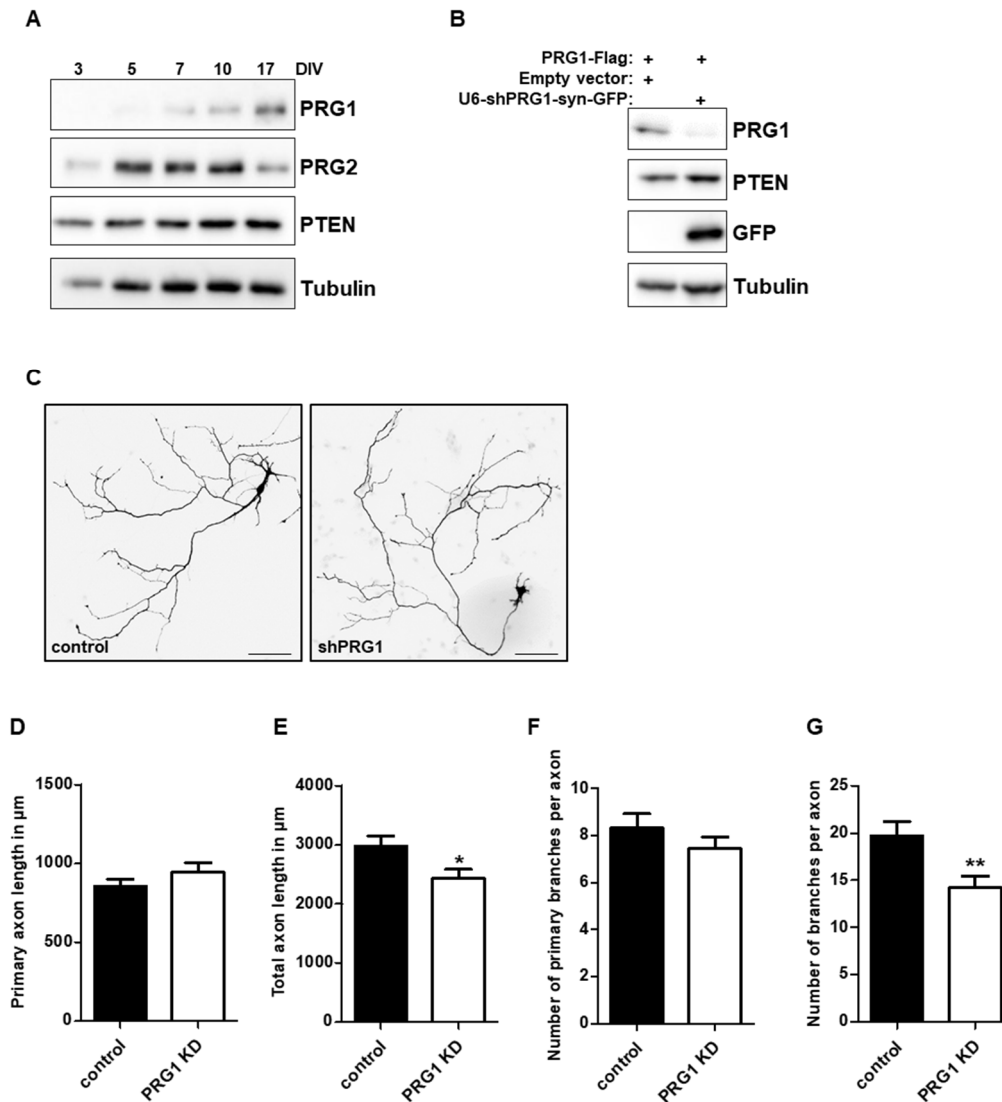


Figure 29: Loss of PRG1 during neuronal development has a minor effect on neuronal arborization.

A) Primary cortical neurons were lysed at indicated time points and analysed by western blotting. PRG1 expression is delayed compared to the related family member PRG2. B) HEK293T cells, transfected with delineated plasmids, were lysed and studied by western blotting. B, C, D, E, F) DIV7 primary hippocampal neurons were analysed after transfection (DIV2) with control-GFP or shPRG1-GFP plasmids. Cells were stained with anti-GFP and anti-Tau antibody. Axonal arborization was assessed using the NeuronJ plugin from ImageJ. D) Representative images of control and shPRG1 transfected neurons. Scale bar: 100 μm . Statistical analysis of primary axon length (D), total axon length (E) and branching (F, G) was performed. $n=3$, total cell number: 70, unpaired Student's t-test, * $p<0.05$, ** $p<0.01$.

In summary, loss of PRG2 during early neurodevelopment impaired axonal branching. In comparison, the loss of the family member PRG1 caused a mild decrease in axonal branching.

Although both PRGs possess a long C-terminal tail and are highly homologous, only the C-terminus of PRG2 contains an accumulation of 20 glutamic acid residues (poly-E-box). This acidic stretch may be responsible for the more severe knock down phenotype of PRG2 compared to PRG1 loss. As described earlier in this thesis, in association with PRG2, PTEN phosphatase activity is inhibited by full length PRG2, but is not affected in conditions using the

PRG2 mutant lacking the poly-E-box. Since the poly-E-box is absent in the PRG1 C-terminus, we predict that this particular domain, by inhibition of PTEN activity, provides a novel regulatory function of PRG2 in neuronal outgrowth.

In order to understand the relationship of PRG1 and PRG2 during axonal branching, we created a third shRNA simultaneously targeting PRG1 and PRG2 (shPRG1/2). Similar to the previously described PRG shRNAs, cell lysates devoid of both PRGs also express GFP (Figure 30A). To test for specificity of each shRNA, we overexpressed PRG1-Flag or PRG2-Flag with each shRNA and performed western blot analysis of HEK293T cell lysate. Results showed PRG1-Flag expression was not decreased in the presence of shPRG2 and PRG2-Flag expression was not affected with shPRG1. HEK293T cells transfected with shPRG1/2-GFP revealed knock down of both, PRG1-Flag and PRG2-Flag. We next used the double knock down shPRG1/2 to examine the impact of shPRG1/2 on axonal branching as previously described (see Figure 28). Measurement of primary axon length, total axon length, including all axonal processes and number of axonal branches exhibited a more severe decrease in axonal arborization compared to single knock down of PRG1 or PRG2 alone (Figure 30B-E).

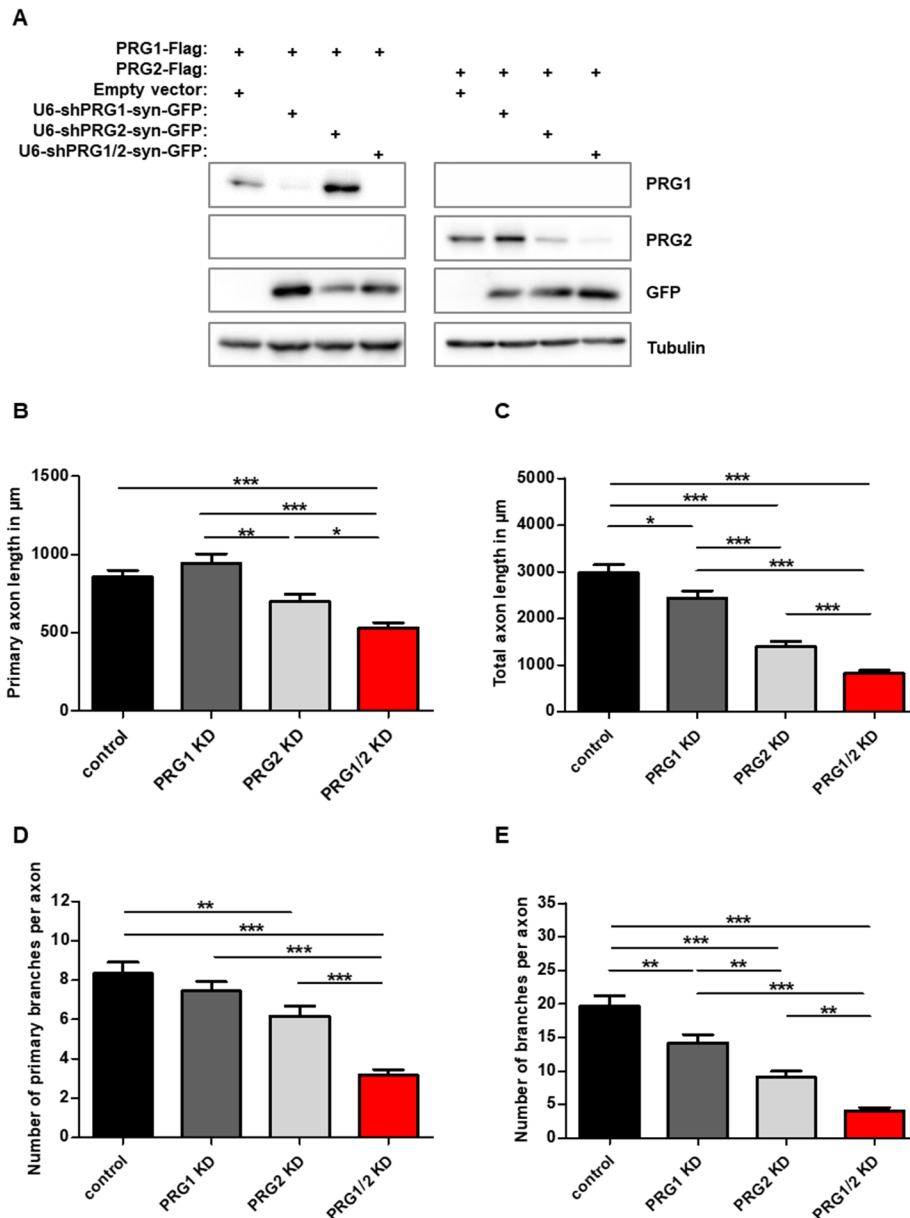


Figure 30: Synchronised loss of PRG1 and PRG2 reveals a more severe decrease in axonal arborization compared to single depletion of both PRGs.

A) HEK293T cells transiently transfected with indicated constructs were lysed and probed by western blotting. B, C, D, E,) DIV7 primary hippocampal neurons were analysed after transfection (DIV2) with control-GFP, shPRG1-GFP, shPRG2-GFP or shPRG1/2-GFP plasmids. Cells were immunolabeled with anti-GFP and anti-Tau antibody. Axonal arborization was assessed using the NeuronJ plugin from ImageJ. Statistical analysis of primary axon length (B), total axon length (C) and branching (D, E) was performed. $n=3$, total cell number: 173, One way ANOVA with Bonferroni post hoc, * $p<0.05$, ** $p<0.01$, *** $p<0.001$.

Given that increased $PI(3,4,5)P_3$, i.e. through PI3K activation or PTEN depletion, promotes the formation of axonal filopodia and branches (Ketschek, Gallo, 2010; Spillane et al., 2011; Ketschek, Spillane, and Gallo, 2011; Jaworski et al., 2005; Kwon et al., 2006), we tested the influence of PTEN and PRG loss on axonal branching.

We used PTEN flox/flox primary hippocampal neurons and infected cells at DIV1 with RFP-Cre virus, which harbours a nuclear localisation sequence on its transgene. In order to generate PRG/PTEN and PTEN depleted neurons, we additionally transfected these neurons with shPRG1/2-GFP or control-GFP constructs, respectively. Again, analysis of axonal morphology was performed at DIV7. Neurons were identified by GFP and nuclear RFP expression. Results are shown in Figure 31. The loss of PTEN in primary hippocampal neurons led to a general overgrowth phenotype. Axonal length (Figure 31A+B) and the number of branches per axon (Figure 31C+D) were increased compared to control. To our surprise, the simultaneous loss of PTEN and PRG1/2 resembled the PRG1/2 knock down phenotype. Total axon length and branch number of PRG1/2/PTEN depleted neurons were significantly decreased compared to control and to PTEN knock down neurons (Figure 31A-D). This demonstrates that the loss of PTEN in addition to PRG knock down does not restore the defect in axonal branching induced by PRG depletion.

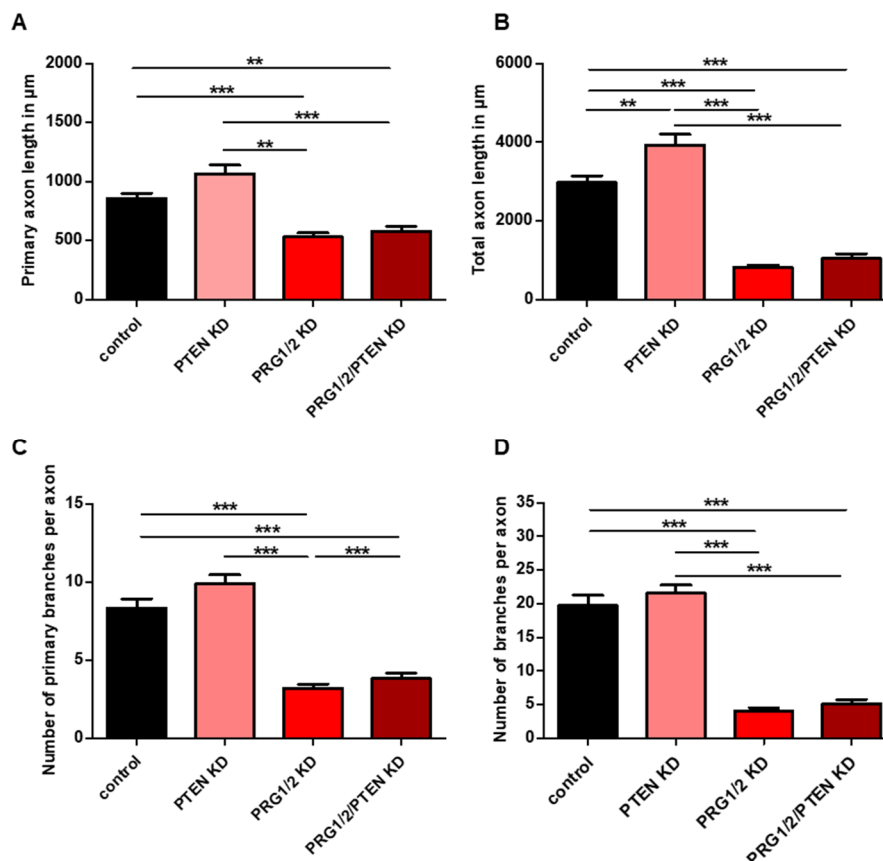


Figure 31: Simultaneous loss of PRGs and PTEN does not restore axonal complexity.

A-D) Primary hippocampal neurons dissociated from PTEN flox/flox mice were infected with RFP-Cre virus at DIV1. PRG and PTEN depleted neurons were additionally transfected with shPRG1/2 at DIV1. Control and PRG knock down condition was generated by transfection of wild type hippocampal neurons with control-GFP or shPRG1/2-GFP plasmids. Neurons were fixed and stained with anti-GFP, anti-Tau1 antibody at DIV7. Axonal arborization was assessed using the NeuronJ plugin from ImageJ. Statistical analysis of primary axon length (B), total axon length (C) and branching (D, E) was performed. n=3, total cell number: 197, One way ANOVA with Bonferroni post hoc, *p<0.05, **p<0.01, ***p<0.001.

Published data, demonstrate a requirement of PI3K activity in the formation of axonal filopodia and branches (Ketschek, Gallo, 2010; Spillane et al., 2011; Ketschek, Spillane, and Gallo, 2011). Our data demonstrates that loss of PRG2 results in decreased axonal branching, whereas depletion of PTEN causes an increase in axonal outgrowth. This could be explained through the inhibition of PTEN enzymatic activity by PRG2 (see Figure 26), which leads to an increase in PI(3,4,5)P₃ levels. If this stands true, axonal branching should increase under simultaneous loss of PRG2 and PTEN. However, the simultaneous loss of PRGs and PTEN was not capable of increasing axonal branching (see Figure 31). This discrepancy prompted us to test the influence of PRG2 on PI(3,4,5)P₃ levels by analysing the phosphorylation of Akt as a readout for PI(3,4,5)P₃.

To address this, one day after plating we infected primary PTEN flox/flox cortical neurons with control-RFP, Cre-RFP to induce knock down of PTEN, shPRG1/2-GFP or RFP-Cre and shPRG1/2-GFP viruses. Western blot analysis of cortical lysates, depicted in Figure 32A-D, demonstrate a robust knock down of PTEN and PRG2 following viral transduction. Under control conditions relative phospho-Akt levels did not change in the course of neuronal development (Figure 32A+E). As known from the literature, knock down of PTEN gradually increased relative phospho-Akt levels during neuronal development (Figure 32B+F). Loss of PRGs moderately decreased phospho-Akt at DIV16, suggesting that PRG2 modulates PI(3,4,5)P₃ signalling (Figure 32C+G). The combined loss of PRG and PTEN in primary neurons displayed high levels of phospho-Akt (Figure 32D+H). The more drastic change of phospho-Akt in PTEN knock down lysates compared to the rather mild decrease upon PRG loss, is probably due to the fact that PTEN is highly enriched in primary neurons, whereas PRGs are present locally in the neuronal plasma membrane. However, this demonstrates that PI(3,4,5)P₃ levels are high in neurons lacking both PTEN and PRGs. This is in contrast, to the previously described effect of decreased axonal branching in these neurons, suggesting that PRGs have additional functions to its effect on PTEN inhibition.

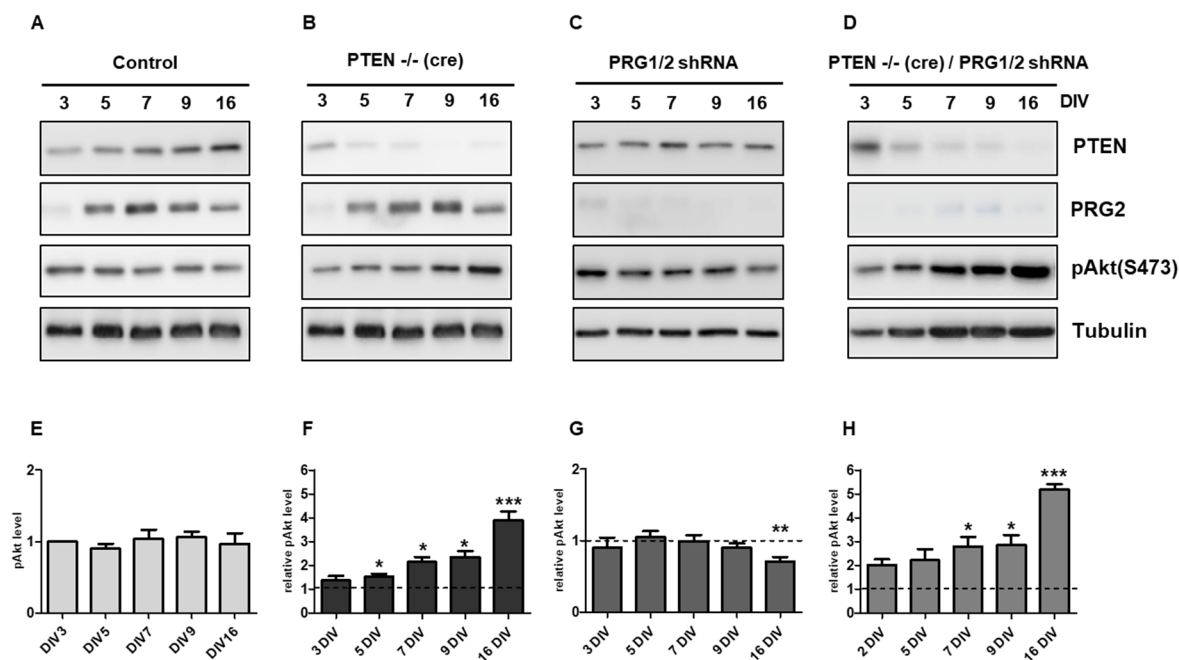


Figure 32: PI3K signalling strength is altered by loss of PRG1/2 and PTEN.

A-D) Primary cortical neurons dissociated from PTEN flox/flox mice were infected with control-RFP, cre-RFP, shPRG1/2-GFP or cre-RFP and shPRG1/2-GFP virus one day after plating. Neurons were lysed at indicated time point during neuronal development. Lysates were probed by western blotting with anti-PRG2, anti-PTEN, anti-phospho-Akt and anti-Tubulin antibody. E-H) Relative phospho-Akt levels were quantified with ImageJ and GraphPad. N=4, unpaired Student's t-test, * $p < 0.05$, ** $p < 0.01$, *** $p < 0.001$.

3.5.4 BDNF facilitates PRG2-PTEN interaction

Growth factor signalling by NGF and BDNF plays prominent roles in developing neurons by regulating PI3K/Akt signalling and neuronal morphology (Cosker and Eickholt, 2007; Kreis et al., 2014; Van Diepen and Eickholt, 2007). For example, NGF has been shown to induce PI3K dependent F-actin patch formation, as well as increase the number of axonal filopodia and branches (Ketschek and Gallo, 2010; Ketschek et al., 2011). BDNF stimulates branching in cortical axons and transfection of the growth factor into dentate granule cells specifically increases axon branching (Danzer et al., 2002; Jeanneteau et al., 2010). Moreover, *in vivo* imaging showed that acute BDNF application induces rapid extension of new branches on retinal axon arbors (Marshak et al., 2007). In order to test the possibility that a bona fide axon branch and arborization factor may affect our identified PTEN-PRG2 scaffold during axon filopodia induction, we evaluated whether protein complex formation is dynamically regulated. For that purpose, cortical neurons were cultured for 9 DIVs, when both, branching behaviour and PRG2 expression are high. Then, cells were stimulated with 50 ng/ml BDNF for a distinct period of time. Cells were lysed and PTEN was immunoprecipitated from protein lysate. Western blot analysis of total cell lysate (input) and immunoprecipitated samples showed a pronounced increase in the association of PRG2 and PTEN as early as 5 minutes after BDNF addition compared to untreated conditions (Figure 33). This result strongly provides evidence

that the application of BDNF positively regulates PRG2-PTEN complex formation and indicates that growth factor induced PI3K activation may leads to a stabilisation of the protein complex.

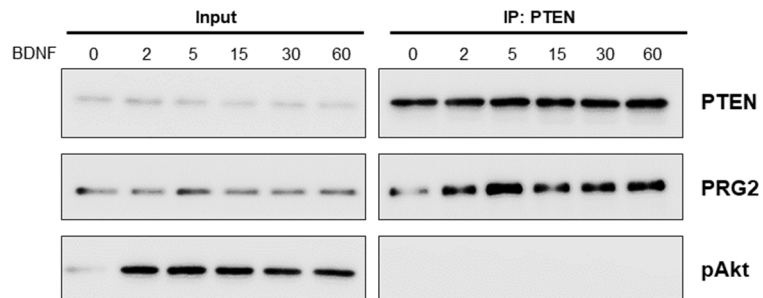


Figure 33: BDNF promotes binding of PRG2 and PTEN.

Cultured cortical neurons (DIV9) were treated with 50 ng/mL BDNF for indicated period of time. Subsequently cells were lysed and PTEN was immunoprecipitated from cortical lysates using anti-PTEN antibody (Santa Cruz). Input and IP samples were examined by western blotting.

4. Discussion

This study proposes a model, in which the presence of a novel membranous protein scaffold, consisting of the lipid phosphatase PTEN and the transmembrane protein PRG2, spatiotemporally regulating axonal arborization during neuronal development.

Major findings of this dissertation encompassed the occurrence of PRG2 as a higher order protein complex, which was also capable to bind other PRG family members. Furthermore, PRG2 was characterised as a highly developmentally regulated protein, displaying strongest protein expression during the phase of neuronal outgrowth and branching of axons and dendrites. Subcellular distribution studies in primary hippocampal neurons revealed a differential localisation of PRG2 in axons and dendrites. Most striking was the periodic appearance of PRG2 puncta along the axonal plasma membrane. Interestingly, this characteristic arrangement of PRG2 puncta was dependent on the actin cytoskeleton. PRG2 interacts with the lipid phosphatase PTEN and inhibited PTEN phosphatase activity. We demonstrated that the interaction of PTEN and PRG2 is facilitated upon application of the bona fide branch inducing factor BDNF. Lastly, we showed a substantial reduction in axonal arborization upon PRG2 depletion in early phases of neuronal maturation. The combined loss of PRG2 and its family member PRG1 strengthened the effect on axonal arborization. However, the simultaneous loss of PRG1 and PRG2 in combination with the loss of the growth repressor PTEN failed to reconstitute the characteristic axonal phenotype.

4.1 PRG2 forms higher order complexes

The present study addressed the complex formation capability of PRG2 in immunoprecipitation assays. Experiments obtained in this thesis exhibited a novel self-association ability of PRG2 in primary neurons. Interestingly, native protein lysates from cortical neurons analysed by SDS-PAGE with subsequent western blotting with anti-PRG2 antibody revealed the recognition of two prominent PRG2 signals. The first one resembling monomeric PRG2. Whereas, the second PRG2 western blot band emerged above the 250 kDa reference, suggesting that in addition to its monomeric state, PRG2 forms higher order protein complexes. The apparent molecular weight of the second western blot signal, suggests that this complex may include two or even three PRG2 molecules. Further analysis of the constitution of PRG2 protein complexes is currently performed in collaboration with the Institute of Biophysics, Charité. Initial data indicates that PRG2 generates tetrameric and/or hexameric PRG2 complexes.

The structural requirements determining PRG2 self-association remain still unclear. We generated PRG2 C-terminal deletion mutants. Experiments showed that co-expression of the

truncated PRG2 mutants with full length PRG2 in N1E-115 cells failed to abolish PRG2 interaction. Further, co-expression of PRG2 mutants lacking the entire C-terminal tail showed interaction of the truncated variants. This indicates that the long intracellular tail of PRG2 is not required for the self-association of PRG2. In agreement with this result is that the generation of heterologous PRG complexes, composed of PRG2 and other PRG family members harbouring rather short intracellular C-tails. PRG2 interacts with PRG3 and PRG5, which in contrast to the 400 aa long C-tail of PRG2 (400 aa) possess a ~50 aa intracellular C-terminal part (Figure 34). During the course of the study, data by Yu et al. (2015) were published, which showed that the association of PRG3 with PRG1, PRG2 and PRG5 occurs independently of the PRG3 C-terminus (P. Yu et al., 2015). Altogether, this indicates that the length of the individual PRG C-terminus is not responsible for the interaction with PRG family members. Both, the longer members (enlarged intracellular C-tail; PRG1, PRG2) and the shorter members (short C-tail; PRG3, PRG5), exhibit multimeric function. Additionally, no specific region within the intracellular C-terminal tail, is responsible for the ability of PRGs to build a heteromeric complex. We believe that the interaction is mediated by the intracellular loops between the transmembrane domains of PRGs. The relevance of PRG complex formation is still unclear. It has been hypothesised that protein stability is enhanced following co-expression of PRG3 and PRG5 leading to an increase in filopodia formation (P. Yu et al., 2015). Another hypothesis to the multimerization is the correct positioning of PRGs, which could contribute to or allow the interaction of other binding partners and may ultimately lead to faster processing of signalling cascades.

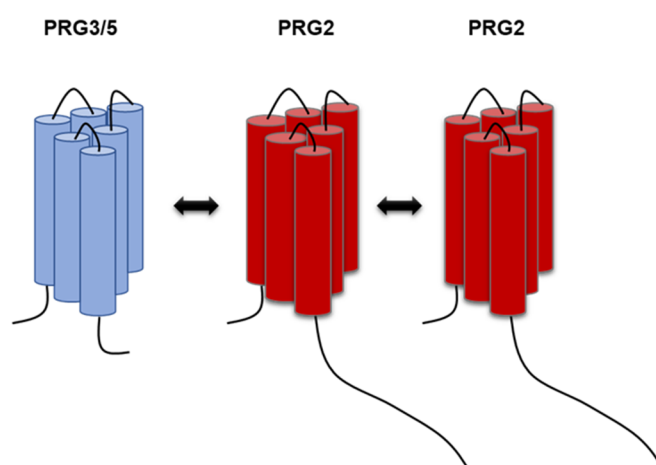


Figure 34: Schematic of interacting PRG family members unravelled in the present thesis. PRG2 interacts with PRG3 and PRG5. Self-association of PRG2 molecules occurs independent of the intracellular C-terminus.

4.2 Spatiotemporal organisation of PRG2

PRGs are brain-enriched proteins (Bräuer and Nitsch, 2008). Previous studies, demonstrated that PRG3 and PRG5 display a differentially regulated expression profile during neuronal development (Coiro et al., 2014; Velmans et al., 2013). However, as yet the regulation of PRG2 is poorly understood. In this thesis, western blot analysis of whole brain lysate from rat and primary cortical lysate from mouse revealed a highly developmentally controlled expression of the PRG2 protein. *In vitro*, highest PRG2 expression coincided with the phase of neuronal outgrowth and branch formation of axon and dendrites (DIV5-DIV12). After DIV12, PRG2 expression declined rapidly. Strikingly, the expression profile of, PRG2s most related family member, PRG1, follows an entirely different profile of expression. Compared to PRG2, PRG1 expression is delayed with first levels detected during the phase of neuronal branching and highest protein levels at DIV17, corresponding to the phase of synapse formation. This indicates that although PRG1 is highly homologous to PRG2 and constitutes its most related family member, both proteins are probably required for distinct functions throughout neuronal development. Whereas PRG2 might be necessary for events during early neuronal maturation, such as neuronal outgrowth and branching, PRG1 presumably is more involved in later stages during neuronal development, in which initial establishment of neuronal architecture has been completed and neurons develop synaptic connectivity and transmission.

In addition to the temporal expression of PRG2 during neuronal development, we further assessed its subcellular distribution in DIV9 primary hippocampal neurons, which corresponds to PRG2 highest expression level, using axonal and dendritic markers. In axons, PRG2 appeared along the axonal plasma membrane. In dendrites it was mainly found to be restricted within the dendritic shaft. Due to the striking association of PRG2 with the plasma membrane of axons, this thesis focused on the functional relevance of PRG2 within the axonal compartment of primary neurons. Subsequent analysis of PRG2 organisation by super-resolution microscopy exhibited a periodic accumulation of consecutive PRG2 puncta along the axonal membrane of DIV9 hippocampal neurons. Analysis of distance measurements between consecutive PRG2 spots revealed PRG2 distances of 220 nm, 240 nm, 260 nm and 280 nm as the most frequent distance. Longer and shorter distances were less present, providing evidence for a highly organised and regulated distribution of the PRG2 puncta.

The sequential arrangement of PRG2 puncta was reminiscent of the lattice like appearance of axonal actin rings in developing neurons, suggesting that these actin structures may influence PRG2 localisation (Xu et al., 2013). Discovered as an additional cytoskeletal structure this periodic skeleton is formed by rings of actin filaments with even spacings underneath the plasma membrane. The actin rings are separated by spectrin, providing a distance between two adjacent actin rings of ~190 nm (Xu et al., 2013; Zhong et al., 2014). Co-staining of PRG2

and actin rings revealed that PRG2 was not exclusively distributed at sites of the actin lattice and only partially co-localised with the actin rings, indicating that actin ring structures are unlikely to mediate the organisation of PRG2 clusters along the axonal membrane. This distribution, however, does not rule out the influence of the actin cytoskeleton on PRG2 localisation, which we tested by SIM microscopy of primary hippocampal neurons pre-treated with the actin destabilizing drug Latrunculin B. Under control conditions, PRG2 periodicity was achieved through high frequency of rather similar distances being 220 nm, 240 nm, 260 nm and 280 nm. Whereas longer or shorter distances did not occur often. Treated neurons showed an increase in the frequency of longer distances between two PRG2 spots and a decrease of distances between 220 nm and 280 nm, when compared to control. This demonstrates that actin disruption affects PRG2 periodicity and suggests that the actin cytoskeleton mediates the arrangement of PRG2 dots along the axonal plasma membrane. As the actin ring structures are unlikely to coordinate PRG2 distribution, it is conceivably that subcortical actin structures underneath the axonal membrane are responsible for PRG2 organisation by, for example, anchorage to the cortical actin cytoskeleton.

In addition to the analysis of PRG2 periodicity, we quantified the level of PRG2 membrane enrichment in control and Latrunculin B treated neurons by immunocytochemistry. Results showed significantly decreased levels of PRG2 at the axonal membrane after 3 h of Latrunculin B application compared to control. This indicates that the actin cytoskeleton may contribute to targeting of PRG2 to the plasma membrane. In this regard, the dynamic actin cytoskeleton may be required for the vesicle transport of proteins from the endoplasmic reticulum (ER) to the destined plasma membrane (Anitei and Hoflack, 2012).

The previously discussed data constitute a novel periodic subcellular distribution of PRG2 along the axonal plasma membrane, which has never been described previously for any PRG family member. In addition, our data demonstrate that the localisation of the transmembrane protein PRG2 is dependent on the axon cytoskeletal dynamics.

4.3 Regulation of the PRG2/PTEN complex

The major suppressor of the PI3K signalling pathway is the protein and lipid phosphatase PTEN. Primarily acting at the plasma membrane by dephosphorylating PI(3,4,5)P₃ to PI(4,5)P₂, PTEN directly antagonises PI3K function (Cantley et al., 2002). Initiated by a mass spectrometry approach, seeking for novel neuronal PTEN interaction partners, this dissertation aimed to understand the role of the newly identified PTEN-PRG2 interaction during neuronal development. We confirmed the predicted binding of PTEN to PRG2 by Co-immunoprecipitation experiments. Analysis of PTEN enzymatic activity demonstrated an inhibition of PTEN lipid phosphatase activity in association with PRG2. Thus, we suggest that

inhibition of PTEN by PRG2 dynamically regulates phosphoinositide composition at the axonal plasma membrane, causing a spatially restricted excess of PI(3,4,5)P₃ at PRG2 clusters. In addition, we provided evidence that PRG2 regulation of PTEN activity is dependent on the PRG2 C-terminus containing the poly-E-box. However, the mechanism of how the C-terminal domain of PRG2 exactly inhibits PTEN is yet unclear. Possibly, the long intracellular C-terminus could function by blocking PTENs phosphatase domain. The self-association capability as well as PRG2s ability to interact with PRG family members, point to a formation of a higher order PRG membrane protein complex at the axonal plasma membrane, which may act by preventing the direct access of PTEN to the membrane, maintaining its inactive state.

Interestingly, reduced PTEN activity and membrane binding is associated with phosphorylation of the PTEN C-terminus leading to a “closed” conformational status (Rahdar et al., 2009). It would be of interest to analyse the phosphorylation status of the amino acid cluster within PTENs C-tail in order to get insight into the structural features of PTEN-PRG2 complex formation.

Regulatory inputs/mechanisms providing PRG2 function are largely unknown. Post-translational modifications, such as phosphorylation, glycosylation or ubiquitination, are described to manipulate protein function. Preliminary data generated in this project, using Λ -phosphatase treated cortical lysates, showed a band shift of PRG2 to a lower molecular weight suggesting that PRG2 can be phosphorylated. Whether phosphorylation dynamically regulates for example, PRG2 protein-protein interaction, including multimerization, conformation or its inhibitory function on PTEN activity, needs to be further characterised.

4.4 Regulation of axonal filopodia and branches by PRG2

An additional key finding of this study is a reduced axonal branching phenotype of primary hippocampal neurons through shRNA mediated depletion of PRG2 during early neuronal maturation. Depletion of the PRG family member, PRG1, showed a milder decrease in axonal branching. Although PRG1 and PRG2 demonstrate high sequence homologies in their long intracellular C-terminal tails, we suggest that the unique poly-E-box within the PRG2 C-terminus functions as a regulatory domain, leading to a more severe branching phenotype in PRG2 depleted neurons compared to PRG1 depleted neurons. The combined loss of both PRGs revealed an increased branching defect compared to single loss of PRG2. This result indicates that PRG1 might assist in PRG2 function during axonal branching.

In complex with PRG2, PTEN enzymatic activity is inhibited, which may cause an excess of PI(3,4,5)P₃ at sites of PRG2 accumulation along the axonal plasma membrane. Published data constitute local PI3K activity and its lipid product PI(3,4,5)P₃ as precursors for F-actin patch

formation, that subsequently form axonal filopodia by elongating actin filaments (Ketschek and Gallo, 2010; Spillane et al., 2011). Axonal filopodia eventually mature into collateral branches. We hypothesise that loss of PRG2 might favour PI(3,4,5)P₃ hydrolysis due to the missing inhibitory function of PRG2 on PTEN. Consequently, less PI(3,4,5)P₃ domains may lead to diminished number of actin patches, thus to a reduced number of filopodia and ultimately less axonal branches. In contrast, loss of PTEN favours PI(3,4,5)P₃ generation by PI3K, creating the opposite effect on axonal branching compared to PRG2 loss. If PRG2s effect on PI3K signalling is only driven by inhibition of PTEN, PI(3,4,5)P₃ levels and axonal branching should increase under synchronous loss of PRG2 and PTEN. Our experiments revealed that indeed neurons depleted of PTEN and both PRG1 and PRG2 showed high pAkt levels, as a readout for PI(3,4,5)P₃ levels. However axonal branching was severely decreased in these neurons, indicating that PTEN loss did not restore axonal branching in PRG1 and PRG2 depleted neurons. This finding was unexpected and questioned our hypothesis as well as the specificity of the PRG1 and PRG2 shRNA.

To test for specificity, we performed a blast of the shRNA sequence, which showed an overlap of only 16 out of 21 bp in the 5'UTR of the formin-homology-domain-containing protein FHOD1. FHOD1 has been shown to promote short actin filaments (Schulze et al., 2014). Expression analysis of FHOD1 in primary neurons by western blotting and immunocytochemistry revealed no change in FHOD1 levels following viral transduction of the shRNA. Although the only apparent off target seems to be unaffected, the binding of the shRNA to another target cannot be completely ruled out and need to be investigated by additional expression analysis.

Nonetheless, preliminary experiments depleting PTEN and the PRG2 member alone using shRNA, restored the axonal branching compared to PRG2 loss only. To investigate this contradiction further, we also generated a PRG2 KO mouse line within this SFB958 project, and preliminary results obtained by Joachim Fuchs in the Eickholt lab showed that the reduction of axonal branching caused by PRG2 loss is restored in the absence of PTEN, confirming the PRG2 shRNA mediated axonal arborization defect presented in this thesis.

4.5 Conclusion

Activation of PI3K drives the formation of PI(3,4,5)P₃ at the plasma membrane. PTEN as the major PI3K antagonist, directly suppresses PI3K signalling strength by dephosphorylating PI(3,4,5)P₃ to PI(4,5)P₂. Published data demonstrates a requirement of active PI3K and PI(3,4,5)P₃ production for the formation of axonal filopodia (Ketschek and Gallo, 2010). Local PI3K activity leads to cytoskeletal rearrangement beneath the axonal plasma membrane, initiated by the emergence of F-actin patches at sides of PI(3,4,5)P₃ accumulations. Subsequently, filopodia originate from actin patches and mature by invading microtubules into

collateral branches. Accordingly, PI3K activity is essential in the establishment of the axonal arbor. The present study also shows that the PTEN phosphatase is highly abundant throughout neuronal development and, is strongly expressed in the axonal compartment of developing neurons. However, to date, a mechanism regulating the generation of PI(3,4,5)P₃ domains along the axonal membrane in the presence of high levels of the lipid phosphatase PTEN is unclear.

Our summarized data provide evidence for the spatiotemporal inhibition of PTEN by the transmembrane protein PRG2 in the course of neuronal development. PRG2 cluster localise along the axonal plasma membrane of developing neurons, exhibiting a specific upregulation of its protein expression from DIV5 to DIV9 during neuronal maturation, a timeframe characterized by the development of axonal and dendritic branches to build the typical elaborated neuronal architecture. During that phase, PRG2 multimers interact with PTEN and effectively inhibit PTEN phosphatase activity along the axonal membrane. This results in the formation of local PI(3,4,5)P₃ domains at sites of PRG2 accumulation, which leads to F-actin patch formation and favours protrusive activity of axonal filopodia.

We hypothesise that PRG2 is a novel axonal regulator of PTEN, spatiotemporally allowing PI(3,4,5)P₃ nanodomains to occur and actively organising axonal filopodia formation preceded by F-actin patch formation, favouring axon branching processes (Figure 35).

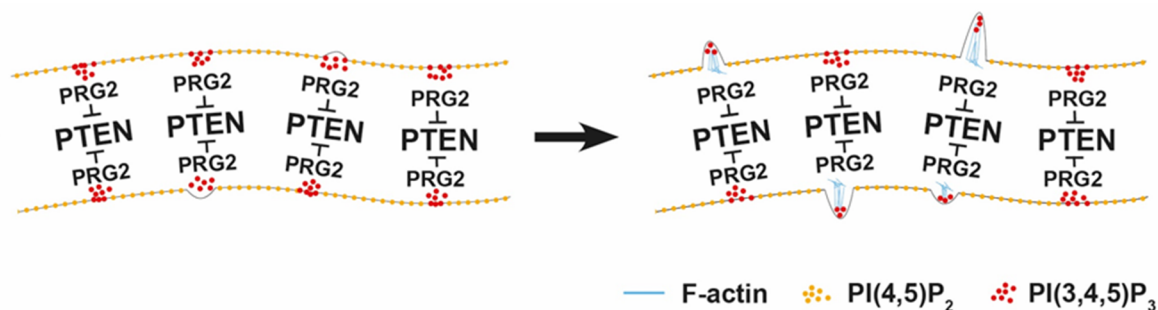


Figure 35: Model of axonal filopodia formation by the PRG2/PTEN protein complex.

The lipid phosphatase PTEN is enriched in the neuronal axon. By interaction of PTEN with PRG2, PTEN lipid phosphatase is actively inhibited. This leads to the formation of local PI(3,4,5)P₃ domains, which drive the formation of F-actin patches along the axonal membrane. Filopodia emerge from F-actin patches by elongating actin filaments.

4.6 Outlook

Our proposed model includes the inhibitory function of PRG2 on PTENs lipid phosphatase activity. We confirmed the interaction of both proteins. Nonetheless, further examination on the structural requirements of this complex formation need to be elucidated. The identification of the exact binding domains within PRG2 and PTEN would gain further insight into the relation of structure and function of this interaction. With regard to our proposed model of PTEN inhibition by PRG2 leading to PI(3,4,5)P₃ nanodomains, PRG2 deficient neurons are

suspected to display an aberrant phosphoinositide composition in the axonal plasma membrane compared to wildtype neurons. Thus, ongoing experiments in the lab aim to study the frequency and organisation of PI(3,4,5)P₃ accumulations within the axonal plasma membrane in the presence and absence of PRG2 by SIM microscopy and live cell imaging. In this vein, restoration of PRG2 and the PRG2 deletion mutant lacking the C-terminus in PRG2 KO neurons, may clarify the importance of PRG2 function in axonal filopodia formation and may provide further evidence for the relevance of the PRG2 C-terminus determining PTEN inhibition.

In the course of my PhD study, a manuscript addressing PRG2 function in axon guidance has been published. Data demonstrated that a protein complex of PRG2 and Radixin mediates LPA dependent guidance of thalamocortical fibers (Cheng et al., 2016). Radixin, together with Ezrin and Moesin, are collectively known as ERM proteins, which link membrane proteins with the actin cytoskeleton (Neisch and Fehon, 2011). With regard to our hypothesised model, in addition to its role in generating PI(3,4,5)P₃ domains through PTEN interaction, the interaction of PRG2 and Radixin may actively contribute to actin dynamics required for filopodia formation. Therefore, it would be interesting to perform co-localisation studies of PRG2 and Radixin in the axon of primary hippocampal neurons and to investigate F-actin patch formation in the absence and presence of Radixin. This would be an interesting hypothesis since little is known between the link of PRG2 and F-actin regulation in filopodia formation.

The present thesis focuses on the role of PRG2 in early stages of neuronal development and reveals a prominent effect on neuronal branching. Subsequent research may also address the effect of PRG2 loss on later stages during neuronal maturation. Diminished axonal branching in PRG2 depleted neurons may presumably result in an decreased number of neuronal connections and may ultimately influence synaptic plasticity. Therefore, it would be of further interest to explore the effect of PRG2 depletion during synaptogenesis.

5. References

- Albrecht, D., Winterflood, C. M., Sadeghi, M., Tschager, T., Noé, F., & Ewers, H. (2016). Nanoscopic compartmentalization of membrane protein motion at the axon initial segment. *Journal of Cell Biology*, *215*(1), 37–46. <https://doi.org/10.1083/jcb.201603108>
- Amiri, A., Cho, W., Zhou, J., Birnbaum, S. G., Sinton, C. M., McKay, R. M., & Parada, L. F. (2012). Pten Deletion in Adult Hippocampal Neural Stem/Progenitor Cells Causes Cellular Abnormalities and Alters Neurogenesis. *Journal of Neuroscience*, *32*(17), 5880–5890. <https://doi.org/10.1523/JNEUROSCI.5462-11.2012>
- Anitei, M., & Hoflack, B. (2012). Bridging membrane and cytoskeleton dynamics in the secretory and endocytic pathways. *Nature Cell Biology*, *14*(1), 11–19. <https://doi.org/10.1038/ncb2409>
- Antal, C. E., & Newton, A. C. (2013). Spatiotemporal dynamics of phosphorylation in lipid second messenger signaling. *Molecular & Cellular Proteomics: MCP*, *12*(12), 3498–3508. <https://doi.org/10.1074/mcp.R113.029819>
- Backman, S. A., Stambolic, V., Suzuki, A., Haight, J., Elia, A., Pretorius, J., ... Mak, T. W. (2001). Deletion of Pten in mouse brain causes seizures, ataxia and defects in soma size resembling Lhermitte-Duclos disease. *Nature Genetics*, *29*(4), 396–403. <https://doi.org/10.1038/ng782>
- BIGNER, S. H., MARK, J., MAHALEY, M. S., & BIGNER, D. D. (1984). Patterns of the early, gross chromosomal changes in malignant human gliomas. *Hereditas*, *101*(1), 103–113. <https://doi.org/10.1111/j.1601-5223.1984.tb00455.x>
- Bradke, F., & Dotti, C. C. (1999). The role of local actin instability in axon formation. *Science*, *283*(5409), 1931–1934. <https://doi.org/10.1126/science.283.5409.1931>
- Bräuer, A. U., & Nitsch, R. (2008). Plasticity-related genes (PRGs/LRPs): A brain-specific class of lysophospholipid-modifying proteins. *Biochimica et Biophysica Acta - Molecular and Cell Biology of Lipids*, *1781*(9), 595–600. <https://doi.org/10.1016/j.bbalip.2008.04.004>
- Bräuer, A. U., Savaskan, N. E., Kühn, H., Prehn, S., Ninnemann, O., & Nitsch, R. (2003). A new phospholipid phosphatase, PRG-1, is involved in axon growth and regenerative sprouting. *Nature Neuroscience*, *6*(6), 572–578. <https://doi.org/10.1038/nn1052>
- Broggini, T., Nitsch, R., & Savaskan, N. E. (2010). Plasticity-related Gene 5 (PRG5) Induces Filopodia and Neurite Growth and Impedes Lysophosphatidic Acid- and Nogo-A-mediated Axonal Retraction. *Molecular Biology of the Cell*, *21*(4), 521–537. <https://doi.org/10.1091/mbc.E09-06-0506>

- Butler, M. G., Dasouki, M. J., Zhou, X., Talebizadeh, Z., Brown, M., Takahashi, T. N., ... Eng, C. (2005). Subset of individuals with autism spectrum disorders and extreme macrocephaly associated with germline PTEN tumour suppressor gene mutations. *Journal of Medical Genetics*, *42*(4), 318–321. <https://doi.org/10.1136/jmg.2004.024646>
- Cantley, L. C., Riezman, H., Chan, C.-H., Lee, S.-W., Campos, A. D., Lamothe, B., ... Lin, H.-K. (2002). The Phosphoinositide 3-Kinase Pathway. *Science*, *296*(5573), 1655–1657. <https://doi.org/10.1126/science.296.5573.1655>
- Cantrell, D. a. (2001). Phosphoinositide 3-kinase signalling pathways. *Journal of Cell Science*, *114*(Pt 8), 1439–1445.
- Chadborn, N. H., Ahmed, A. I., Holt, M. R., Prinjha, R., Dunn, G. A., Jones, G. E., & Eickholt, B. J. (2006). PTEN couples Sema3A signalling to growth cone collapse. *Journal of Cell Science*, *119*(Pt 5), 951–7. <https://doi.org/10.1242/jcs.02801>
- Chae, H.-D., & Broxmeyer, H. E. (2011). SIRT1 Deficiency Downregulates PTEN/JNK/FOXO1 Pathway to Block Reactive Oxygen Species-Induced Apoptosis in Mouse Embryonic Stem Cells. *Stem Cells and Development*, *20*(7), 1277–1285. <https://doi.org/10.1089/scd.2010.0465>
- Chen, R., Chen, Q., Kim, H., Siu, K.-H., Sun, Q., Tsai, S.-L., & Chen, W. (2014). Biomolecular scaffolds for enhanced signaling and catalytic efficiency. *Current Opinion in Biotechnology*, *28*, 59–68. <https://doi.org/10.1016/j.copbio.2013.11.007>
- Cheng, J., Sahani, S., Hausrat, T. J., Yang, J. W., Ji, H., Schmarowski, N., ... Vogt, J. (2016). Precise Somatotopic Thalamocortical Axon Guidance Depends on LPA-Mediated PRG-2/Radixin Signaling. *Neuron*, *92*(1), 126–142. <https://doi.org/10.1016/j.neuron.2016.08.035>
- Coiro, P., Stoenica, L., Strauss, U., & Braüer, A. U. (2014). Plasticity-related gene 5 promotes spine formation in murine hippocampal neurons. *Journal of Biological Chemistry*, *289*(36), 24956–24970. <https://doi.org/10.1074/jbc.M114.597880>
- Conde, C., & Cáceres, A. (2009). Microtubule assembly, organization and dynamics in axons and dendrites. *Nature Reviews. Neuroscience*, *10*(5), 319–332. <https://doi.org/10.1038/nrn2631>
- Cosker, K. E., & Eickholt, B. J. (2007). Phosphoinositide 3-kinase signalling events controlling axonal morphogenesis. *Biochemical Society Transactions*, *35*(Pt 2), 207–10. <https://doi.org/10.1042/BST0350207>
- D'Este, E., Kamin, D., Göttfert, F., El-Hady, A., & Hell, S. W. (2015). STED Nanoscopy Reveals

- the Ubiquity of Subcortical Cytoskeleton Periodicity in Living Neurons. *Cell Reports*, 10(8), 1246–1251. <https://doi.org/10.1016/j.celrep.2015.02.007>
- Danzer, S. C., Crooks, K. R. C., Lo, D. C., & McNamara, J. O. (2002). Increased expression of brain-derived neurotrophic factor induces formation of basal dendrites and axonal branching in dentate granule cells in hippocampal explant cultures. *The Journal of Neuroscience : The Official Journal of the Society for Neuroscience*, 22(22), 9754–9763. <https://doi.org/22/22/9754> [pii]
- Diepen, M. T. Van, Parsons, M., Downes, C. P., Leslie, N. R., Hindges, R., & Eickholt, B. J. (2009). MyosinV controls PTEN function and neuronal cell size_M.T. vanDiepen 2009.pdf, 11(10). <https://doi.org/10.1038/ncb1961.nature>
- Dotti, C. G., Sullivan, C. a, & Banker, G. a. (1988). The establishment of polarity by hippocampal neurons in culture. *The Journal of Neuroscience : The Official Journal of the Society for Neuroscience*, 8(4), 1454–1468. [https://doi.org/10.1016/0012-1606\(89\)90269-8](https://doi.org/10.1016/0012-1606(89)90269-8)
- Endersby, R., & Baker, S. J. (2008). PTEN signaling in brain: Neuropathology and tumorigenesis. *Oncogene*, 27(41), 5416–5430. <https://doi.org/10.1038/onc.2008.239>
- Escriva, M., Peiro, S., Herranz, N., Villagrasa, P., Dave, N., Montserrat-Sentis, B., ... Garcia de Herreros, A. (2008). Repression of PTEN Phosphatase by Snail1 Transcriptional Factor during Gamma Radiation-Induced Apoptosis. *Molecular and Cellular Biology*, 28(5), 1528–1540. <https://doi.org/10.1128/MCB.02061-07>
- Fraser, M. M., Zhu, X., Kwon, C. H., Uhlmann, E. J., Gutmann, D. H., & Baker, S. J. (2004). Pten loss causes hypertrophy and increased proliferation of astrocytes in vivo. *Cancer Research*, 64(21), 7773–7779. <https://doi.org/10.1158/0008-5472.CAN-04-2487>
- Funamoto, S., Meili, R., Lee, S., Parry, L., & Firtel, R. A. (2002). Spatial and temporal regulation of 3-phosphoinositides by PI 3-kinase and PTEN mediates chemotaxis. *Cell*, 109(5), 611–623. [https://doi.org/10.1016/S0092-8674\(02\)00755-9](https://doi.org/10.1016/S0092-8674(02)00755-9)
- Gahbauer, S., & Böckmann, R. A. (2016). Membrane-mediated oligomerization of G protein coupled receptors and its implications for GPCR function. *Frontiers in Physiology*, 7(OCT), 1–17. <https://doi.org/10.3389/fphys.2016.00494>
- Gallent, E. A., & Steward, O. (2018). Neuronal PTEN deletion in adult cortical neurons triggers progressive growth of cell bodies, dendrites, and axons. *Experimental Neurology*, 303(December 2017), 12–28. <https://doi.org/10.1016/j.expneurol.2018.01.005>
- Ganguly, A., Tang, Y., Wang, L., Ladit, K., Loi, J., Dargent, B., ... Roy, S. (2015). A dynamic

- formin-dependent deep F-actin network in axons. *Journal of Cell Biology*, 210(3), 401–417. <https://doi.org/10.1083/jcb.201506110>
- García, J. M., Silva, J., Peña, C., Garcia, V., Rodriguez, R., Cruz, M. A., ... Bonilla, F. (2004). Promoter methylation of the PTEN gene is a common molecular change in breast cancer. *Genes Chromosomes and Cancer*, 41(2), 117–124. <https://doi.org/10.1002/gcc.20062>
- Gil, A., Andrés-Pons, A., Fernández, E., Valiente, M., Torres, J., Cervera, J., & Pulido, R. (2006). Nuclear Localization of PTEN by a Ran-dependent Mechanism Enhances Apoptosis: Involvement of an N-Terminal Nuclear Localization Domain and Multiple Nuclear Exclusion Motifs. *Molecular Biology of the Cell*, 17, 4002–4013.
- Gu, T., Zhang, Z., Wang, J., Guo, J., Shen, W. H., & Yin, Y. (2011). CREB Is a Novel Nuclear Target of PTEN Phosphatase Tingtong. *Cancer Research*, 71(8), 2821–2825. <https://doi.org/10.1158/0008-5472.CAN-10-3399>
- Hammarlund, M., Jorgensen, E. M., & Bastiani, M. J. (2007). Axons break in animals lacking β -spectrin. *Journal of Cell Biology*, 176(3), 269–275. <https://doi.org/10.1083/jcb.200611117>
- Hanna, S., & El-Sibai, M. (2013). Signaling networks of Rho GTPases in cell motility. *Cellular Signalling*, 25(10), 1955–1961. <https://doi.org/10.1016/j.cellsig.2013.04.009>
- Haugh, J. M., Codazzi, F., Teruel, M., & Meyer, T. (2000). Spatial sensing in fibroblasts mediated by 3' phosphoinositides. *Journal of Cell Biology*, 151(6), 1269–1279. <https://doi.org/10.1083/jcb.151.6.1269>
- Heiman, M. G., & Shaham, S. (2010). Twigs into branches: how a filopodium becomes a dendrite. *Current Opinion in Neurobiology*, 20(1), 86–91. <https://doi.org/10.1016/j.conb.2009.10.016>
- Hellwig, N. (2005). Homo- and heteromeric assembly of TRPV channel subunits. *Journal of Cell Science*, 118(5), 917–928. <https://doi.org/10.1242/jcs.01675>
- Ho, C. M., Lin, M. C., Huang, S. H., Huang, C. J., Lai, H. C., Chien, T. Y., & Chang, S. F. (2009). PTEN promoter methylation and LOH of 10q22-23 locus in PTEN expression of ovarian clear cell adenocarcinomas. *Gynecologic Oncology*, 112(2), 307–313. <https://doi.org/10.1016/j.ygyno.2008.09.040>
- Hollander, M. C., Blumenthal, G. M., & Dennis, P. A. (2011). PTEN loss in the continuum of common cancers, rare syndromes and mouse models. *Nature Reviews Cancer*, 11(4), 289–301. <https://doi.org/10.1038/nrc3037>
- Hoogenraad, C. C., & Bradke, F. (2009). Control of neuronal polarity and plasticity - a

- renaissance for microtubules? *Trends in Cell Biology*, 19(12), 669–676. <https://doi.org/10.1016/j.tcb.2009.08.006>
- Horiguchi, K., Hanada, T., Fukui, Y., & Chishti, A. H. (2006). Transport of PIP3 by GAKIN, a kinesin-3 family protein, regulates neuronal cell polarity. *The Journal of Cell Biology*, 174(3), 425–36. <https://doi.org/10.1083/jcb.200604031>
- Hu, J., Bai, X., Bowen, J. R., Dolat, L., Korobova, F., Yu, W., ... Spiliotis, E. T. (2012). Septin-driven coordination of actin and microtubule remodeling regulates the collateral branching of axons. *Current Biology*, 22(12), 1109–1115. <https://doi.org/10.1016/j.cub.2012.04.019>
- Iijima, M., Huang, Y. E., & Devreotes, P. (2002). Temporal and spatial regulation of chemotaxis. *Developmental Cell*, 3(4), 469–478. [https://doi.org/10.1016/S1534-5807\(02\)00292-7](https://doi.org/10.1016/S1534-5807(02)00292-7)
- Jaworski, J., Spangler, S., Seeburg, D. P., Hoogenraad, C. C., & Sheng, M. (2005). Control of Dendritic Arborization by the Phosphoinositide-3 Kinase – Akt – Mammalian Target of Rapamycin Pathway, 25(49), 11300–11312. <https://doi.org/10.1523/JNEUROSCI.2270-05.2005>
- Jeanneteau, F., Deinhardt, K., Miyoshi, G., Bennett, A. M., & Chao, M. V. (2010). The MAP kinase phosphatase MKP-1 regulates BDNF-induced axon branching. *Nat Neurosci*, 13(11), 1373–1379. <https://doi.org/10.1038/nn.2655> [pii]r10.1038/nn.2655
- Jiang, H., Guo, W., Liang, X., & Rao, Y. (2005). Both the establishment and the maintenance of neuronal polarity require active mechanisms: critical roles of GSK-3 β and its upstream regulators. *Cell*, 120(1), 123–135. <https://doi.org/10.1016/j.cell.2004.12.033>
- Jurado, S., Benoist, M., Lario, A., Knafo, S., Petrok, C. N., & Esteban, J. A. (2010). PTEN is recruited to the postsynaptic terminal for NMDA receptor-dependent long-term depression. *EMBO Journal*, 29(16), 2827–2840. <https://doi.org/10.1038/emboj.2010.160>
- Kapitein, L. C., & Hoogenraad, C. C. (2015). Building the Neuronal Microtubule Cytoskeleton. *Neuron*, 87(3), 492–506. <https://doi.org/10.1016/j.neuron.2015.05.046>
- Ketschek, Andrea; Gallo, G. (2010). NGF-induces Axonal Filopodia through Localized Microdomains of Phosphoinositide 3-kinase (PI3K) Activity that Drive the Formation of Cytoskeletal Precursors to Filopodia, 48(Suppl 2), 1–6. <https://doi.org/10.1097/MPG.0b013e3181a15ae8>.Screening
- Ketschek, A., & Gallo, G. (2010). Nerve Growth Factor Induces Axonal Filopodia through Localized Microdomains of Phosphoinositide 3-Kinase Activity That Drive the Formation of Cytoskeletal Precursors to Filopodia. *Journal of Neuroscience*, 30(36), 12185–12197.

<https://doi.org/10.1523/JNEUROSCI.1740-10.2010>

- Ketschek, A., Spillane, M., & Gallo, G. (2011). Mechanism of NGF-induced formation of axonal filopodia: NGF turns up the volume, but the song remains the same? *Communicative & Integrative Biology*, 4(1), 55–8. <https://doi.org/10.4161/cib.4.1.13647>
- Kreis, P., Hendricusdottir, R., Kay, L., Papageorgiou, I. E., van Diepen, M., Mack, T., ... Eickholt, B. J. (2013). Phosphorylation of the Actin Binding Protein Drebrin at S647 Is Regulated by Neuronal Activity and PTEN. *PLoS ONE*, 8(8), 1–12. <https://doi.org/10.1371/journal.pone.0071957>
- Kreis, P., Leondaritis, G., Lieberam, I., & Eickholt, B. J. (2014). Subcellular targeting and dynamic regulation of PTEN: implications for neuronal cells and neurological disorders. *Frontiers in Molecular Neuroscience*, 7(April), 23. <https://doi.org/10.3389/fnmol.2014.00023>
- Kwon, C. H., Luikart, B. W., Powell, C. M., Zhou, J., Matheny, S. A., Zhang, W., ... Parada, L. F. (2006). Pten Regulates Neuronal Arborization and Social Interaction in Mice. *Neuron*, 50(3), 377–388. <https://doi.org/10.1016/j.neuron.2006.03.023>
- Kwon, C. H., Zhu, X., Zhang, J., Knoop, L. L., Tharp, R., Smeyne, R. J., ... Baker, S. J. (2001). Pten regulates neuronal soma size: a mouse model of Lhermitte-Duclos disease. *Nature Genetics*, 29(december), 404–411. <https://doi.org/10.1038/ng781>
- Lee, J. O., Yang, H., Georgescu, M. M., Cristofano, A. Di, Maehama, T., Shi, Y., ... Pavletich, N. P. (1999). Crystal structure of the PTEN tumor suppressor: Implications for its phosphoinositide phosphatase activity and membrane association. *Cell*, 99(3), 323–334. [https://doi.org/10.1016/S0092-8674\(00\)81663-3](https://doi.org/10.1016/S0092-8674(00)81663-3)
- Lee, S. R., Yang, K. S., Kwon, J., Lee, C., Jeong, W., & Rhee, S. G. (2002). Reversible inactivation of the tumor suppressor PTEN by H₂O₂. *Journal of Biological Chemistry*, 277(23), 20336–20342. <https://doi.org/10.1074/jbc.M111899200>
- Leterrier, C., Dubey, P., & Roy, S. (2017). The nano-architecture of the axonal cytoskeleton. *Nature Reviews Neuroscience*. <https://doi.org/10.1038/nrn.2017.129>
- Lewis, T. L., Courchet, J., & Polleux, F. (2013). Cell biology in neuroscience: Cellular and molecular mechanisms underlying axon formation, growth, and branching. *The Journal of Cell Biology*, 202(6), 837–48. <https://doi.org/10.1083/jcb.201305098>
- Li, J., Yen, C., Liaw, D., Podsypanina, K., Bose, S., Wang, S. I., ... Parsons, R. (1997). PTEN, a putative protein tyrosine phosphatase gene mutated in human brain, breast, and prostate cancer. *Science*, 275(5308), 1943–7.

<https://doi.org/10.1126/science.275.5308.1943>

- Li, Z., Dong, X., Wang, Z., Liu, W., Deng, N., Ding, Y., ... Wu, D. (2005). Regulation of PTEN by Rho small GTPases. *Nature Cell Biology*, 7(4), 399–404. <https://doi.org/10.1038/ncb1236>
- Liu, K., Lu, Y., Lee, J. K., Samara, R., Willenberg, R., Sears-Kraxberger, I., ... He, Z. (2010). PTEN deletion enhances the regenerative ability of adult corticospinal neurons. *Nature Neuroscience*, 13(9), 1075–1081. <https://doi.org/10.1038/nn.2603>
- Liu, X., Huai, J., Endle, H., Schlüter, L., Fan, W., Li, Y., ... Vogt, J. (2016). PRG-1 Regulates Synaptic Plasticity via Intracellular PP2A/ β 1-Integrin Signaling. *Developmental Cell*, 1–16. <https://doi.org/10.1016/j.devcel.2016.06.019>
- Loudon, R. P., Silver, L. D., Yee, H. F., & Gallo, G. (2006). RhoA-kinase and myosin II are required for the maintenance of growth cone polarity and guidance by nerve growth factor. *Journal of Neurobiology*, 66(8), 847–867. <https://doi.org/10.1002/neu.20258>
- Lu, J., Jeong, H., Kong, N., Yang, Y., Carroll, J., Luo, H. R., ... Chai, L. (2009). Stem cell factor SALL4 represses the transcriptions of PTEN and SALL1 through an epigenetic repressor complex. *PLoS ONE*, 4(5), 1–13. <https://doi.org/10.1371/journal.pone.0005577>
- Lukinavičius, G., Reymond, L., D'Este, E., Masharina, A., Göttfert, F., Ta, H., ... Johnsson, K. (2014). Fluorogenic probes for live-cell imaging of the cytoskeleton. *Nature Methods*, 11(7), 731–3. <https://doi.org/10.1038/nmeth.2972>
- Lumb, C. N., & Sansom, M. S. P. (2013). Defining the membrane-associated state of the PTEN tumor suppressor protein. *Biophysical Journal*, 104(3), 613–621. <https://doi.org/10.1016/j.bpj.2012.12.002>
- Maehama, T., Taylor, G. S., Slama, J. T., & Dixon, J. E. (2000). A Sensitive Assay for Phosphoinositide Phosphatases. *Analytical Biochemistry*, 279(2), 248–250. <https://doi.org/10.1006/abio.2000.4497>
- Manning, B., & Cantley, L. (2007). AKT/PKB Signalling: Navigating Downstream. *Cell*, 129(7), 1261–1274. <https://doi.org/10.1016/j.cell.2007.06.009>.AKT/PKB
- Marshak, S., Nikolakopoulou, A. M., Dirks, R., Martens, G. J., & Cohen-Cory, S. (2007). Cell-autonomous TrkB signaling in presynaptic retinal ganglion cells mediates axon arbor growth and synapse maturation during the establishment of retinotectal synaptic connectivity. *The Journal of Neuroscience: The Official Journal of the Society for Neuroscience*, 27(10), 2444–2456. <https://doi.org/10.1523/JNEUROSCI.4434-06.2007>
- McDermott, M. I., Sigal, Y. J., Sciorra, V. a, & Morris, A. J. (2004). Is PRG-1 a new lipid

- phosphatase? *Nature Neuroscience*, 7(8), 789; author reply 789-790. <https://doi.org/10.1038/nn0804-789b>
- Ménager, C., Arimura, N., Fukata, Y., & Kaibuchi, K. (2004). PIP3 is involved in neuronal polarization and axon formation. *Journal of Neurochemistry*, 89(1), 109–118. <https://doi.org/10.1046/j.1471-4159.2004.02302.x>
- Meng, F., Henson, R., Wehbe-Jane, H., Ghosal, K., Jacobs, S. T., & Patel, T. (2015). MicroRNA-21 Regulates Expression of the PTEN Tumor Suppressor Gene in Human Hepatocellular Cancer. *Gastroenterology*, 133(2), 647–658. <https://doi.org/10.1053/j.gastro.2007.05.022>.MicroRNA-21
- Neisch, Amanda., Fehon, Rl. (2011). Ezrin, Radixin and Moesin: Key regulators of membran-cortex interactions and signaling. *Curr Opin Cell Biol*, 23(4), 377–382. <https://doi.org/10.1016/j.ceb.2011.04.011>.Ezrin
- Okumura, K., Mendoza, M., Bachoo, R. M., DePinho, R. A., Cavenee, W. K., & Furnari, F. B. (2006). PCAF modulates PTEN activity. *Journal of Biological Chemistry*, 281(36), 26562–26568. <https://doi.org/10.1074/jbc.M605391200>
- Olive, V., Bennett, M. J., Walker, J. C., Ma, C., Jiang, I., Cordon-Cardo, C., ... He, L. (2009). miR-19 is a key oncogenic component of mir-17-92. *Genes and Development*, 23(24), 2839–2849. <https://doi.org/10.1101/gad.1861409>
- Papa, A., Wan, L., Bonora, M., Salmena, L., Song, M. S., Hobbs, R. M., ... Pandolfi, P. P. (2014). Cancer-associated PTEN mutants act in a dominant-negative manner to suppress PTEN protein function. *Cell*, 157(3), 595–610. <https://doi.org/10.1016/j.cell.2014.03.027>
- Park, K. K., Liu, K., Hu, Y., Smith, P. D., Wang, C., Cai, B., ... Zhigang, H. (2008). Promoting Axon Regeneration in the Adult CNS by Modulation of the PTEN/mTOR Pathway. *Science*, 322(Dezember).
- Pollard, T. D. (2009). Actin, a Central Player in Cell Shape and Movement Thomas D. Pollard, 1208(November), 1208–1213. <https://doi.org/10.1126/science.1175862>
- Polleux, F., & Snider, W. (2010). Initiating and growing an axon. *Cold Spring Harbor Perspectives in Biology*, 2(4), 1–19. <https://doi.org/10.1101/cshperspect.a001925>
- Rahdar, M., Inoue, T., Meyer, T., Zhang, J., Vazquez, F., & Devreotes, P. N. (2009). A phosphorylation-dependent intramolecular interaction regulates the membrane association and activity of the tumor suppressor PTEN. *Proceedings of the National Academy of Sciences*, 106(2), 480–485. <https://doi.org/10.1073/pnas.0811212106>
- Rivero-Müller, A., Jonas, K. C., Hanyaloglu, A. C., & Huhtaniemi, I. (2013). Di/Oligomerization

- of GPCRs - Mechanisms and functional significance. *Progress in Molecular Biology and Translational Science*, 117, 163–185. <https://doi.org/10.1016/B978-0-12-386931-9.00007-6>
- Rodgers, E. E., & Theibert, A. B. (2002). Functions of PI 3-kinase in development of the nervous system. *International Journal of Developmental Neuroscience*, 20(3–5), 187–197. [https://doi.org/10.1016/S0736-5748\(02\)00047-3](https://doi.org/10.1016/S0736-5748(02)00047-3)
- Roy, S. (2016). Waves, rings, and trails: The scenic landscape of axonal actin. *Journal of Cell Biology*, 212(2), 131–134. <https://doi.org/10.1083/jcb.201511016>
- Saarikangas, J., Zhao, H., & Lappalainen, P. (2010). Regulation of the actin cytoskeleton-plasma membrane interplay by phosphoinositides. *Physiological Reviews*, 90, 259–289. <https://doi.org/10.1152/physrev.00036.2009>
- Salvesen, H. B., MacDonald, N., Ryan, A., Jacobs, I. J., Lynch, E. D., Akslen, L. A., & Das, S. (2001). Pten Methylation Is Associated With Advanced Stage and. *Int. J. Cancer*, 26(November 2000), 22–26.
- Schermelleh, L., Heintzmann, R., & Leonhardt, H. (2010). A guide to super-resolution fluorescence microscopy. *Journal of Cell Biology*, 190(2), 165–175. <https://doi.org/10.1083/jcb.201002018>
- Schindl, R., & Romanin, C. (2007). Assembly domains in TRP channels. *Biochemical Society Transactions*, 35(Pt 1), 84–85. <https://doi.org/10.1042/BST0350084>
- Schulze, N., Graessl, M., Blancke Soares, A., Geyer, M., Dehmelt, L., & Nalbant, P. (2014). FHOD1 regulates stress fiber organization by controlling the dynamics of transverse arcs and dorsal fibers. *Journal of Cell Science*, 127(7), 1379–1393. <https://doi.org/10.1242/jcs.134627>
- Senju, Y., Kalimeri, M., Koskela, E. V., Somerharju, P., Zhao, H., Vattulainen, I., & Lappalainen, P. (2017). Mechanistic principles underlying regulation of the actin cytoskeleton by phosphoinositides. *Proceedings of the National Academy of Sciences*, 201705032. <https://doi.org/10.1073/pnas.1705032114>
- Servant, G., Weiner, O. D., Herzmark, P., Balla, T., Sedat, J. W., & Bourne, H. R. (2000). Polarization of Chemoattractant Receptor Signaling During Neutrophil Chemotaxis, 287(5455), 1037–1040.
- Shen, W. H., Balajee, A. S., Wang, J., Wu, H., Eng, C., Pandolfi, P. P., & Yin, Y. (2007). Essential Role for Nuclear PTEN in Maintaining Chromosomal Integrity. *Cell*, 128(1), 157–170. <https://doi.org/10.1016/j.cell.2006.11.042>

- Shenoy, S., Shekhar, P., Heinrich, F., Daou, M. C., Gericke, A., Ross, A. H., & Lösche, M. (2012). Membrane association of the PTEN tumor suppressor: Molecular details of the protein-membrane complex from SPR binding studies and neutron reflection. *PLoS ONE*, *7*(4). <https://doi.org/10.1371/journal.pone.0032591>
- Shi, S., Jan, L. Y., & Jan, Y. (2003). Hippocampal Neuronal Polarity Specified by Spatially Localized mPar3 / mPar6 and PI 3-Kinase Activity. *Cell.*, *112*(1), 63–75.
- Sigal, Y. J., McDermott, M. I., & Morris, A. J. (2005). Integral membrane lipid phosphatases/phosphotransferases: common structure and diverse functions. *The Biochemical Journal*, *387*(Pt 2), 281–93. <https://doi.org/10.1042/BJ20041771>
- Sigal, Y. J., Quintero, O. a, Cheney, R. E., & Morris, A. J. (2007). Cdc42 and ARP2/3-independent regulation of filopodia by an integral membrane lipid-phosphatase-related protein. *Journal of Cell Science*, *120*(Pt 2), 340–52. <https://doi.org/10.1242/jcs.03335>
- Song, M. S., Salmena, L., Carracedo, A., Egia, A., Lo-, F., Teruya-feldstein, J., & Pandolfi, P. P. (2012). The deubiquitylation and localization of PTEN are regulated by a HAUSP–PML network, *455*(7214), 813–817. <https://doi.org/10.1038/nature07290>.The
- Song, M. S., Salmena, L., & Pandolfi, P. P. (2012). The functions and regulation of the PTEN tumour suppressor. *Nature Reviews Molecular Cell Biology*, *13*(5), 283–296. <https://doi.org/10.1038/nrm3330>
- Spillane, M., Ketschek, A., Jones, S. L., Korobova, F., Marsick, B., Lanier, L., ... Gallo, G. (2011). The actin nucleating Arp2/3 complex contributes to the formation of axonal filopodia and branches through the regulation of actin patch precursors to filopodia. *Developmental Neurobiology*, *71*(9), 747–758. <https://doi.org/10.1002/dneu.20907>
- Stankiewicz, T. R., & Linseman, D. a. (2014). Rho family GTPases: key players in neuronal development, neuronal survival, and neurodegeneration. *Frontiers in Cellular Neuroscience*, *8*(October), 314. <https://doi.org/10.3389/fncel.2014.00314>
- Steck, P., Pershouse, M., Jasser, S., Alfred Yung, W., Lin, H., Ligon, A., ... Tavtigian, S. (1997). Identification of a candidate tumour suppressor gene, MMAC1, at chromosome 10q23.3 that is mutated in multiple advanced cancers. *Nature Genetics*, *15*, 356–362. <https://doi.org/10.1038/ng0797-270>
- Stiles, J., & Jernigan, T. L. (2010). The basics of brain development. *Neuropsychology Review*, *20*(4), 327–348. <https://doi.org/10.1007/s11065-010-9148-4>
- Strittmatter, S. M., & Cafferty, W. B. J. (2017). Identification of Intrinsic Axon Growth Modulators for Intact CNS Neurons after Injury Article Identification of Intrinsic Axon

- Growth Modulators for Intact CNS Neurons after Injury, 2687–2701.
<https://doi.org/10.1016/j.celrep.2017.02.058>
- Sumitomo, M., Iwase, A., Zheng, R., Navarro, D., Kaminetzky, D., Shen, R., ... Nanus, D. M. (2004). Synergy in tumor suppression by direct interaction of Neutral Endopeptidase with PTEN. *Cancer Cell*, 5(1), 67–78. [https://doi.org/10.1016/S1535-6108\(03\)00331-3](https://doi.org/10.1016/S1535-6108(03)00331-3)
- Takahashi, Y., Morales, F. C., Kreimann, E. L., & Georgescu, M. M. (2006). PTEN tumor suppressor associates with NHERF proteins to attenuate PDGF receptor signaling. *EMBO Journal*, 25(4), 910–920. <https://doi.org/10.1038/sj.emboj.7600979>
- Tokumitsu, H., Hatano, N., Tsuchiya, M., Yurimoto, S., Fujimoto, T., Ohara, N., ... Sakagami, H. (2010). Identification and characterization of PRG-1 as a neuronal calmodulin-binding protein. *Biochem. J*, 431, 81–91. <https://doi.org/10.1042/BJ20100637>
- Torres, J., & Pulido, R. (2001). The tumor suppressor PTEN is phosphorylated by the protein kinase CK2 at its C terminus. Implications for PTEN stability to proteasome-mediated degradation. *Journal of Biological Chemistry*, 276(2), 993–998. <https://doi.org/10.1074/jbc.M009134200>
- Trimbuch, T., Beed, P., Vogt, J., Schuchmann, S., Maier, N., Kintscher, M., ... Nitsch, R. (2009). Synaptic PRG-1 Modulates Excitatory Transmission via Lipid Phosphate-Mediated Signaling. *Cell*, 138(6), 1222–1235. <https://doi.org/10.1016/j.cell.2009.06.050>
- Van Diepen, M. T., & Eickholt, B. J. (2007). Function of PTEN during the formation and maintenance of neuronal circuits in the brain. *Developmental Neuroscience*, 30(1–3), 59–64. <https://doi.org/10.1159/000109852>
- Vanhaesebroeck, B., Guillermet-Guibert, J., Graupera, M., & Bilanges, B. (2010). The emerging mechanisms of isoform-specific PI3K signalling. *Nature Reviews Molecular Cell Biology*, 11(5), 329–341. <https://doi.org/10.1038/nrm2882>
- Vazquez, F., Matsuoka, S., Sellers, W. R., Yanagida, T., Ueda, M., & Devreotes, P. N. (2006). Tumor suppressor PTEN acts through dynamic interaction with the plasma membrane. *Proceedings of the National Academy of Sciences of the United States of America*, 103(10), 3633–8. <https://doi.org/10.1073/pnas.0510570103>
- Velmans, T., Battenfeld, A., Geist, B., Farrés, A. S., Strauss, U., & Bräuer, A. U. (2013). Plasticity-related gene 3 promotes neurite shaft protrusion. *BMC Neuroscience*, 14, 36. <https://doi.org/10.1186/1471-2202-14-36>
- Virolle, T., Adamson, E. D., Baron, V., Birlé, D., Mercola, D., Mustelin, T., & De Belle, I. (2001). The Egr-1 transcription factor directly activates PTEN during irradiation-induced

- signalling. *Nature Cell Biology*, 3(December), 1–5. Retrieved from <http://cellbio.nature.com>
- Wu, X., Hepner, K., Castelino-Prabhu, S., Do, D., Kaye, M. B., Yuan, X. J., ... Whang, Y. E. (2000). Evidence for regulation of the PTEN tumor suppressor by a membrane-localized multi-PDZ domain containing scaffold protein MAGI-2. *Proceedings of the National Academy of Sciences of the United States of America*, 97(16), 4233–4238. <https://doi.org/10.1073/pnas.97.8.4233>
- Xu, K., Zhong, G., & Zhuang, X. (2013). Actin, spectrin, and associated proteins form a periodic cytoskeletal structure in axons. *Science (New York, N.Y.)*, 339(6118), 452–6. <https://doi.org/10.1126/science.1232251>
- Yoshimura, T., Kawano, Y., Arimura, N., Kawabata, S., Kikuchi, A., & Kaibuchi, K. (2005). GSK-3beta regulates phosphorylation of CRMP-2 and neuronal polarity. *Cell*, 120(1), 137–149. <https://doi.org/10.1016/j.cell.2004.11.012>
- Yu, P., Agbaegbu, C., Malide, D. A., Wu, X., Katagiri, Y., Hammer, J. A., & Geller, H. M. (2015). Cooperative interactions of LPPR/PRG family members in membrane localization and alteration of cellular morphology. *Journal of Cell Science*, 128(July), 3210–3222. <https://doi.org/10.1242/jcs.169789>
- Yu, W., Qiang, L., Solowska, J. M., Karabay, A., Korulu, S., & Baas, P. W. (2008). The Microtubule-severing Proteins Spastin and Katanin Participate Differently in the Formation of Axonal Branches. *Molecular Biology of the Cell*, 19(1), 1485–1498. <https://doi.org/10.1091/mbc.E07-09-0878>
- Zhang, J. guang, Wang, J. jun, Zhao, F., Liu, Q., Jiang, K., & Yang, G. hai. (2010). MicroRNA-21 (miR-21) represses tumor suppressor PTEN and promotes growth and invasion in non-small cell lung cancer (NSCLC). *Clinica Chimica Acta*, 411(11–12), 846–852. <https://doi.org/10.1016/j.cca.2010.02.074>
- Zhong, G., He, J., Zhou, R., Lorenzo, D., Babcock, H. P., Bennett, V., & Zhuang, X. (2014). Developmental mechanism of the periodic membrane skeleton in axons. *eLife*, 3, e04581. <https://doi.org/10.7554/eLife.04581>
- Zhou, J., & Parada, L. F. (2012). PTEN signaling in autism spectrum disorders. *Current Opinion in Neurobiology*, 22(5), 873–879. <https://doi.org/10.1016/j.conb.2012.05.004>
- Zhou, X.-P., Marsh, D. J., Morrison, C. D., Chaudhury, A. R., Maxwell, M., Reifenberger, G., & Eng, C. (2003). Germline Inactivation of PTEN and Dysregulation of the Phosphoinositol-3-Kinase/Akt Pathway Cause Human Lhermitte-Duclos Disease in Adults. *The American Journal of Human Genetics*, 73(5), 1191–1198. <https://doi.org/10.1086/379382>

6. Supplementary information

6.1 Curriculum vitae

Der Lebenslauf ist in der Online-Version aus Gründen des Datenschutzes nicht enthalten.

6.2 Poster and talks

Membranes and Modules 2014, Berlin, Germany. “Regulation of PTEN by transmembrane lipid pseudo-phosphatases of the plasticity-related gene family and implications for neuronal growth” (poster presentation)

FENS 2014, Milan, Italy. “Regulation of PTEN by transmembrane lipid pseudo-phosphatases of the plasticity-related gene (PRG) family: Implications for neuronal growth responses” (poster presentation)

FEBS 2015, Berlin, Germany. “Identification of transmembrane pseudo-phosphatase Plasticity related gene 2 as an interacting partner of PTEN” (poster presentation)

SFB958 retreat 2016, Kloster Lehnin, Germany. “Regulation of localized PI3K signaling by a PTEN-associated protein scaffold containing a transmembrane lipid pseudo-phosphatase of the Plasticity-Related Gene (PRG) family” (poster presentation)

PI3K-mTOR-PTEN Network in Health & Disease (CSHL) 2016, New York, USA. “A PTEN-associated membrane protein scaffold controls axonal phosphoinositides and neuronal morphogenesis” (poster presentation)

EMBO Conference, Cell Biology of the Neuron, 2017, Heraklion, Greece. “A PTEN-associated membrane protein controls phosphoinositide distribution and axon morphogenesis” (poster presentation)

SFB958 retreat 2017, Brandenburg, Germany. “A PTEN-associated membrane protein controls phosphoinositide distribution and axon morphogenesis” (poster presentation)

Biochemistry/ Biophysics Institute Seminar, 2017. “A PTEN-based protein scaffold containing Plasticity Related Gene 2 (PRG2) influences neuronal morphology” (oral presentation)

7. Statement of authorship

I declare that my PhD thesis entitled “Analysis of a PTEN-associated protein scaffold containing the transmembrane protein PRG2” has been written independently and with no other sources and aids than quoted.

Berlin,

Annika Brosig